CHARACTERIZING AND CONTROLLING THE EFFECTS OF DIFFERENTIAL DRAG ON SATELLITE FORMATIONS

THESIS

James T. Wedekind, Captain, USAF

AFIT/GSS/ENY/06-M14

DEPARTMENT OF THE AIR FORCE
AIR UNIVERSITY

AIR FORCE INSTITUTE OF TECHNOLOGY

Wright-Patterson Air Force Base, Ohio

The views expressed in this thesis are those of the author and do not reflect the official policy or position of the United States Air Force, Department of Defense, or the U.S. Government.

AFIT/GSS/ENY/06-M14

CHARACTERIZING AND CONTROLLING THE EFFECTS OF DIFFERENTIAL DRAG ON SATELLITE FORMATIONS

THESIS

Presented to the Faculty

Department of Aeronautics and Astronautics

Graduate School of Engineering and Management

Air Force Institute of Technology

Air University

Air Education and Training Command

In Partial Fulfillment of the Requirements for the

Degree of Master of Science in Space Systems

James T. Wedekind, BSE

Captain, USAF

March 2006

AFIT/GSS/ENY/06-M14

CHARACTERIZING AND CONTROLLING THE EFFECTS OF DIFFERENTIAL DRAG ON SATELLITE FORMATIONS

James T. Wedekind, BSE

Captain, USAF

Approved:

// Signed //	2 Mar 06
Nathan A. Titus, Lt Col, USAF (Chairman)	Date
// Signed //	2 Mar 06
Kerry D. Hicks, Lt Col, USAF (Member)	Date
// Signed //	2 Mar 06
Dr. William E. Wiesel (Member)	Date

Abstract

The ability to fly satellites in close formations represents a capability that could revolutionize the way satellite missions are designed in the future. This study examines three of the primary formation flying designs and characterizes the affect that an anomalous satellite with a slightly different cross-sectional area would have on the stability of the formation. Following the characterization of the effects, a controller is implemented to mitigate the cross-sectional area differences between the satellites. With the addition of a straightforward controller, small cross-sectional area differences can be mitigated and corrected such that the satellites will remain in close proximity and in some cases the formation will remain stable.

Acknowledgments

I would like to express my sincere appreciation to my faculty advisor, Lt Col Nathan Titus, for his guidance and support throughout the course of this thesis effort. His insight and knowledge made many of the difficult problems I faced seem much simpler and easier to understand. Without his advice and thoughts my task would have been much more daunting. Finally I would like to thank my wonderful wife and my new son for providing continuous support and infectious smiles that instantly put the longest days back into the correct perspective.

James T. Wedekind

Table of Contents

Page

Page

List of Figures

CHARACTERIZING AND CONTROLLING THE EFFECTS OF DIFFERENTIAL DRAG ON SATELLITE FORMATIONS

I. Background

The old axiom that information is power remains one of the primary tenets of military operations. The ability to observe ground events from overhead platforms can be traced back to the French Revolution when France organized a company of aerostiers, or balloonists in the spring of 1794 (Richelson, 1999). Balloon platforms were also used with limited success during the American Revolution, and many scholars originally believed that the airplane's primary wartime mission would revolve around aerial surveillance (Richelson, 1999). When presented the opportunity to gather more intelligence about their adversaries military leaders throughout history have jumped at the idea.

Upon the Soviet launch of Sputnik on October 4, 1957, the world of overhead surveillance changed forever. The Sputnik launch led directly to the creation of the National Aeronautics and Space Administration (NASA) and pushed the United States' space program into catch-up mode. Fortunately for the United States, the gears of progress had already been set in motion. On March 16, 1955, more than two years prior to the launch of Sputnik, the Air Force issued General Operational Requirement No. 80, officially establishing a high-level requirement for an advanced reconnaissance satellite. The document defined the Air Force objective to be the provision of continuous surveillance of "preselected areas of the earth" in order "to determine the status of a

potential enemy's warmaking capability." (Richelson, 1999). The Air Force program, originally Advanced Reconnaissance System (ARS) then renamed SAMOS, which evolved from this directive experienced a number of problems and delays. Concern about the time schedule for SAMOS prompted President Eisenhower to approve the CIA reconnaissance program CORONA. After 12 unsuccessful launches the 13th mission finally returned a canister of film from space that was successfully recovered by the United States on August 18, 1960 (Richelson, 1999). With the success of CORONA, the high ground of surveillance had irreversibly been shifted to space borne platforms.

Modern satellite systems give the United States military an immense strategic advantage by providing unparalleled intelligence, surveillance, and reconnaissance (ISR) capabilities. Traditionally these satellites have been large complex satellites that operate independently or as part of a larger formation that provides near global coverage. These complex systems require extra redundancy and extremely detailed integration and test procedures because the failure of a single subsystem can not only impact the operability of the individual satellite, but also endanger the mission of the entire formation. However in recent years mission planners have begun to explore alternative mission profiles and satellite configurations that could reduce cost, size, and complexity while increasing imaging resolution.

One idea that has gained credence recently is the idea of distributing the functionality of large satellites among a group of smaller cooperative satellites. This concept involves flying a group of satellites (often called a cluster) within very close range of each other (250m – 5km) (Mohammed, 2001: 58). The cluster approach offers mission planners much more flexibility in mission design and lifecycle planning because

of the ability to re-position satellites in the cluster to accomplish different missions or to compensate for malfunctioning members of the cluster. It offers additional redundancy and the promise of graceful capability degradation. Adding satellites to the cluster post-initial launch is also a very real option that allows for implementing new technologies and enhancing cluster performance (Mohammed, 2001: 58).

Many scientific, military, and commercial space applications are exploring the use of clustered satellites to perform distributed observations from space, synthetic aperture radar (SAR) earth mapping, magnetosphere sensing, interferometry, and a variety of other missions (Kitts, 1999: 217). Many of these missions are drawn to the cluster approach because clusters can provide a very large virtual aperture. Since imaging resolution is a function of aperture size, the larger the aperture (real or virtual) the better the resolution. The separation between instruments can be used to create apertures that allow for orders of magnitude improvements in ISR capabilities (Kitts, 1999: 217).

In fact several current missions are being developed to validate cluster flying dynamics, command and control, and other cluster specific problems. The French MoD recently launched a cluster of satellites, Essaim, designed to demonstrate the electro-magnetic signal interception feasibility from space, and the possibilities of a formation flying (swarm) system to prepare for coming fully operational systems (de Selding, 2004). The Orion mission was developed to demonstrate true formation flying using spaceborne carrier differential GPS aboard low-cost LEO satellites. It is scheduled to be a single satellite flying in formation with the two Emerald vehicles (Bauer et al, 1999: 379). In addition many earth and space science mission require the use of satellite

constellations in order to accomplish their mission. Some of these mission ideas will be further discussed later in the text.

There are numerous mission profiles that would benefit from the use of clustered satellites. A number of those profiles can be accomplished with very loose formation knowledge (1-100 km). Unfortunately on the other end of the spectrum many of the possible science and ISR missions would require much finer knowledge and control. Providing the necessary accuracy of micro-meter and sometimes even pico-meter position knowledge presents a difficult challenge for today's command and control systems (Baeur et al, 1999: 370). Given the large distances from space down to the Earth, it follows that small errors in the relative positions of the clustered satellites can cause huge accuracy and fidelity issues with the final data. Therefore one of the primary areas of research concerning clustered satellites is in the area of command and control. Currently there are a number of proposed solutions to the command and control problem, but none of them have been successfully tested to the precision necessary to achieve pico-meter accuracy. The technologies and algorithms for implementing these command and control schemes are still being refined, but given the potential cost savings and flexibilities that satellite clusters could offer it is only a matter of time.

Satellites in orbit experience a number of perturbations that will test the command and control system of any clustered formation. In low Earth orbit (LEO), where most of the Earth pointing systems will be deployed, one of the primary perturbations is atmospheric drag. Atmospheric drag is a perturbing nonconservative force that acts to lower a satellite's orbit while increasing its mean velocity (Vallado, 2000: 632). While the acceleration due to drag does not noticeably effect satellites on an hour to hour basis,

it is a major perturbation factor for satellites in orbits with an altitude of less than 500 km. It becomes even more important to understand when clustered satellites need to maintain separation accuracy on the order of micro meters.

Problem Statement

Satellite clusters will ideally deploy and operate in an optimal manner every time. However given harsh launch environments, excessive radiation in space and a myriad of other issues many satellites are not deployed in the desired manner or develop problems after a period of operation. An anomalous deployment or change in the physical size of a satellite in a cluster can be particularly difficult to deal with because of the precise command and control that is necessary for the cluster to operate as designed. This study will investigate the effects of how differential drag among satellites in a cluster formation will affect the stability and configuration of the cluster.

Objective

The objective of this research is to study the effects of drag on anomalous satellites within a cluster and determine how quickly the cluster formation will deteriorate. This research will examine the effects of differential drag for satellites within an in-plane formation, an in-track formation, and a circular formation. In addition to inspecting the effects of drag on these formations, a controller will be employed and tested to determine if a simple control mechanism may be able to alleviate the disturbances created by atmospheric drag on the formations.

II. Literature Review

Chapter Overview

There has been a surge of interest in recent years regarding the enabling technologies for high precision formation flying satellites. This literature review will examine three of the major areas that are distinctive to formation flying (formation design, formation navigation & control, and inter-satellite communication) and the current technology situation with regard to those specific areas. In addition it will briefly look at the history and current state of modeling atmospheric drag.

Formation Flying Overview

In addition to the advantages discussed in the chapter one, the distributed sensor platform that formation flying promises is becoming more and more enticing due to the volume and mass constraints that current launch vehicle fairings place on payloads. These constraints will restrict new monolithic apertures to slightly larger or the same size as that of the Hubble Space Telescope. There are some image resolution enhancements that can be made by using segmented optics similar to the optics planned for the James Webb Space Telescope, however this approach is limited due to structural dynamics and control issues (Leitner, 2004).

There are three primary areas that are distinctive to the formation flying problem. Those areas are formation design, formation navigation and control, and inter-satellite communication (Leitner, 2004).

Formation Design

Formation design can be defined as the positioning of satellites into a desired geometry to meet the demands of the mission. It is a difficult "give and take" problem between optimal positioning and fuel consumption. Designing a formation that maintains a useful formation with very little or no fuel consumption is the ultimate goal.

Sabol et al (2001: 271) used the relative equations of motion of two satellites known as Hill's equations or the Clohessy-Wiltshire equations (Chlohessy and Wiltshire, 1960) to examine satellite formation design. They examined the initial Hill's equations and used a detailed derivation from Vallado's text (Vallado, 2001: 374-399) that describe the unperturbed motion of two bodies (in close proximity) in circular orbits as a preliminary design tool.

$$\ddot{x} - 2n\dot{y} - 3n^2 x = 0 \tag{2.1}$$

$$\ddot{y} + 2n\dot{x} = 0 \tag{2.2}$$

$$\ddot{z} + n^2 z = 0 \tag{2.3}$$

After solving analytically for these and complementing the solution with numerical simulation of the fully nonlinear dynamics with realistic force modeling they set the secular term to zero through the constraint

$$\dot{y}_0 = -2x_0 n \tag{2.4}$$

"Then through algebraic manipulation they showed that this constraint results in a displaced orbit with the same energy and thus the same semimajor axis, as the reference orbit neglecting higher-order terms in eccentricity. When the constraint is enforced Hill's equations become (Sabol et al, 2001: 271)"

$$x(t) = (\dot{x}_0 / n)\sin(nt) + x_0 \cos(nt) \tag{2.5}$$

$$y(t) = (2\dot{x}_0 / n)\cos(nt) - 2x_0 \sin(nt) - 2\dot{x}_0 / n + y_0 \tag{2.6}$$

$$z(t) = (\dot{z}_0 / n)\sin(nt) + z_0 \cos(nt) \tag{2.7}$$

The above equations provided the basis for Sabol's formation flying design.

Three of the formation flying designs that were considered in their analysis were the in-plane formation, the in-track formation and the circular formation. Sabol et al (2001: 271) describes the in-plane cluster design as the simplest of all cluster designs. The formation consists of a group (2+) of satellites occupying the same orbital plane, but separated by mean anomaly. This in-plane formation offers the advantages of a simple design, straightforward deployment, and uncomplicated control. However this type of formation is limited in the style of configurations it can support and the number of satellites that can be deployed into a reasonable cluster (Sabol et al, 2001: 271).

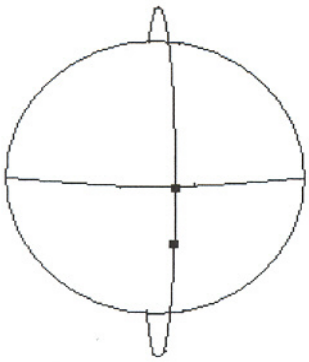

Figure 1. In-plane formation

The in-track formation consists of satellites that all share the same ground track. At first this concept seems identical to the in-plane design, and it would be if the Earth did not rotate. However since the Earth does rotate satellites can only follow the same ground track if their orbital planes are separated by a delta in the right ascension of the ascending node, which compensates for the rotating Earth. This formation offers the advantage of identical ground tracks, but will also have a difficult time supporting multiple configuration shapes with numerous satellites (Sabol et al, 2001: 272).

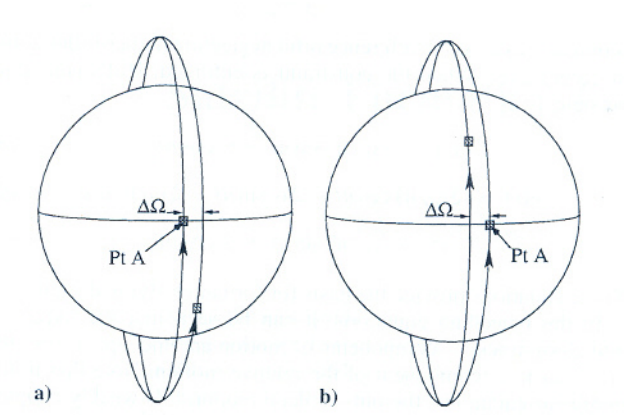

Figure 2. In-track formation (Sabol et al, 2001: 272)

The final type of formation that this study examines is the circular formation. In the circular formation the satellites maintain a constant distance from each other. For two arbitrary points in the cluster their will most likely be differences in inclination, right ascension of the ascending node, argument of perigee, and mean anomaly. Sabol et al (2001: 272) give the following insight into the circular formation design in terms of Keplerian mechanics,

> "Consider a circular reference orbit inclined at 90 degrees with a satellite at the equator (ascending node). Now consider another satellite in a slightly elliptical orbit also on the equator and separated from the reference orbit by a small amount of ascending node. The second satellite is at apogee and, therefore will fall behind the reference satellite as they both proceed towards the North Pole. Because both orbits are polar, the satellites' paths will cross at the poles, but the reference satellite reaches the pole first. On the other side of the North Pole, the second satellite is lower in altitude than the reference satellite and begins to catch up. Both satellites reach their descending nodes at the same time, and the second satellite is now at perigee. The second satellite continues to advance ahead of the reference satellite and reaches the South Pole first, where the paths cross once again. On the other side of the South Pole, the reference satellite begins to catch up as the second satellite increases in altitude towards its apogee and ascending node."

The circular formation offers two characteristics make it attractive to cluster designers. One advantage is that the two satellites maintain a constant distance from each other at all times. The other advantage that is unique to the circular formation is that unlike the in-plane and in-track formations the circular formation presents a two-dimensional array (Sabol et al, 2001: 272-273).

Formation Navigation and Control

The implementation of formation flying satellites acting in harmony to achieve military and scientific Earth sensing objectives will require stringent control thresholds. Formation control is responsible for rejecting disturbances and keeping the formation in the desired geometry. Formation maintenance and control at the necessary level is one of the more difficult problems facing the widespread deployment of clustered satellites. Formation control and relative navigation pose some very interesting challenges in the areas of (Bauer el al, 1999: 376):

1. Onboard sensing of relative and absolute vehicle position/attitudes.
2. Maneuvering, retargeting, collision avoidance, and aperture optimization including resource/task allocation within the fleet.
3. Modeling the orbital mechanics and the impact of differential drag and solar disturbances
4. Fleet and vehicle autonomy, including high-level fault detection and recovery to enhance mission robustness

5. Decentralized control and computation for a fleet of many (e.g. from 16 to hundreds) vehicles.
6. Testbeds and simulations to validate the various sensing and control concepts.

Many current spacecraft systems rely on ground based command and control to ensure proper positioning and attitude of individual spacecrafts. However nearly all of those systems are single satellites that are widely spaced and don't depend on the relative positioning data between spacecraft. When dealing with a clustered group of satellites ground based command and control becomes much more cumbersome. Attitude and position data are needed instantaneously. Ground-based systems would be very intricate, weighed down by data, and possibly unable to provide timely corrective commands. Thus, a number of institutions have been focusing on developing autonomous satellite-based command and control algorithms and schema to facilitate clustered satellite flight (Bauer et al, 1999: 376).

Ideally, autonomous formation flying involves taking continuous position and velocity data that determine the state of the formation. Those measurements are then used to maintain the current configuration or to transition to a new formation style without the application of any outside controls. The configuration of the cluster includes not only the distances between all pairs of spacecraft in the cluster, but also the orientation of the satellites in a coordinate frame defined by the array's internal geometry (Bauer et al, 1999: 376). Initializing, targeting, and maneuvering will all task the autonomous command and control system in different manners such that the control

system must be designed and implemented to switch between the various system models and control schemas.

Cooperative formation control can be achieved in several manners. A typical control design for a small number of satellites (16 or less) in formation is to employ a master/slave control structure. Master/slave scenarios involve a single spacecraft that acts as the leader (master) and issues commands to the other spacecrafts (deputies or slaves). This can be accomplished by actual commands being sent to the other members of the cluster or by the slaves autonomously reacting to the maneuvers of the master in order to maintain the proper configuration (Bauer et al, 1999: 376). This master/deputy control structure works well with a small number of satellites, and can be scaled up slightly by dividing the cluster into a number of subsets. However as the number of satellites increase the overhead becomes unbearable and the system begins to break down, necessitating a distributed control system when the formation is large (Bauer et al, 1999: 376).

A decentralized control system demands that each node in the system process its own measurement data in parallel with all of the other nodes. Detected failures then can be mitigated so that the cluster performance degrades gracefully (Bauer et al, 1999: 376). However none of these navigation and control systems have been tested and verified in a relative environment or for the desired amount of time that formations would stay on orbit.

Inter-Satellite Communication

Along with precise navigation and control requirements, the communication link between the formation flyers is critical to success. The data buses must be extremely robust and reliable. There remains a substantial amount of work to be done in defining requirements for communication bandwidth, time synchronization, and the transfer of precision control commands (Francis et al, 2003).

The importance of this system is akin to the mailman in the postal system. Everything else may go perfectly but nobody receives the mail without the mailman. The formation control laws will all be implemented through the communication system, so a lack of integrity in the system will mean a loss of control that could be catastrophic even if it happens for only a few seconds. This is especially true if the formation is to employ a decentralized command structure that relies heavily on each communication unit functioning flawlessly.

State of the Technology

Formation Design

Sabol et al (2001: 274) also examined the relative stability of two identical satellites initially separated by 1 km, placed into in-plane formations and in-track formations. They looked at two different cases for each formation. The initial case was a 100-revolution-per-seven-nodal-day repeat ground track cycle and the second situation involved a 14 revolution per nodal day repeat ground track cycle. They then propagated

the orbit scenarios using the DSST Averaged Orbit Generator (AOG) which includes the following modeled perturbations: geopotential, atmospheric drag, luni-solar third body point mass effects, and solar radiation pressure (Sabol et al, 2001: 274).

The in-plane formation proved to be extremely stable in the (100:7) case and only showed a diversion of a few meters over a year long timeframe. During the daily repeat ground track (14:1) tesseral resonance had a much greater effect and caused the satellites to drift nearly 0.2 km closer together over a year. Over time (the next year) the satellites should drift back to near their original positions (Sabol et al, 2001: 274).

The in-track formation satellites share the same ground tracks so they encounter the same gravitational effects. However the two satellites are in slightly different orbital planes so the high-density atmosphere simulation causes a slight along-track drift between the two satellites. This drift can be shown to be on the order of about 50m after one year (Sabol et al, 2001: 274).

Both of these simple formation styles offer promising stable designs that should require minimal station keeping propulsion and maintenance. However these studies all examined perfectly identical satellites in the formations, any slight differences in the satellites would produce different results.

The circular formation was also studied, albeit in a slightly different manner (Sabol et al, 2001: 274). Three satellite trajectories were generated for the circular cluster. Satellite one represents the center of the circular formation and the reference satellite. Satellites two and three are on the circle phased at 270 degrees and 180 degrees. This design puts satellite two directly in front of satellite one in the in-track direction and satellite three to the right in the negative normal (cross-track) direction. For their study

Sabol et al (2001: 274) used an orbit of 800 km and began propagating the orbit scenarios using the DSST AOG. They found the propagations in the presences of perturbations showed that the circular formation was unstable at an altitude of 800 km. The primary disrupting factor was found to be the Earth's oblateness or the J2 effect. The J2 effect disturbs the formation in two primary manners: 1) through the differential precession of the orbital planes and 2) through the shifting of the argument of perigee (Sabol et al, 2001: 274-275).

Because satellites one and two have slightly different inclinations the secular J2 effect causes the right ascension of the ascending node for the different orbits to precess at different rates. This results in the orbital planes drifting apart and error growth in the normal (or cross-track) direction. This error growth expands fairly quickly and after four days in the 800 km orbit the separation between satellite one and two could increase by up to 25% (Sabol et al, 2001: 276). For the worst case circular formation, formation maintenance can cost up to 38 m/s per year per kilometer of formation radius (Sabol et al, 2001: 276).

Rotation of the argument of perigee is another major disruption on the circular formation. This effect is independent of formation size, but the budget for maintaining constant argument of perigees is nearly 11 m/s per year (Sabol et al, 2001: 276).

Given the major disrupting force that the J2 effect causes upon circular formations it will be necessary to make formation keeping maneuvers on a near daily basis (Sabol et al, 2001: 276).

Formation Navigation and Control

NASA/GSFC is currently pursuing a decentralized approach that involves using a stand-alone GPS point solution to maintain the spacecraft formation (Carpenter et al, 2003: 3). In this decentralized approach each satellite transmits and receives data to and from each of the other satellites in the formation. This allows relative states to be computed without the need for direct measurement of the inter-satellites states. If enough processor capacity is available the GPS measurement data could be processed for improved accuracy. The addition of instruments that would allow one or more of the vehicles to take relative measurements between itself and the other formation members would provide additional data that could maximize the relative navigation accuracy. This particular approach with the multi-faceted measurements will demand a lot of processing power. In addition an approach similar to this may be necessary to obtain the necessary pico-meter accuracy that will be necessary for a number of the desired satellite cluster missions (Carpenter et al, 2003: 3).

Stanford University has also been developing methods for centralized and decentralized control of a satellite cluster. Their team has demonstrated several estimation architectures that could be used in a differential carrier-phase GPS relative sensing for larger (>16) cluster of satellites (Corazzini et al, 1997). They have used the Formation Flying Testbed at Stanford to demonstrate a multi-level cluster control system that includes a coordinator, a planner, and distributed regulators using a high fidelity orbit simulator. A linear programming approach allows their system to rapidly solve for the optimal formation maneuvers using linearized group dynamics. A portion of their

experimentally analyzed autonomous formation flying algorithms will be demonstrated on Orion (How et al, 1998).

Currently the NASA Goddard Space Flight Center Earth Observing 1 (E0-1) is on orbit and employing a manner of formation flying. The EO-1 formation flying demonstration is controlled from the ground (not cross-linked) using magnetospheric measurements. However it is only important that the satellites be arranged in a particular shape (tetrahedron) at a single point (apogee) in the orbit (Folta et al, 2002). Similarly the Solar Imaging Radio Array (SIRA) mission will require only a loose control of positions and spacing such that all spacecraft are within a spherical region (MacDowell et al 2005). These two missions are both formation flying systems, but their controlling schemes are loose enough that controls need to be applied only once or twice an orbit.

In addition, a number of other agencies are developing formation flying technologies and base lining clusters for use in future missions. The European Space Agency has developed a sophisticated cluster formation to study the Earth's magnetosphere (Roux, 1998). The low-cost technology demonstration Orion-Emerald program developed by a group of universities will demonstrate the use of carrier-phase differential GPS as a primary sensor for formation flying (Kitts et al, 1999)(How et al, 1998).

Air Force Research Laboratory's (AFRL) technology demonstration missions TechSat 21 attempted to tackle some of the extreme system level challenges and technology hurdles that face future formation flying missions. Their efforts uncovered even more technology challenges and eventually led to the program cancellation (Cobb, 2005).

For many of the envisioned formation flying missions continuous six degrees of freedom formation control must be implemented at levels that are orders of magnitude more precise than any spacecraft on orbit today. "This will necessitate propulsion systems with constantly varying levels of thrust, unlike impulsive systems currently in use today," (Leitner, 2004).

Inter-Satellite Communication

Current satellite communication systems are primarily designed for uplink and downlink purposes. Inter-satellite communication offers a different type of challenge that will require increased precision and robustness. A full analysis of the effect of variable distance communication delays between formation flying satellites and how it will affect closed-loop control performance must be completed and evaluated (Leitner, 2004).

Modeling Atmospheric Drag (Vallado, 2001: 524-537)

Satellites orbit around the Earth based upon the laws of two-body motion described by Kepler. During their orbits they experience a number of perturbations that affect the basic equations of two-body motion; four of the largest perturbations are atmospheric drag, third-body effects, Earth oblateness, and solar radiation pressure. The relative importance of these effects varies greatly based upon the height of the satellite's orbit. In low Earth orbit (LEO) up to an altitude of about 500 km, atmospheric drag is the primary perturbation force. The Earth's oblateness also causes a pronounced departure from two body motion and is the second most pronounced perturbation for LEO

satellites. When satellites move into orbits above the LEO range, solar radiation pressure and third-body effects begin to play a dominant effect on the orbital perturbations.

Atmospheric drag is caused by atmospheric particles colliding with the satellite and impeding the satellite's motion. The acceleration due to the drag force changes based upon the density of the particular atmosphere, and it can be expressed as:

$$A_d = -\frac{1}{2}\frac{(C_d A)}{m}\rho v^2 \tag{2.8}$$

The coefficient of drag, C_d, is a dimensionless quantity that expresses the satellite's susceptibility to drag forces. The exposed cross-sectional area, A, is the area of the satellite that is normal to the velocity vector of the satellite. It can be a difficult quantity to estimate accurately unless the configuration and attitude of the satellite is precisely known. The atmospheric density, ρ, comes from one of the numerous atmosphere models that are available, but is difficult to predict because of it's variable nature. All three of these quantities are difficult to accurately measure and predict so the science of determining precise accelerations due to atmospheric drag still suffers from some ambiguity.

To accurately predict the effects of drag on satellites in specific orbits we need to be able to accurately model the atmosphere at the altitude of interest. Unfortunately the Sun's interaction with the upper atmosphere and the Earth's magnetic field cause the properties of the atmosphere to shift and change such that there will always be a level of uncertainty while modeling the Earth's atmosphere.

Despite the known difficulties, scientists and astronomers have developed numerous atmospheric density models over the past twenty years in order to meet the changing accuracy demands of specific projects. Most of these models include some manner of exponential decay as altitude goes up. Those models can be separated into two main groups: static models and time-varying models. Gaposhkin and Coster (1998) discuss many of the atmospheric density models in detail and come to the conclusion that no model is best for all applications. Computing power and accuracy requirements are the primary deciding factors when choosing the best drag model for a particular application. However more computing power does not necessarily mean better accuracy and other factors such as length of simulation and sections of atmosphere pertinent to the given experiment need to be considered when determining which atmospheric model best fits the application.

III. Methodology

Chapter Overview

The objective of this research is to study the effects of drag on anomalous satellites within a cluster and determine how quickly the cluster formation will deteriorate. This research will examine the effects of differential drag for satellites within an in-plane formation, an in-track formation, and a circular formation. In addition to inspecting the effects of drag on these formations, a controller will be employed and tested to determine if a simple control mechanism may be able to alleviate the disturbances created by atmospheric drag on the formations.

The selected approach for this research is to simulate all of the cluster formations with two satellites in the formation. This approach reduces the complexities of dealing with numerous satellites, but allows detailed study of the anomalous satellite and its position relative to a control satellite. One of the satellites in the formation is considered the control satellite and its orbital characteristics will remain constant throughout all of the experiments (unless explicitly stated). The second satellite's (the deputy's) orbital elements will change based upon the specific scenario that is being examined.

Control Satellite

Throughout the different test cases, the control satellite maintains constant initial orbital elements (excluding true anomaly). It is orbiting the Earth in a circular orbit (eccentricity = 0) at an altitude of 250 kilometers in a polar orbit (inclination = $\pi/2$

radians). The control satellite has a right ascension of the ascending node of zero radians and the simulation starts when the control satellite is on the equator (argument of latitude = 0).

Deputy Satellite

The deputy satellite's orbital elements will change for each cluster formation scenario that is run. In addition to the changes in orbital elements that determine the specific formation style, the deputy satellite will also experience anomalies that will cause it to have a different cross sectional area (and thus experience a different acceleration due to drag) than the control satellite.

Atmospheric Drag Modeling

Satellites in low orbits are constantly fighting against the forces of drag, and the lower the orbit altitude the stronger the forces of drag. Because satellites are fighting against the air particles to move forward, atmospheric drag decreases the energy of the satellite's orbit. Therefore, the acceleration due to drag is a negative (opposite of the satellite's velocity vector) acceleration and it can be expressed as:

$$A_d = -\frac{1}{2}\frac{(C_d A)}{m}\rho v^2 \tag{3.1}$$

Where:

- A_d is the acceleration due to drag

- C_d is the coefficient of drag
- A is the cross sectional area perpendicular to velocity vector
- m is the mass of the satellite
- ρ is the density of the atmosphere at position of the satellite
- v is the magnitude of the velocity

The cross sectional area perpendicular to the velocity vector can be estimated if you know the attitude of the satellite in relation to the direction of travel. For this study a cross sectional area of 2 square meters was used for the control satellite. This simulates a small to medium sized satellite with solar arrays deployed. This study also used a cross sectional area of 1.5 meters squared to simulate a satellite experiencing an anomaly such as a partially deployed solar array. At times in this research, a much larger cross sectional area difference will be used to demonstrate the effects of drag in a timelier manner. The coefficient of drag is usually determined experimentally and is based upon the complex dependencies of shape, attitude, flow conditions, and spacecraft drag. This study uses a number of 2.2, which is a typical value for satellites (Larson and Wertz, 1991: 143). This research uses an arbitrary mass of 100 kilograms for each satellite in the simulation. This mass is the upper limit for micro-satellites.

As discussed in the literature review there are numerous different methods for modeling the atmosphere and computing atmospheric density. For this study a relatively simple, but accurate, exponential atmospheric model will be used (Vallado, 2001:534-535). This simple model assumes the density of the atmosphere decays exponentially

with increasing altitude. It also assumes a spherically symmetrical distribution of particles, in which the density, ρ, varies exponentially according to Vallado (2001: 535):

$$\rho = \rho_0 EXP[-\frac{h_{ellp} - h_0}{H}] \tag{3.2}$$

Where:

- ρ_0 is the reference density
- h_0 is the reference altitude
- h_{ellp} is the actual altitude above the Earth
- H is the scale height

By using the following table to determine values for specific bands of the atmosphere, the exponential atmospheric model can become quite accurate in predicting the nominal density at a given altitude.

Altitude h_{ellp} (km)	Base Altitude h_o (km)	Nominal Density ρ_o (kg/m^3)	Scale Height H (km)	Altitude h_{ellp} (km)	Base Altitude h_o (km)	Nominal Density ρ_o (kg/m^3)	Scale Height H (km)
0–25	0	1.225	7.249	150–180	150	2.070×10^{-9}	22.523
25–30	25	3.899×10^{-2}	6.349	180–200	180	5.464×10^{-10}	29.740
30–40	30	1.774×10^{-2}	6.682	200–250	200	2.789×10^{-10}	37.105
40–50	40	3.972×10^{-3}	7.554	250–300	250	7.248×10^{-11}	45.546
50–60	50	1.057×10^{-3}	8.382	300–350	300	2.418×10^{-11}	53.628
60–70	60	3.206×10^{-4}	7.714	350–400	350	9.518×10^{-12}	53.298
70–80	70	8.770×10^{-5}	6.549	400–450	400	3.725×10^{-12}	58.515
80–90	80	1.905×10^{-5}	5.799	450–500	450	1.585×10^{-12}	60.828
90–100	90	3.396×10^{-6}	5.382	500–600	500	6.967×10^{-13}	63.822
100–110	100	5.297×10^{-7}	5.877	600–700	600	1.454×10^{-13}	71.835
110–120	110	9.661×10^{-8}	7.263	700–800	700	3.614×10^{-14}	88.667
120–130	120	2.438×10^{-8}	9.473	800–900	800	1.170×10^{-14}	124.64
130–140	130	8.484×10^{-9}	12.636	900–1000	900	5.245×10^{-15}	181.05
140–150	140	3.845×10^{-9}	16.149	1000–	1000	3.019×10^{-15}	268.00

Figure 3. Exponential atmosphere modeling table (Vallado, 2001: 537)

This atmospheric density modeling approach works sufficiently well for design level studies such as the one being conducted; however, highly accurate studies might choose to use more sophisticated and accurate models. The atmospheric density derived from the above equations and tables will then be incorporated into equation 3.1 and assimilated into the orbit propagator.

Orbit propagation

This study uses an orbit propagator based solely on two body motion and the effects of drag. Third body and non-spherical Earth perturbations (J2 effect) were not taken into account because the focus of this work is to understand how differential drag will affect satellite formations. The primary effects these perturbations have upon orbits

are shifting the longitude of the ascending node and moving the argument of perigee (Wiesel 1997: 88). While important, it will not significantly effect the relative position of satellites in an in-plane or an in-track cluster (Sabol et al, 2001: 274-275). The J2 effect changes the ascending node (Ω) by causing it to precess at the rate (Wiesel, 2001: 88)

$$\dot{\Omega} = -\frac{3nJ_2R_E^{\ 2}}{2a^2(1-e^2)^2}\cos i \tag{3.3}$$

where:

- n is the mean anomaly
- J_2 is a dimensionless number that characterizes the departure of a body from a true sphere, for the Earth J_2=0.001082
- R_E is the radius of the Earth
- a is the satellite's semi-major axis
- e is the eccentricity of the orbit
- i is the inclination of the orbit

In addition the J2 effect causes elliptical orbits to rotate in their own plane at a rate of (Wiesel, 2001: 88):

$$\dot{\omega} = -\frac{3nJ_2R_E^{\ 2}}{2a^2(1-e^2)^2}(\frac{5}{2}\sin^2 i - 2) \tag{3.4}$$

As previously discussed in the literature review and to be discussed further later in this chapter both the in-plane and in-track formations offer formations where all of the orbits of the satellites in the cluster have the same inclination, semi-major axis, and eccentricity. This will cause $\dot{\Omega}$ and $\dot{\omega}$ to remain equal for the satellites clustered in and in-plane and in-track formations.

However the J2 effect does play a significant role in the stability of satellites in a circular cluster (Sabol et al, 2001: 274). Equations 3.3 and 3.4 show that satellite orbits with different inclinations and eccentricities will experience different $\dot{\Omega}$ and $\dot{\omega}$. As discussed in the literature review the J2 effect is the primary reason that the circular formation is unstable and a two satellite circular formation may require up to 50 m/s per year per kilometer of separation and daily orbital corrections to maintain a stable formation (Sabol et al, 2001: 276). This particular study is done under the context that a controller of some type is already in place that mitigates the effect of the non-spherical Earth (and other less disruptive perturbations) on the circular formation. Without the controller that accomplishes this task the circular formation is unstable from the very beginning and cannot be considered a feasible long term formation. Thus it would not be important how differential drag would effect the formation. In addition, solar radiation perturbations were not considered because of the low relative magnitude of the perturbation in comparison with atmospheric drag (Vallado, 2001: 646). The differential equations expressed in the Earth centered inertial (ECI) frame used in the propagator are as follows:

$$\ddot{x} = -(\mu / r^3)x - \frac{1}{2}\frac{(C_d A)}{m}\rho v^2 \dot{x} / v \tag{3.5}$$

$$\ddot{y} = -(\mu / r^3) y - \frac{1}{2} \frac{(C_d A)}{m} \rho v^2 \dot{y} / v \tag{3.6}$$

$$\ddot{z} = -(\mu / r^3) z - \frac{1}{2} \frac{(C_d A)}{m} \rho v^2 \dot{z} / v \tag{3.7}$$

For the initial cases that examine the effects of drag on the formation, the orbits of the control satellite and the deputy satellite are propagated independently and then compared at specific time intervals (every 10 seconds) to determine the difference in the orbits.

Initial Conditions Conversion

The MATLAB program written for this research accepts the classical orbital elements as input parameters. However in order to propagate the orbits of the satellites we need to convert from the initial classical orbital elements to an ECI frame. This is done by first converting the traditional orbital elements into the perifocal coordinate system and then completing a coordinate transformation that transforms them into the ECI frame.

Convert from Orbital Elements to ECI Frame

For the chosen equations of motion the coordinates of the satellites must be expressed in x, y, and z components in the ECI frame. The MATLAB program written for this research accepts the traditional six orbital elements; inclination (i), right ascension of the ascending node (Ω), eccentricity (e), argument of perigee (ω), semi-major axis (a), and either mean anomaly or true anomaly (υ) and converts these elements

to position and velocity vectors in the perifocal coordinate system. The perifocal position and velocity vectors are obtained by the following equations (Wiesel, 1997: 65)

$$r_{perifocal} = \begin{bmatrix} p\cos\upsilon/(1+e\cos\upsilon) \\ p\sin\upsilon/(1+e\cos\upsilon) \\ 0 \end{bmatrix} \tag{3.8}$$

$$v_{perifocal} = \begin{bmatrix} -\sqrt{\mu/p}\sin\upsilon \\ \sqrt{\mu/p}(e)+\cos\upsilon \\ 0 \end{bmatrix} \tag{3.9}$$

where:

- p is the orbit semi-parameter, = $a(1-e^2)$
- μ is the gravitational parameter of the Earth

Then, those perifocal position and velocity vectors go through a coordinate transformation that transforms them from perifocal coordinates to ECI coordinates. That coordinate transformation can be expressed as:

$$r_{eci} = R_\Omega R_i R_\omega r_{perifocal} \tag{3.10}$$

$$v_{eci} = R_\Omega R_i R_\omega v_{perifocal} \tag{3.11}$$

Where the rotation matrices are as follows:

$$R_{\omega} = \begin{bmatrix} \cos(-\omega) & \sin(-\omega) & 0 \\ -\sin(-\omega) & \cos(-\omega) & 0 \\ 0 & 0 & 1 \end{bmatrix} \tag{3.12}$$

$$R_{i} = \begin{bmatrix} 1 & 0 & 0 \\ 0 & \cos(-i) & \sin(-i) \\ 0 & -\sin(-i) & \cos(-i) \end{bmatrix} \tag{3.13}$$

$$R_{\Omega} = \begin{bmatrix} \cos(-\Omega) & \sin(-\Omega) & 0 \\ -\sin(-\Omega) & \cos(\Omega) & 0 \\ 0 & 0 & 1 \end{bmatrix} \tag{3.14}$$

ECI to RTN

Traditionally two satellite motion has been expressed in the Radial, Tangential, Normal (RTN) frame with one (the control satellite in this case) of the satellites representing the origin of the coordinate system. In order to transform coordinates expressed in the ECI frame to coordinates in the RTN frame, the argument of perigee, the right ascension of the ascending node, the true anomaly, and the inclination of the orbit must be known. The only one of these elements that varies over the course of the orbit is the true anomaly and it can be calculated by

$$\upsilon = (rem(T / P))2\pi \tag{3.15}$$

where:

- υ is the true anomaly

- T is the time passed since beginning of simulation
- P is the orbital period

This process will determine the true anomaly of the given satellite at the desired instant in time. Therefore the position and velocity vectors in the ECI frame can be converted to the RTN frame by the following transformations

$$r_{RTN} = R_{\omega} R_i R_{\Omega} R_{\upsilon} r_{eci} \tag{3.16}$$

$$v_{RTN} = R_{\omega} R_i R_{\Omega} R_{\upsilon} v_{eci} \tag{3.17}$$

where the rotation matrices are as follows:

$$R_{\omega} = \begin{bmatrix} \cos(\omega) & \sin(\omega) & 0 \\ -\sin(\omega) & \cos(\omega) & 0 \\ 0 & 0 & 1 \end{bmatrix} \tag{3.18}$$

$$R_i = \begin{bmatrix} 1 & 0 & 0 \\ 0 & \cos(i) & \sin(i) \\ 0 & -\sin(i) & \cos(i) \end{bmatrix} \tag{3.19}$$

$$R_{\Omega} = \begin{bmatrix} \cos(\Omega) & \sin(\Omega) & 0 \\ -\sin(\Omega) & \cos(\Omega) & 0 \\ 0 & 0 & 1 \end{bmatrix} \tag{3.20}$$

$$R_{\upsilon} = \begin{bmatrix} \cos(\upsilon) & \sin(\upsilon) & 0 \\ -\sin(\upsilon) & \cos(\upsilon) & 0 \\ 0 & 0 & 1 \end{bmatrix} \tag{3.21}$$

In-Plane Formation

For the in-plane formation the deputy satellite has all of the same initial conditions as the control satellite except that it is a pre-determined distance (1 km for this study) behind the control satellite in the same orbital plane. So the following constraints, expressed in RTN frame coordinates, must be met for the satellites to meet the in-plane formation criteria:

$$x(t) = 0 \tag{3.22}$$

$$y(t) = y_0 \tag{3.23}$$

$$z(t) = 0 \tag{3.24}$$

The argument of latitude separation can be determined by inputting the desired separation distance between the master and deputy satellites into the following equation

$$u_d = s/r \tag{3.25}$$

where:

- u_d is the argument of latitude of the deputy satellite
- s is the separation distance between the deputy and control

- r is the orbital radius

In-Track Formation

For the in-track experiments the deputy satellite not only has a different argument of latitude, but it also has a different right ascension of the ascending node such that its ground track matches that of the control satellite's. Hill's equations for this formation are very similar to the in-plane formation except that a cross-track oscillation represents the difference in right ascension of the ascending node. Hill's equations for this type of formation can be expressed in the RTN frame as:

$$x(t) = 0 \tag{3.26}$$

$$y(t) = y_0 \tag{3.27}$$

$$z(t) = -(\omega_e / n) y_0 \sin i \cos nt \tag{3.28}$$

To calculate the correct right ascension of the ascending node to keep the deputy satellite following the control satellite's ground track the following equation was used

$$\Omega_d = ((2\pi - u_d)/(2\pi))T\omega_E \tag{3.29}$$

where:

- Ω_d is the right ascension of the ascending node for the deputy
- u_d is the argument of latitude of the deputy satellite
- T is period of the orbit

- ω_E is the rotational rate of the Earth

Circular Formation

As previously discussed the circular formation is designed such that the satellites will maintain a constant distance from each other. By examining Hill's equations the relation between the initial conditions must meet the following constraint equation where *r* is the radius of the formation from the reference point at the control satellite:

$$x^2 + y^2 + z^2 = r^2 \tag{3.30}$$

The geometric approach takes advantage of the fact that the relative motion in the radial/tangential planes (x/y) is fixed in eccentricity. By substituting the constraints into Hill's equations the following relations are found.

$$\dot{y}_0 = -2nx_0 \tag{3.31}$$

$$y_0 = 2\dot{x}_0 / n \tag{3.32}$$

$$z_0 = \pm\sqrt{3}x_0 \tag{3.33}$$

$$\dot{z}_0 = \pm\sqrt{3}\dot{x}_0 \tag{3.34}$$

The first two equations set the along track (tangential) drift and offset to zero. The second two equations must be of the same sign for any particular case. These constraints demonstrate that there are two planes in which a circular formation is possible.

Initial Conditions (Circular Orbit)

For the test scenario the design will mimic the design presented by Sabol, et al (2001: 272) in their paper and recounted earlier in the literature review. The reference orbit is circular and inclined at 90 degrees with the satellite at the equator (ascending node). The deputy satellite is also at the equator, but at its ascending node and in a slightly elliptical orbit. The two satellites are also offset by a small amount of right ascension of the ascending node. Given this type of formation where both satellites have the same inclination, it also helps to diminish the disruptive effects of the Earth's oblateness.

In order to ensure that both satellites in the circular formation have the same period (and thus will not quickly drift apart) it is essential to the formation stability that all satellites in the formation have the same orbital energy. Therefore to set the initial conditions of the control satellite and the deputy satellite use the energy equation

$$E = \frac{1}{2}v^2 - \frac{\mu}{r} \tag{3.35}$$

and set the energy of the control satellite equal to the energy of the deputy satellite. For the initial conditions in our test scenario, the difference in position is due to differences in the radial and normal direction and the difference in velocity is solely due to a delta in the tangential direction. Setting the energy (and consequently the period) of the two orbits to

equal values ensures that the satellites will remain in the same vicinity and that tiny differences in the orbital energy will not interfere with the simulation.

Controller (Ogata, 1970: 156-157)

An automated controller compares the actual value of the system to the desired value, determines the difference, and produces a modifying control that will minimize or eliminate the difference. In this experiment a proportional and integral controller will be used help keep the clustered satellites in formation. For a controller with a proportional control action the relationship between the output of the controller m(t) and the actuating error signal e(t) is:

$$m(t) = K_p e(t) \tag{3.36}$$

where K_p is termed the proportional sensitivity or the gain. This type of system can be used in many different environments, but whatever the actual mechanism and operating power, the proportional controller is basically an amplifier with an adjustable gain.

In addition to the proportional control action, an integral control action is also employed such that the control of the satellite will become more stable. In a controller with integral control action, the rate of change of the controller output m(t) is proportional to the actuating error signal e(t):

$$\frac{dm(t)}{dt} = K_i e(t) \tag{3.37}$$

For the simulations done in this experiment the following values were chosen to obtain fairly well controlled results:

$$K_p = 150000 \tag{3.38}$$

$$K_i = 20000 \tag{3.39}$$

This controller is then used to continuously alter the cross sectional area of the deputy satellite so that it remains consistent with the cross sectional area of the control satellite. This controlling action should mitigate the differential drag that was originally present and allow the satellites to remain relatively close.

This type of control (proportional-integral) is typically used for linear systems. In this case, it has been applied to a non-linear system and thus stability cannot be assumed. During the scenarios tested for this thesis the controller performed well despite operating outside of its intended environment. If this technique is pursued in the future, it may be necessary and prudent to perform a more rigorous analysis.

IV. RESULTS

Chapter Overview

This section is broken down into two primary parts. The first part deals with how drag affects satellites in each of the three discussed formations (in-plane, in-track, and circular). Plots and analysis will be included that illustrate how the formation is reacting over a period of time. Generally the analysis and plots will be over a ten hour period; however certain configurations will require longer observation periods in order to see the disturbing effects. The second part of this chapter will focus on using a controller to alleviate the drift that the differential drag is causing between the satellites in the cluster.

Un-Controlled Formations

In-Plane Formation

The first formation examined in this research is the in-plane formation. As expected, when there is a differential drag force present between the two satellites in an in-plane formation they begin to move apart and will continue to move further and further apart along an ever-increasing curve. The following graphs show the separation between the two satellites in the radial, tangential and normal directions as well as the total separation.

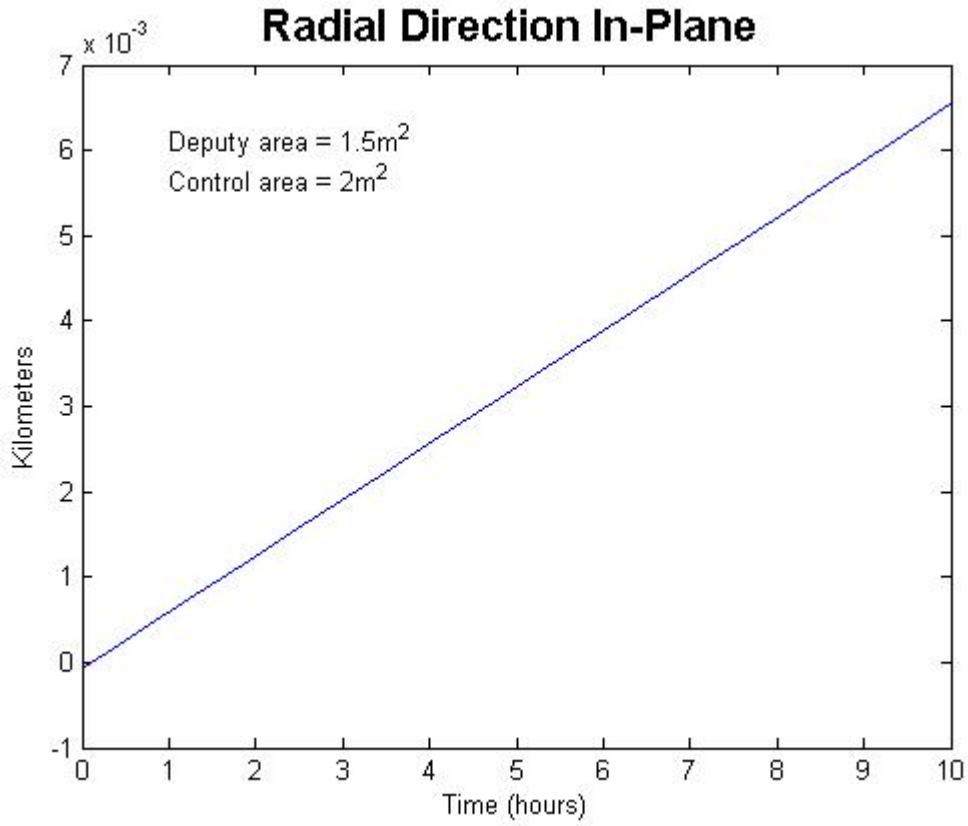

Figure 4. In-plane radial separation

The radial direction separation in the in-plane formation begins to slowly grow as the differential drag between the control and deputy satellites causes the control satellite to speed up and enter a slightly lower orbit. Figure 4 shows that after ten hours the radial separation is 6.5 meters and growing at a steady rate. This separation is in the radial direction and means that the control satellite now has a slightly smaller semi-major axis and thus a different period. The separation in this direction will continue to grow linearly unless some type of contrary force can be applied or the differential drag can be equalized.

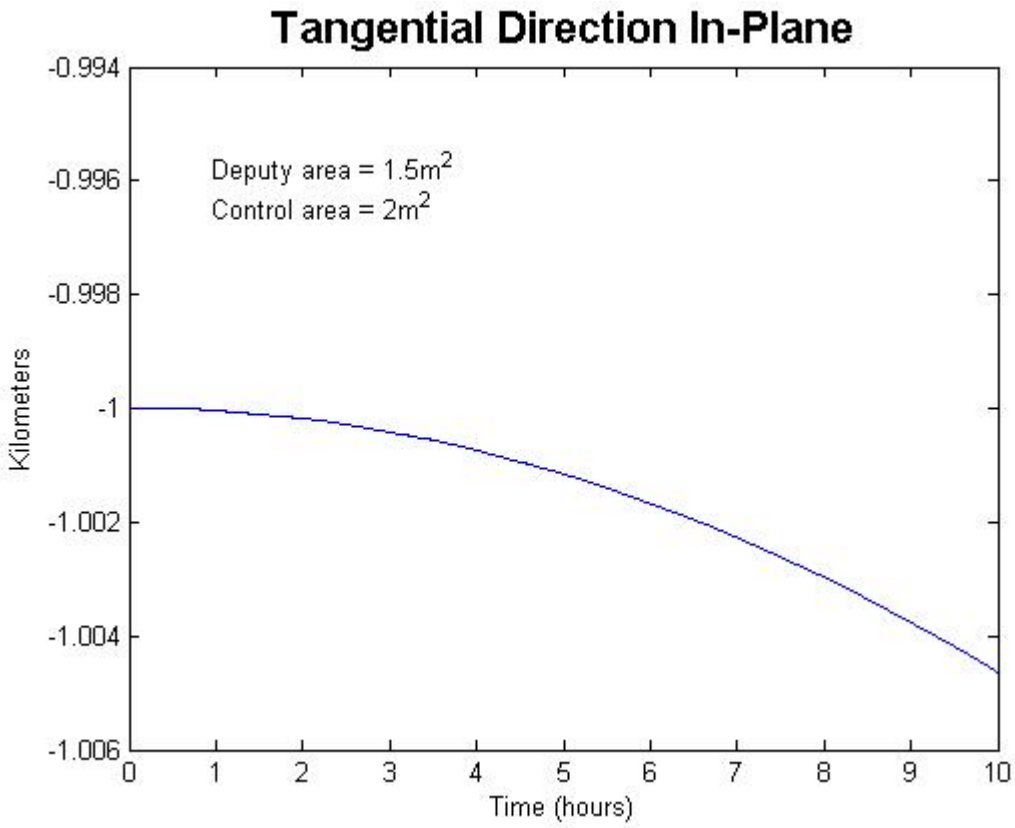

Figure 5. In-plane tangential separation

Originally the two satellites are one kilometer apart in the tangential direction in the in-plane formation. However because the satellite in the formation lead (the control satellite) has a slightly larger cross sectional area due to an anomaly on the deputy satellite it will experience a larger (negative) acceleration due to drag. This will cause the control satellite's semi-major axis to decrease and force it to speed up. As the control satellite continues to accelerate away from the deputy the tangential separation will continue growing at an ever-increasing rate.

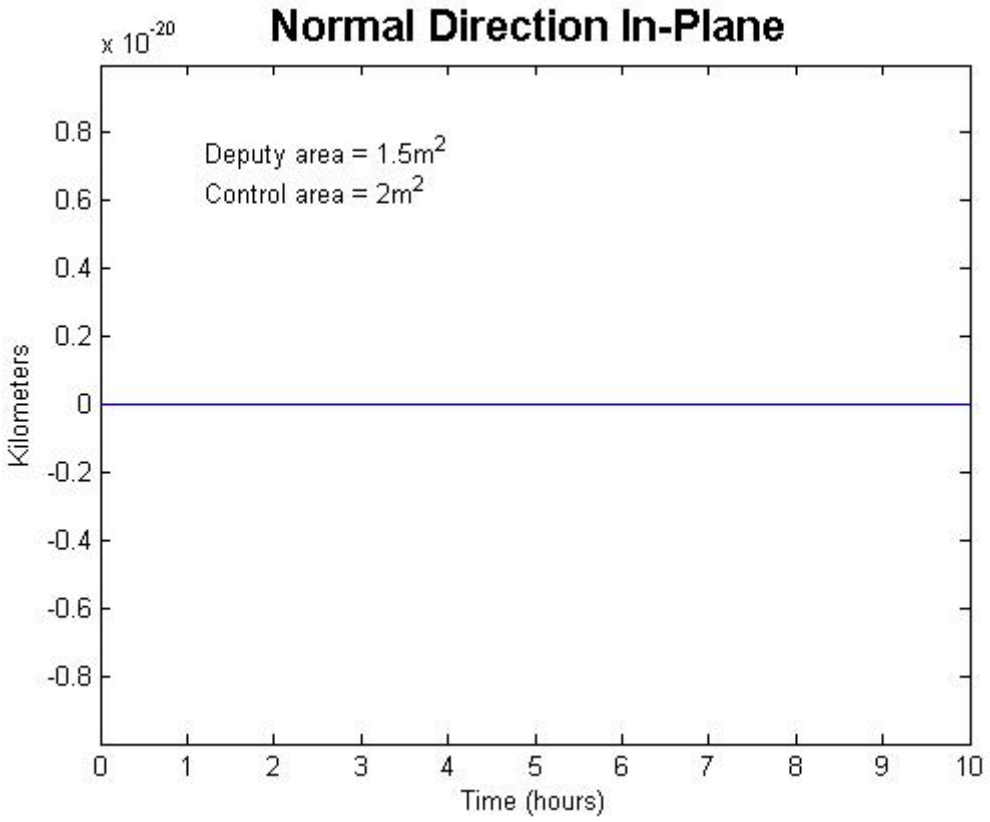

Figure 6. In-plane normal separation

The in-plane formation calls for two satellites to be in the same plane and separated by mean anomaly. Their separation in the normal direction should remain at zero since drag acts solely in the orbital plane and no other perturbing forces were considered. Figure 6 demonstrates that the satellites do maintain their separation of zero in the normal direction.

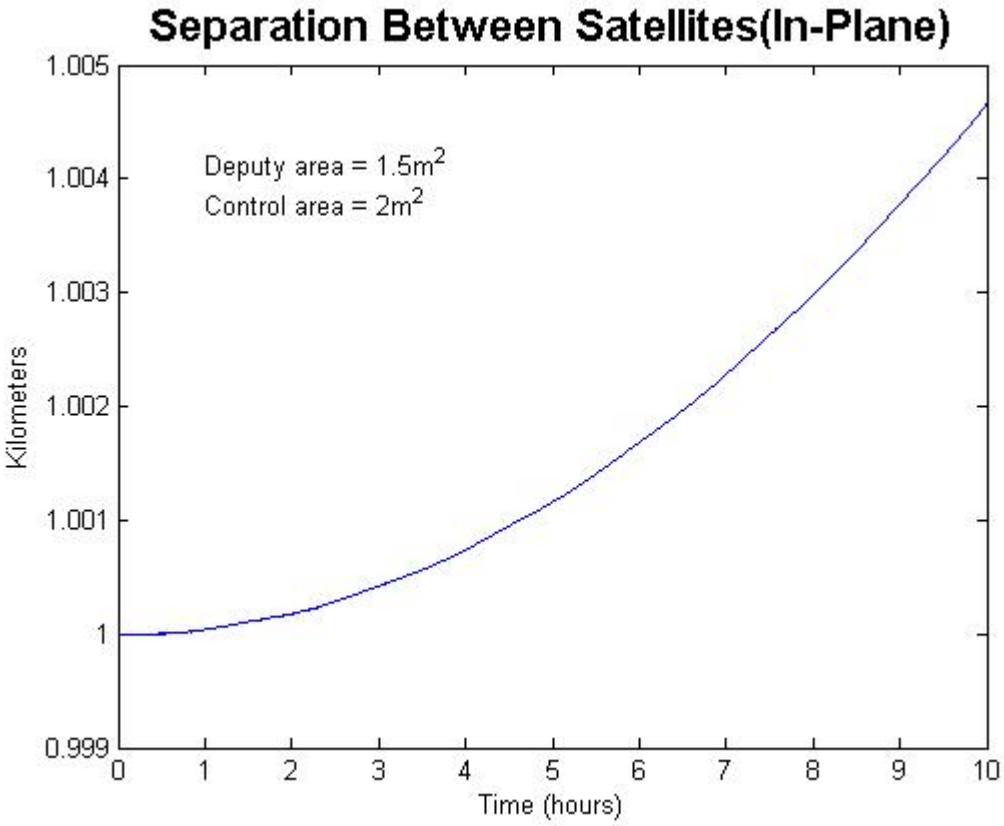

Figure 7. Total separation between satellites (in-plane)

Because the two satellites occupy the same orbital plane, their separation distance will be solely in the radial and tangential directions (as shown in Figure 4, Figure 5, and, Figure 6). In addition, as drag begins to affect the control satellite more than the deputy satellite, the control satellite will begin to speed up, decrease orbital altitude, and move away from the deputy satellite at a faster and faster rate.

In-Track Formation

The in-track formation radial direction separation begins to slowly grow as the drag on the control satellite slowly pulls it closer to Earth. Figure 8 shows that after ten hours the radial separation is 6.5 meters. This separation is in the radial direction and means that the control satellite now has a slightly smaller semi-major axis and thus a different period. The separation in this direction will continue to grow linearly unless some type of contrary force can be applied or the differential drag can be equalized.

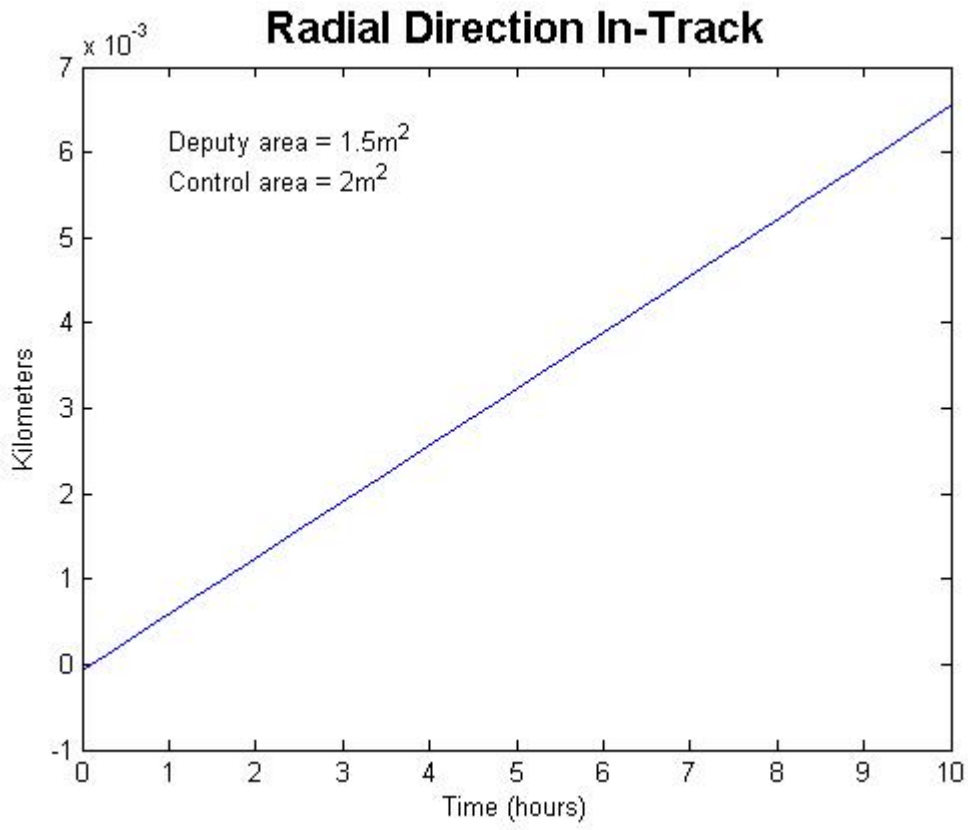

Figure 8. In-track radial separation

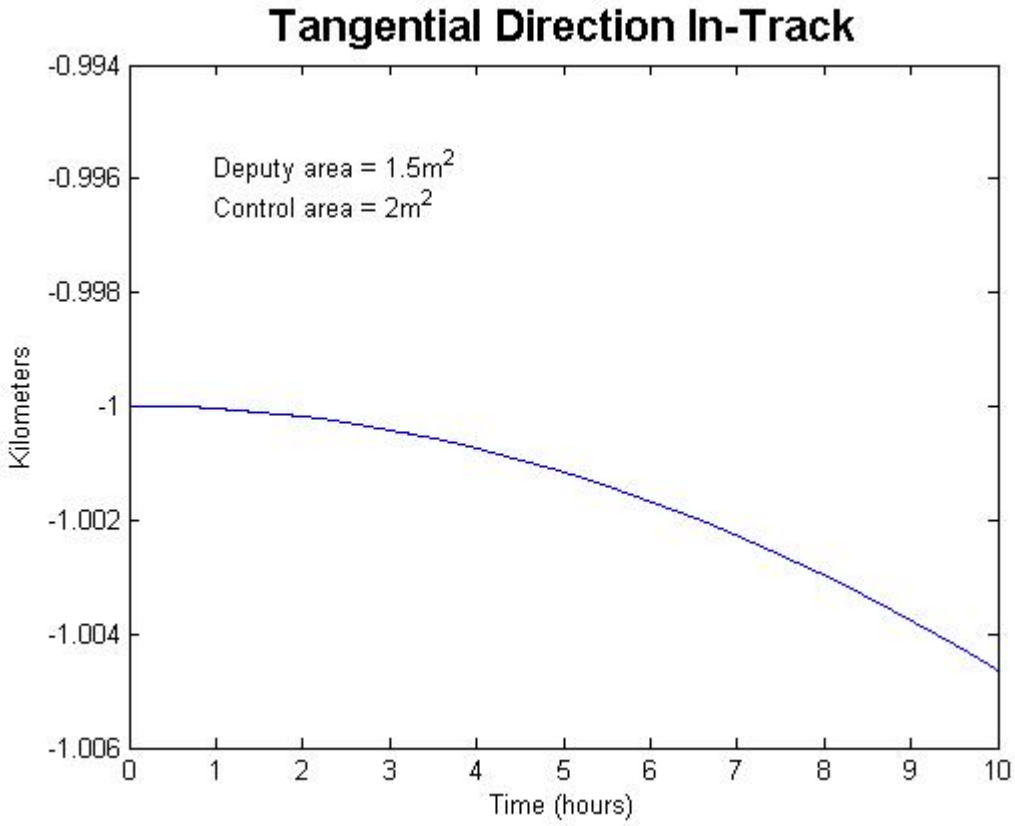

Figure 9. In-track tangential separation

While the radial separation is slowly growing, the tangential separation is also growing at a similar pace for the first ten hours. However because the tangential separation is growing along a quadratic curve it will soon become the dominant direction of separation. As the periods of the two satellites diverge, the satellite with a larger cross sectional area (control satellite in this case) will begin to speed up and pull farther and farther away from the deputy satellite. The control satellite will continue to accelerate away from the deputy satellite and the tangential separation will continue to increase at an ever-increasing rate.

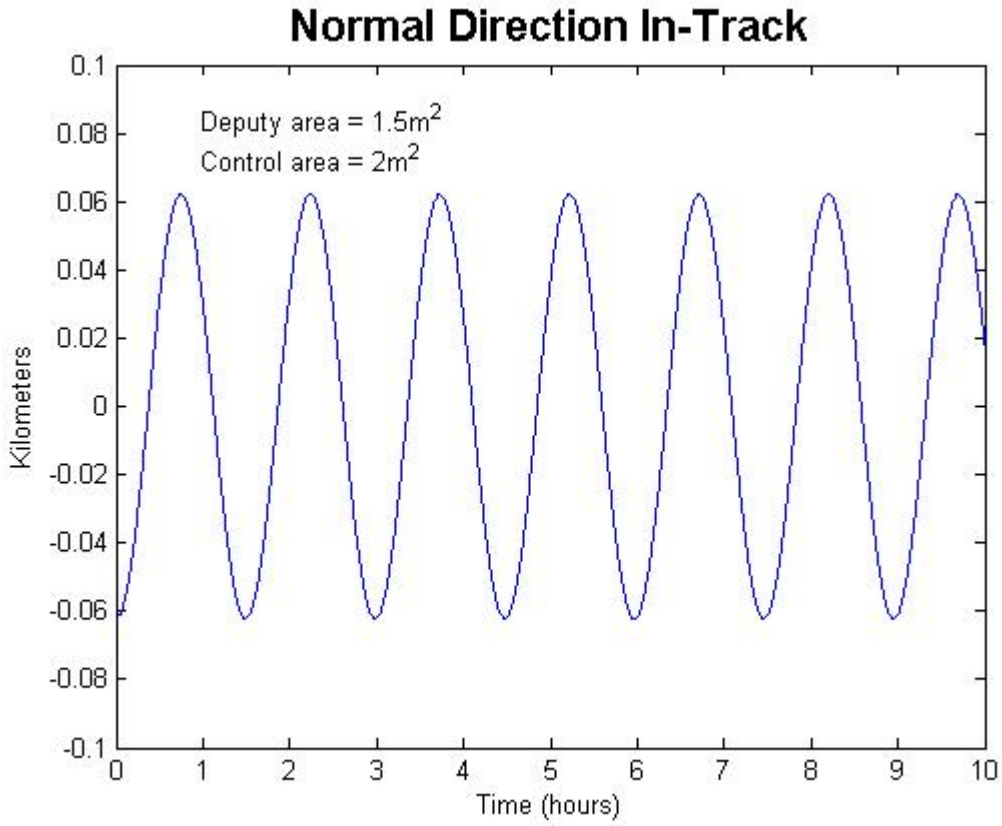

Figure 10. In-track normal separation

Because the two satellites have slightly different ascending nodes, their separation in the normal direction is periodic, with a period equal to that of the orbits. This is illustrated in Figure 10. The magnitude of the separation will vary depending on the altitude of the orbits. Higher satellite orbits will increase the magnitude of the separation (assuming their initial separations are equal in each case).

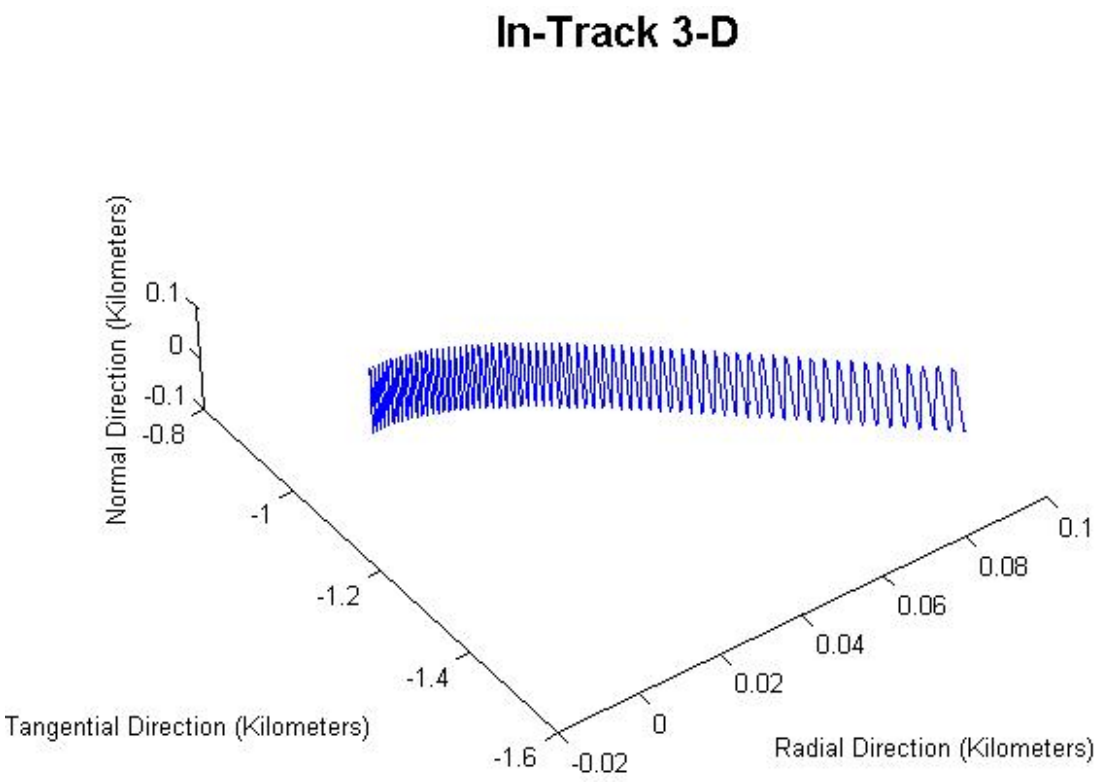

Figure 11. In-track 3-D (100 hours)

Figure 11 demonstrates how the in-track formation changes over 100 hours. As expected, the tangential separation becomes the dominant direction of separation.

Circular Formation

For the circular formation the orbits were also initially propagated for 10 hours. However, some of the motion was not easily discernable over the ten hour period so additional plots are included with different parameters to show the motion of the satellites in the circular formation.

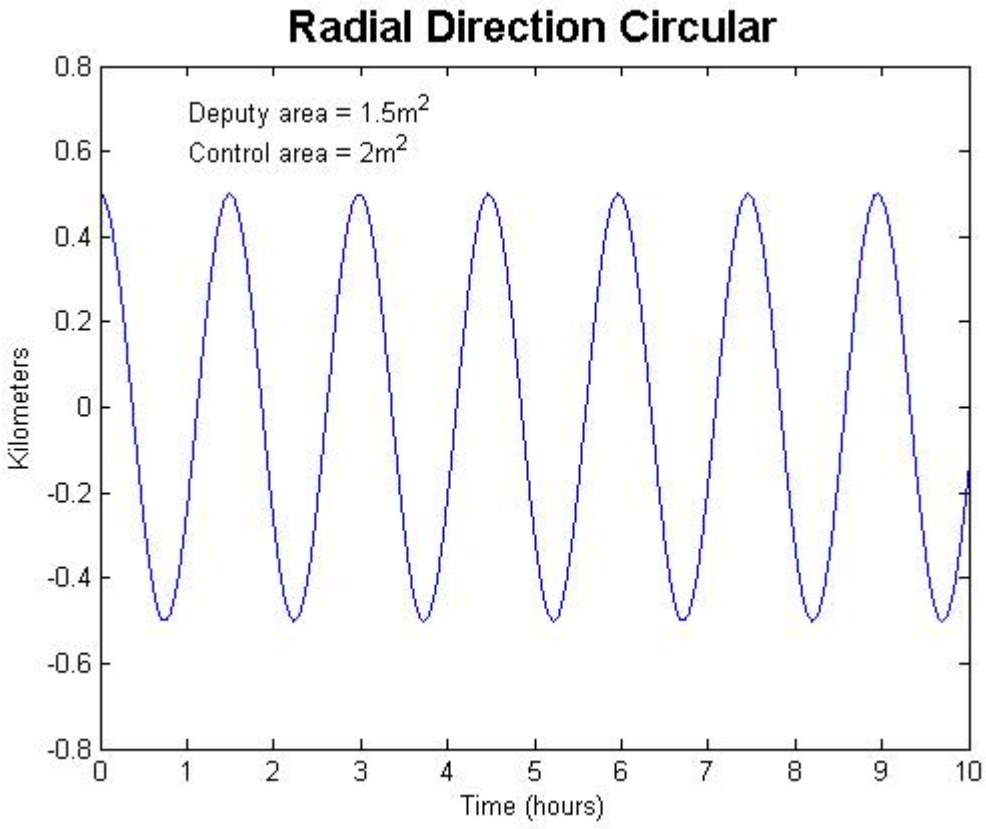

Figure 12. Circular radial separation

As previously described, in the circular formation both the deputy and control satellite have the same period but the deputy satellite has a slightly eccentric orbit that causes it to oscillate around the control satellite in regards to the radial direction. The chosen radial separation at the beginning of the simulation was 0.5 km. Because the deputy satellite was at apogee, that separation distance should also be the maximum separation.

Given the scale of Figure 12, and the small difference in cross sectional areas between the control and deputy, it is difficult to discern any change in maximum separation between the two satellites. To better illustrate how the formation will change over time the cross sectional area difference is exaggerated in the case shown in Figure 13 to illustrate how the formation will change over time as the differential drag affects the formation.

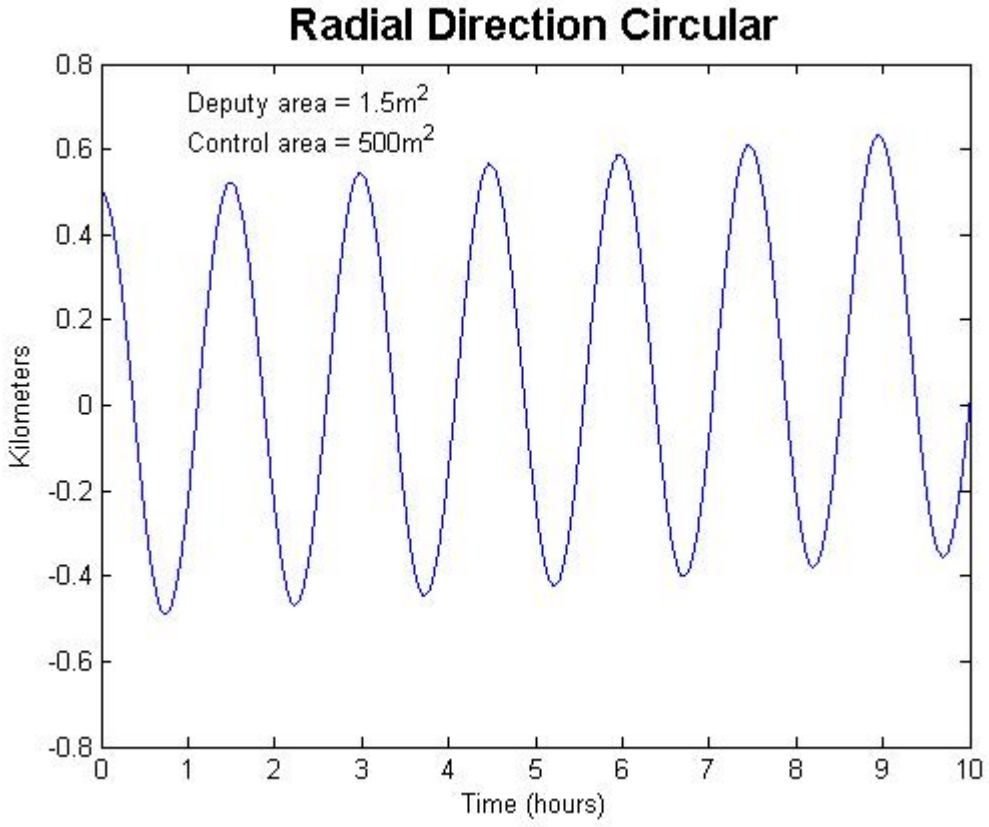

Figure 13. Circular radial separation (exaggerated)

The control satellite's altitude drops faster than the deputy's altitude because of the greater deceleration due to drag that it experiences. As the semi-major axes change the radial separation between the two satellites will increase.

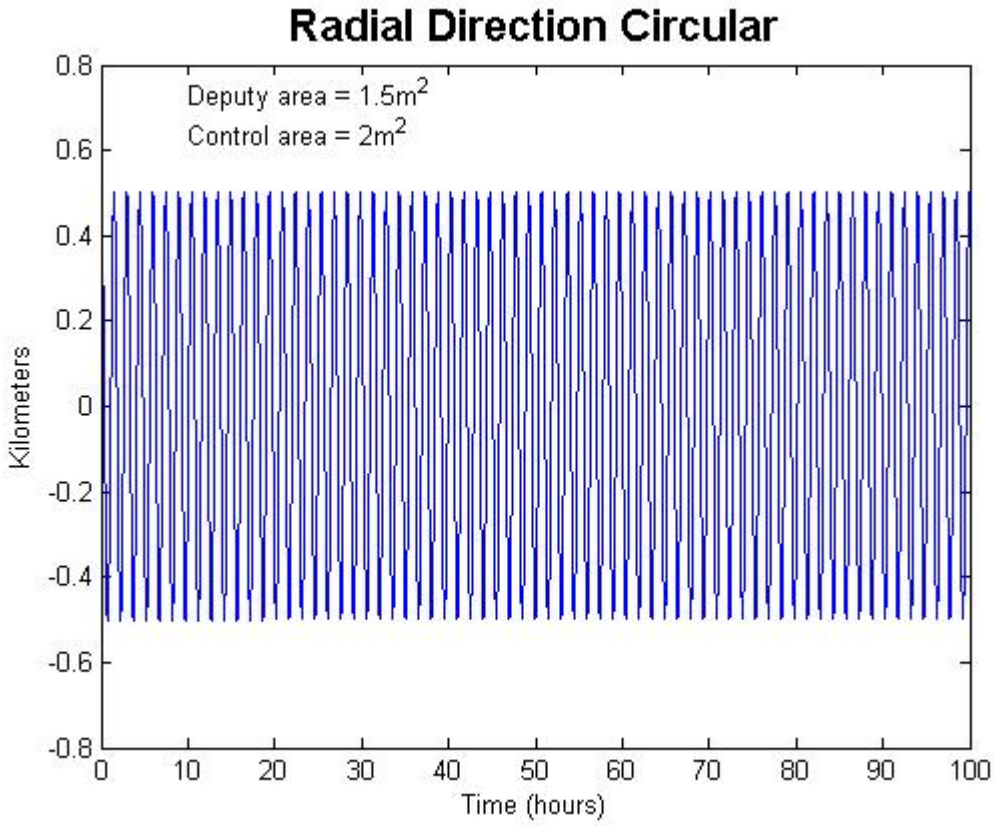

Figure 14. Circular radial separation (100 hours)

It is not obvious from Figure 14 that the radial separation is changing over the 100 hour time period because of the large scale that must be used to show the radial separation distance oscillating. However in Figure 15 the top edge of the plot is amplified so that it becomes apparent that the separation distance in the radial direction is increasing.

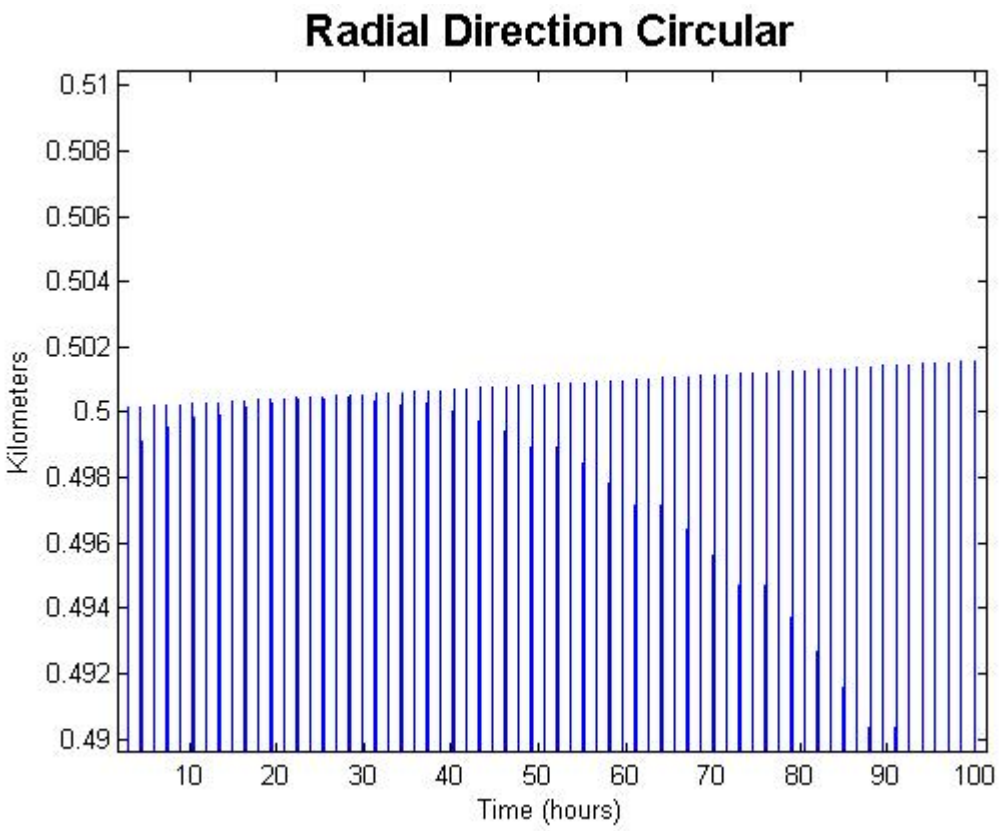

Figure 15. Circular radial separation zoomed (100 hours)

The radial separation is not growing quickly, but it is growing. Over the 100 hour propagation time the radial separation grew by slightly less than two meters. This change is expected because of the differential drag forces that the two satellites are experiencing.

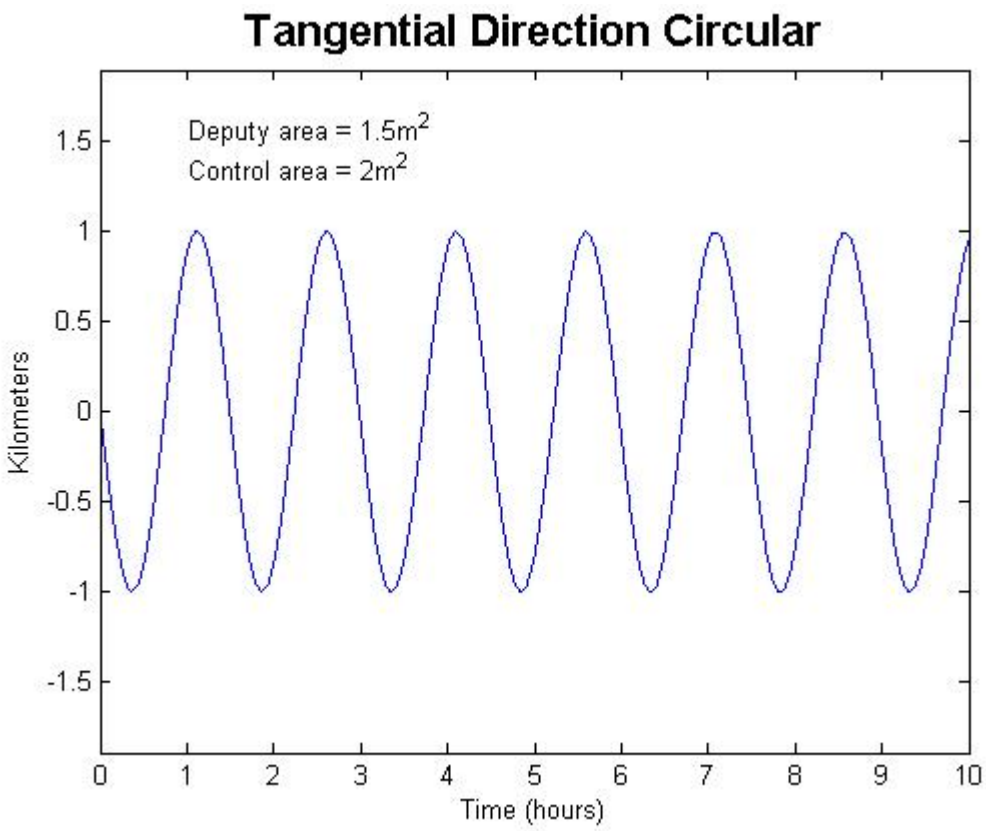

Figure 16. Circular tangential separation

At the start of the simulation both the control and deputy satellite have the same semi-major axis. The control satellite is in a circular orbit and the deputy is in slightly elliptical orbit so their tangential separation will oscillate depending on where the two satellites are located in their respected orbits. Their maximum separation will occur when the deputy satellite is either at apogee or perigee.

Given the scale of Figure 16, and the small difference in cross sectional areas between the control and deputy, it is difficult to discern any change in maximum tangential separation between the two satellites. To better illustrate the changes to the formation over time a graph with exaggerated parameters is shown in Figure 17.

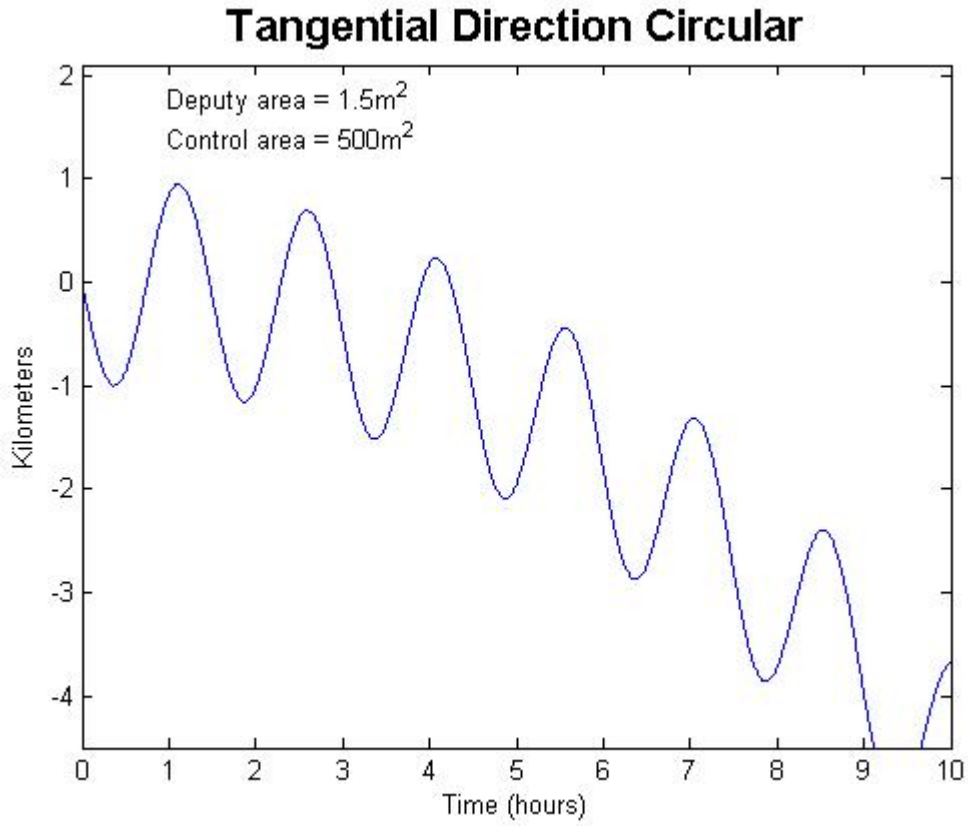

Figure 17. Circular tangential separation (exaggerated)

The tangential separation in the circular formation begins to grow in a similar manner to the tangential separation in the in-plane and in-track formations. However because of the elliptical nature of the deputy's orbit there is an oscillation in the separation distance. The control satellite continues to drop in altitude due to the drag deceleration and as it drops it accelerates away from the deputy satellite. Therefore the faster the control satellite goes, the farther back the deputy will fall and the tangential separation will continue to grow along a quadratic curve unless the differential drag can be corrected.

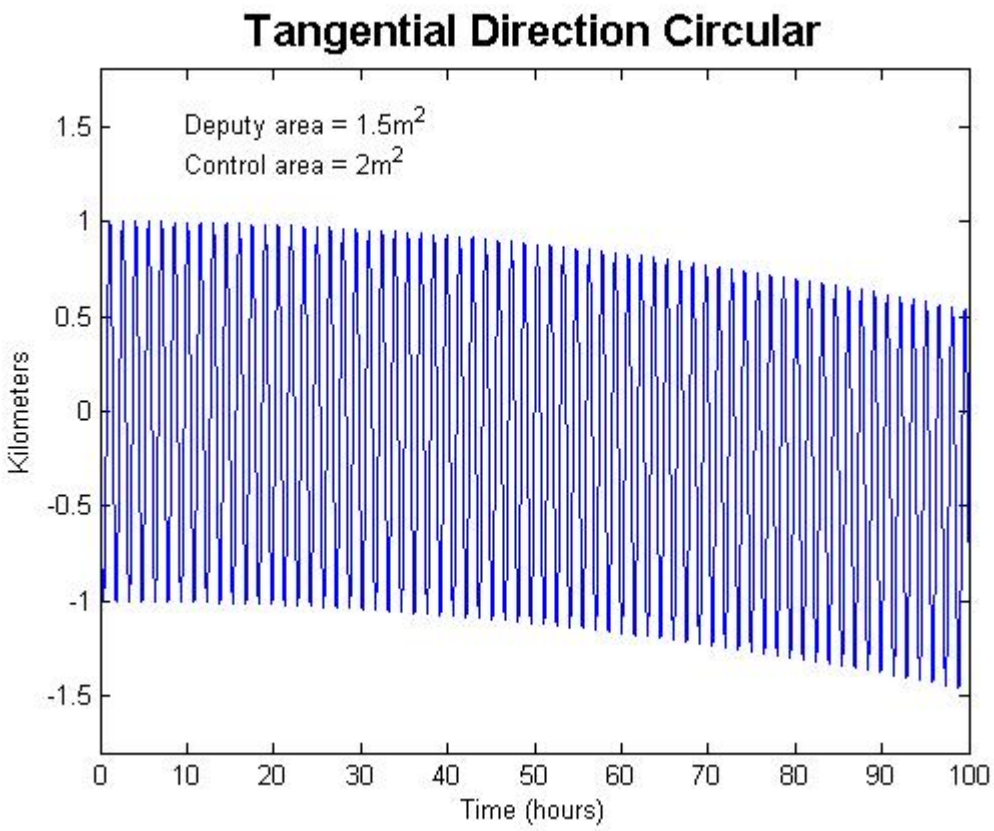

Figure 18. Circular tangential separation (100 hours)

Even with the initial cross sectional areas (control = 2 meters squared and deputy = 1.5 meters squared) a major change in the tangential separation is evident if the orbits are propagated out over 100 hours. The distance continues to oscillate around a mean value, but as more time passes the mean value of the oscillation slowly drifts away from zero. After 100 hours the center of the oscillation has drifted nearly 500 meters away from the starting position. The tangential separation quickly becomes the dominant direction of separation in the circular formation.

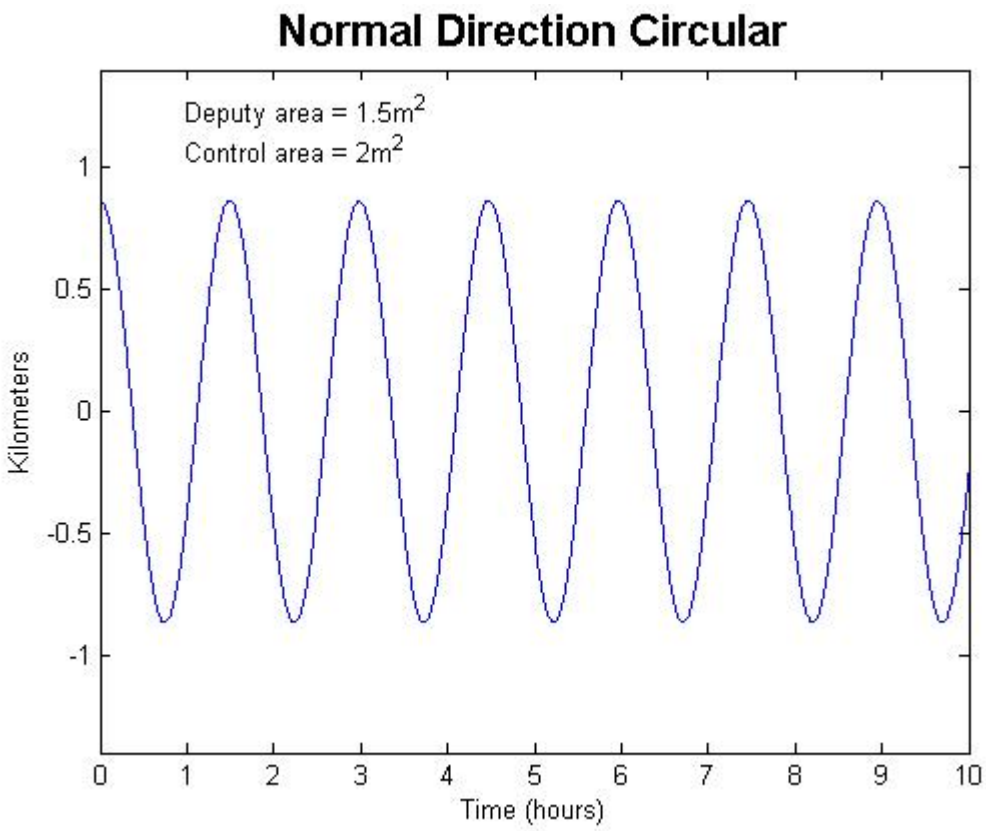

Figure 19. Circular normal separation

Because the two satellites have slightly different ascending nodes, their separation in the normal direction is periodic with a period equal to the orbital period. This is illustrated in Figure 19. Because the drag force acts in a direction opposite the velocity vector, and both the control and deputy satellites are in a polar orbit there should be no appreciable change to the normal separation over the life of the formation.

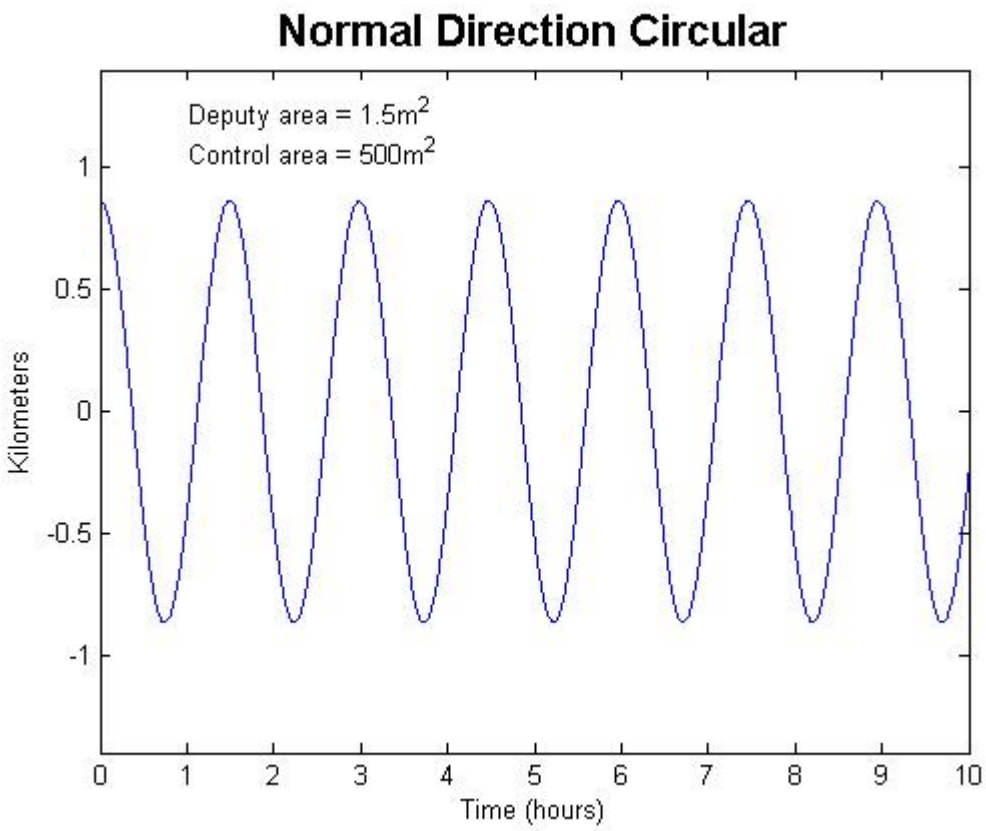

Figure 20. Circular tangential separation (exaggerated)

Looking at the separation in the normal direction, Figure 20 confirms the belief that differential drag will not appreciably affect the separation in the normal direction.

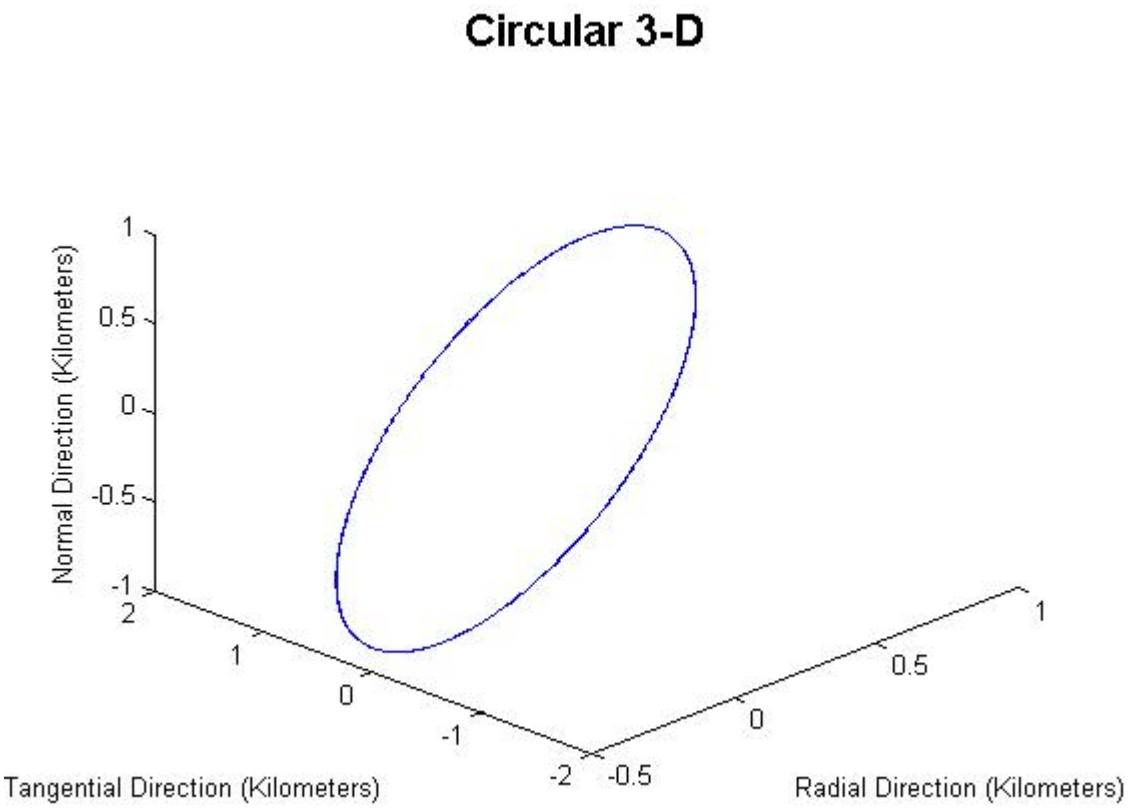

Figure 21. Circular tangential separation with small drag differences (10 hours)

Figure 21 is a three dimensional plot of the motion of the two satellites in a circular formation. The control satellite has a cross sectional area of 2 meters squared and the deputy has a cross sectional area of 1.5 meters squared. The circular formation appears to maintain its integrity pretty well for the first ten hours of the simulation. Figure 22 and Figure 23 show the motion of the formation over 100 hours using the same cross sectional areas for the control and deputy satellites.

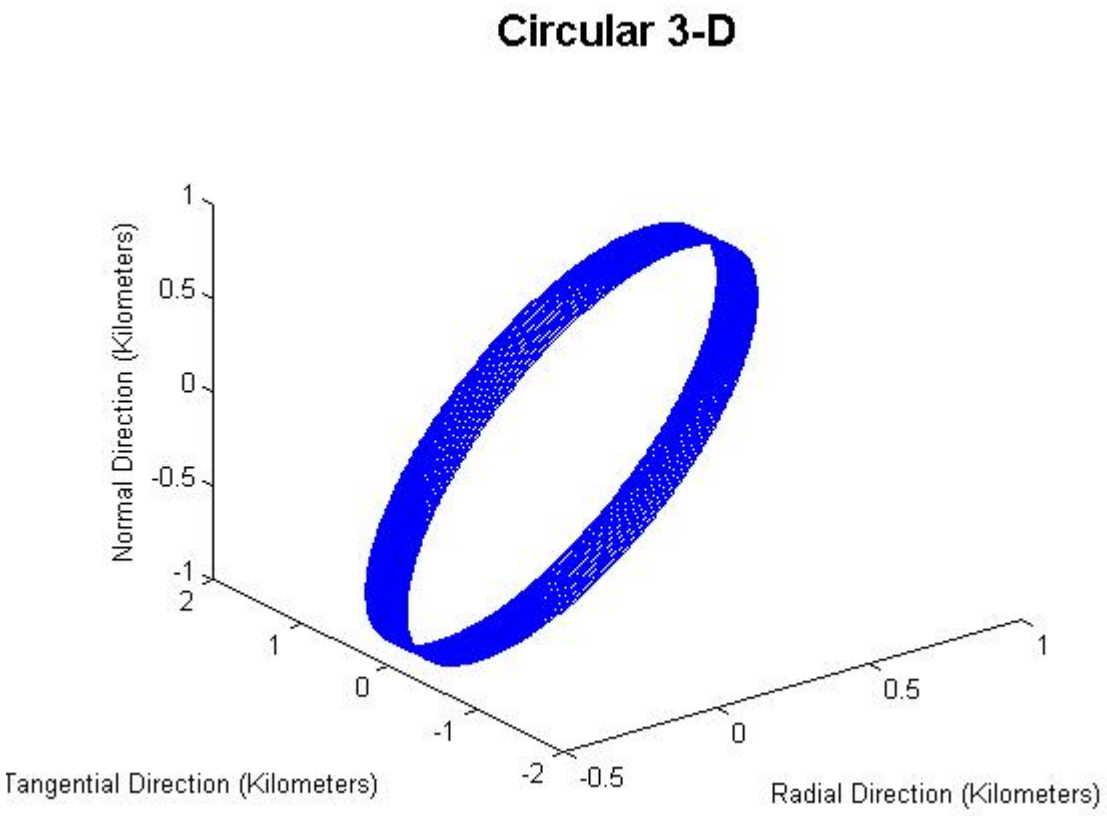

Figure 22. Circular 3-D separation with small drag differences (100 hours)

Figure 22 is a three dimensional plot of the motion between the two satellites in the circular formation over a 100 hour time period. Despite the differential drag situation the formation still maintains a somewhat circular formation; however it is obvious that the formation is beginning to degrade.

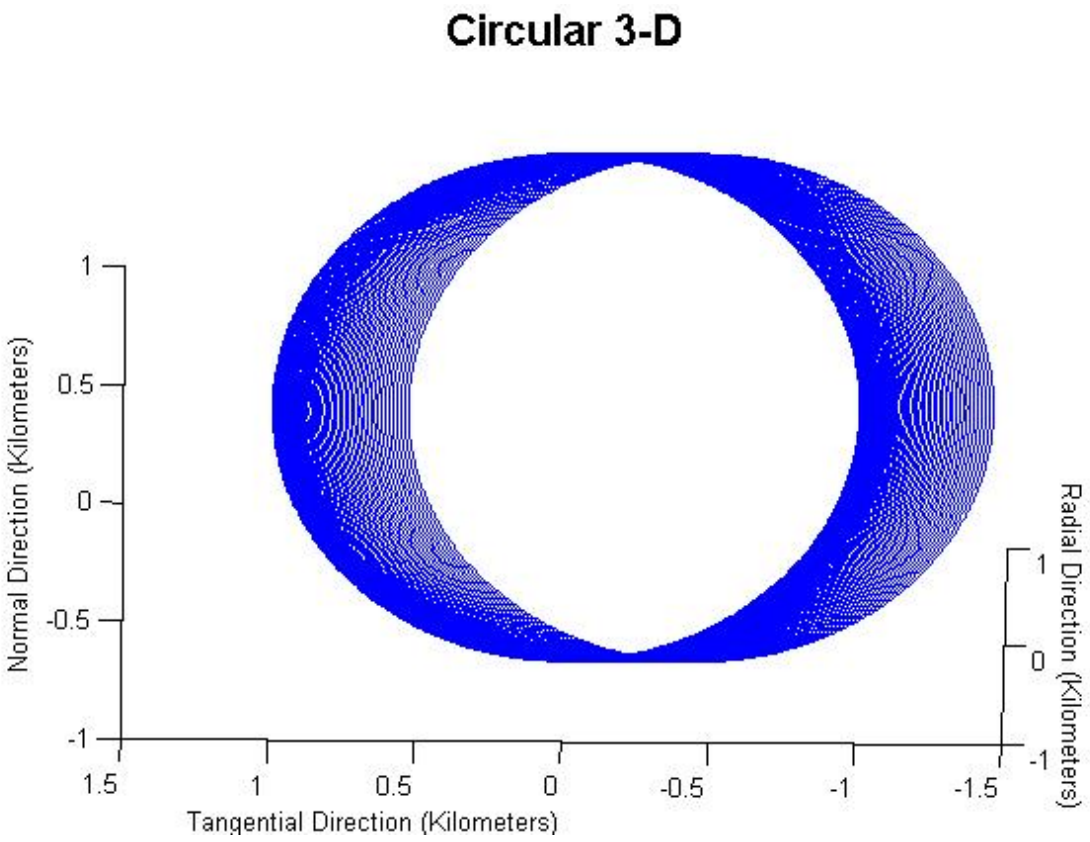

Figure 23. Circular 3-D separation with small drag differences rotated (100 hours)

Figure 23 shows the same case as Figure 22 from a different angle. In this figure (Figure 23) it is clear that the formation degrades primarily in the tangential direction. Over time, the tangential separation will continue to dominate the total separation distance.

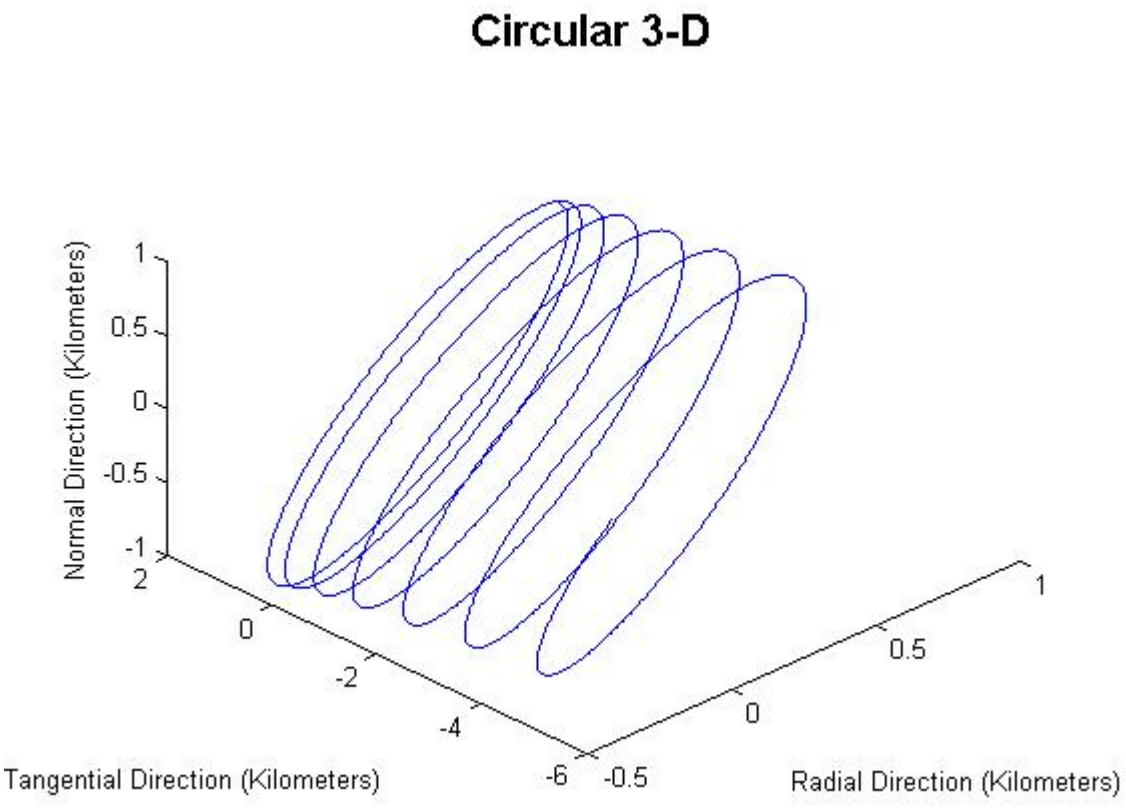

Figure 24. Circular 3-D separation (exaggerated, 10 hours)

Earlier in this section a few plots were displayed where the control and deputy satellites had exaggerated differences in their cross sectional areas (500 meters squared vs. 1.5 meters squared). Figure 24 shows a three dimensional combination of those graphs. Once again it is clear that, as the control satellite loses altitude and speeds up, it will cause ever increasing separations in the tangential direction.

Controlled Formations

The previous section displayed graphs and analysis describing how different formations reacted to satellites in the formation experiencing different drag forces. In all cases it was obvious that over a period of time the satellites fell out of formation as their positions continued to diverge. This presents a problem for formations whose deployment does not go perfectly.

If one satellite in the formation has a solar array that does not completely deploy, or a piece of thermal blanketing comes loose, or an antenna is bent slightly, or any number of other things happen that change the physical configuration of a satellite then one (or more than one) of the satellites in the formation will have a slightly different cross-sectional area than the normal and it will experience a different acceleration due to drag This differential drag will eventually disrupt the configuration of the cluster and possibly jeopardize the mission of the clustered satellites.

However, if this slight difference in cross sectional area can be corrected then the two satellites will not experience the differential drag forces and they will remain in the formation (subject to other perturbations). In order to accomplish this effect a proportional and integral controller was introduced into the code. The controller compares the specific mechanical energy of the control's and deputy's orbit and then assigns a cross sectional area to the deputy satellite that is proportional to the energy difference. This type of controller could be implemented on a satellite by adding drag plates that can be shifted to different angles in relation to the velocity vector to change the satellite's cross sectional area. Unless otherwise specified all of the following

graphs have been generated using the following controller gains for the proportional and integral controllers:

$$K_p = 150000 \tag{4.1}$$

$$K_i = 20000 \tag{4.2}$$

In addition, a controller with much smaller gains will be characterized on the in-plane scenarios to determine if a less capable controller can still maintain the desired configurations. This controller has proportional and integral gains of:

$$K_p = 15 \tag{4.3}$$

$$K_i = 2 \tag{4.4}$$

When the controller gains specified by equations (4.3) and (4.4) is used to generate graphs the proportional and integral control values will be specified on the graph.

Controlled In-Plane Formation

The controller discussed above and in the methodology chapter was used to change the cross sectional area of the deputy satellite in the following graphs. The initial values for cross sectional areas (1.5 meters squared for the deputy and 2 meters squared for the control) are displayed on each graph.

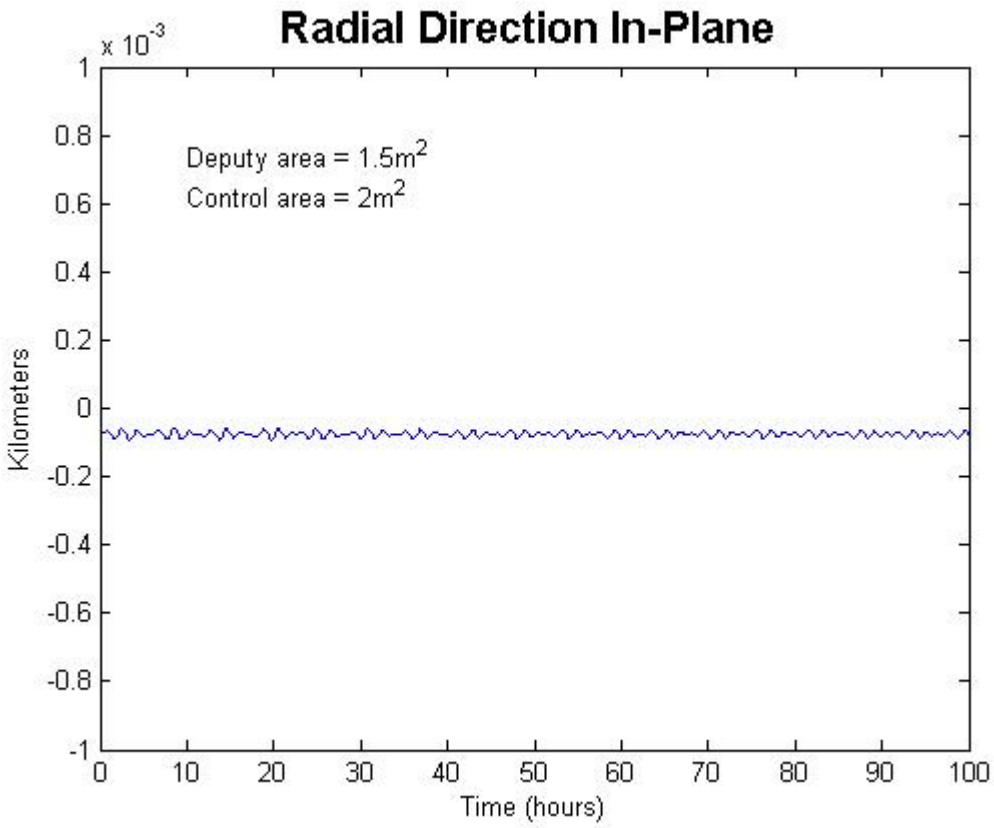

Figure 25. In-plane radial separation with controller (100 hours)

In the previous uncontrolled example for the in-plane formation there was an obvious divergence between the control and deputy satellite after 10 hours. In this case the scenario was run for 100 hours and the controller demonstrates the ability to correct for the drag differences and keep the formation close together in the radial direction.

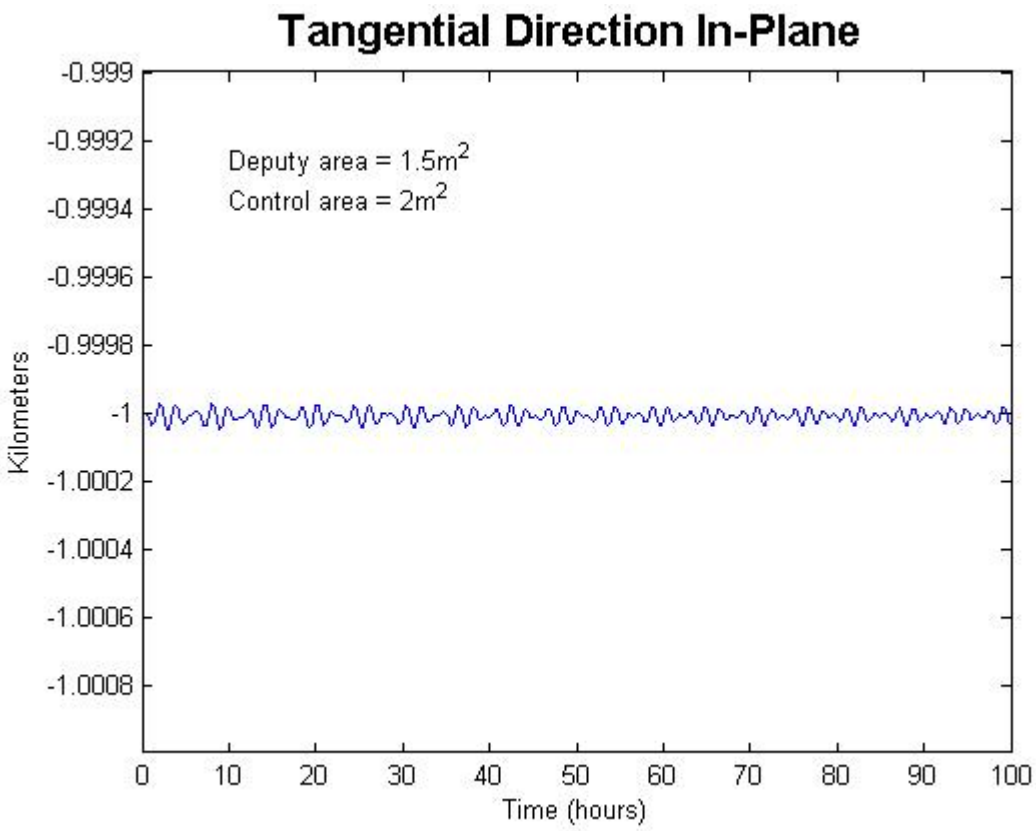

Figure 26. In-plane tangential separation with controller (100 hours)

For the uncontrolled in-plane formation the tangential separation began to quickly grow and continued growing along a quadratic curve. However, with the addition of the controller, the tangential separation stays within centimeters of the starting separation (1 km).

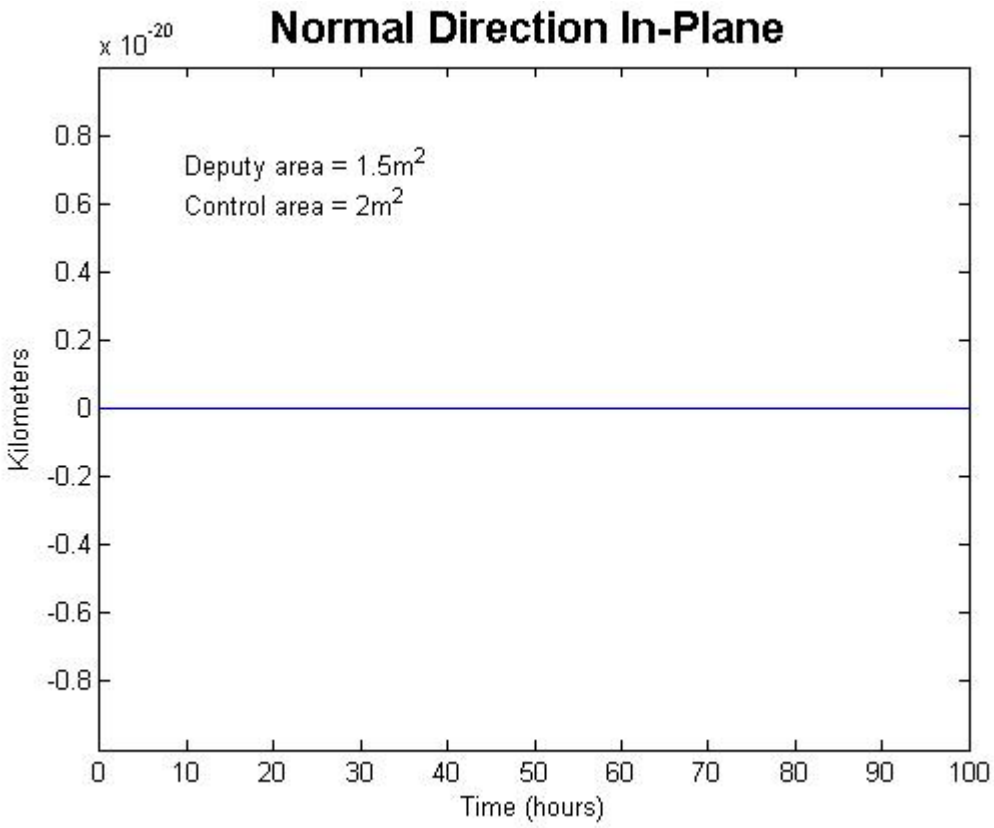

Figure 27. In-plane radial separation with controller (100 hours)

The separation in the normal direction did not increase in the uncontrolled scenario so there is no reason to believe that it will change in the controlled scenario. The above graph demonstrates that the normal separation remains right at zero as expected.

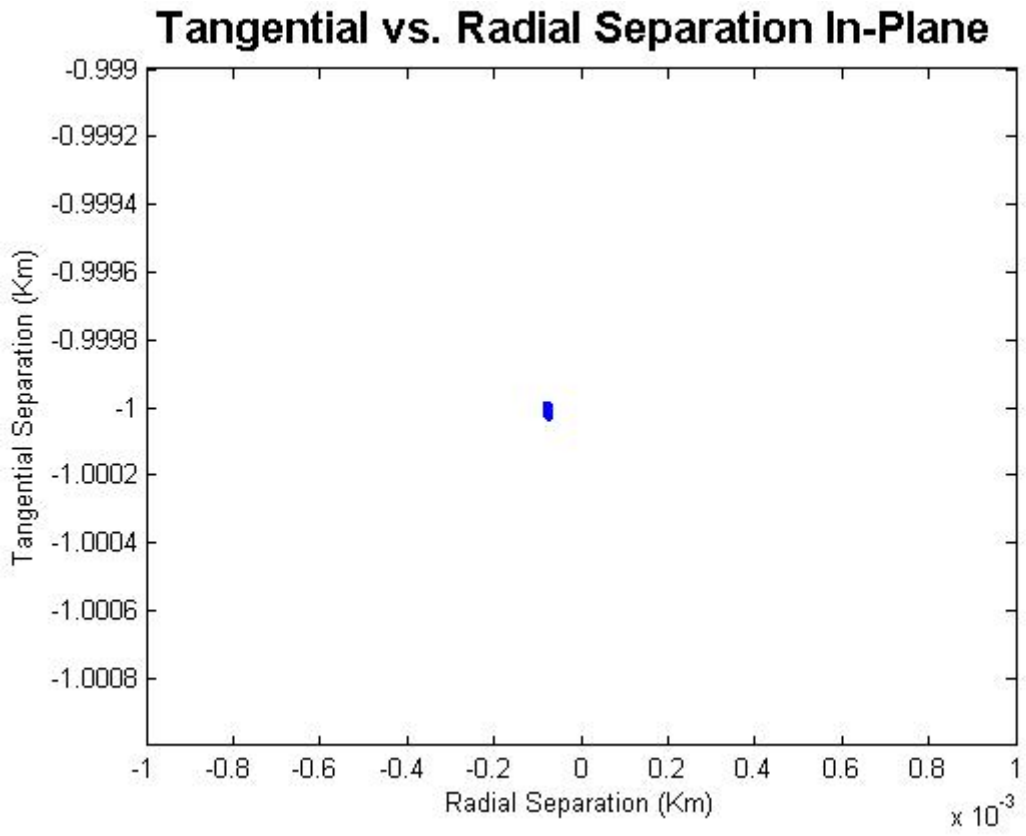

Figure 28. In-plane tangential vs. radial separation with controller (100 hours)

As expected when the tangential and radial separation plots are combined, it is easy to see that the formation is stable when the controller is functioning properly. A three-dimensional plot is not necessary because the separation in the normal direction is zero for all intents and purposes.

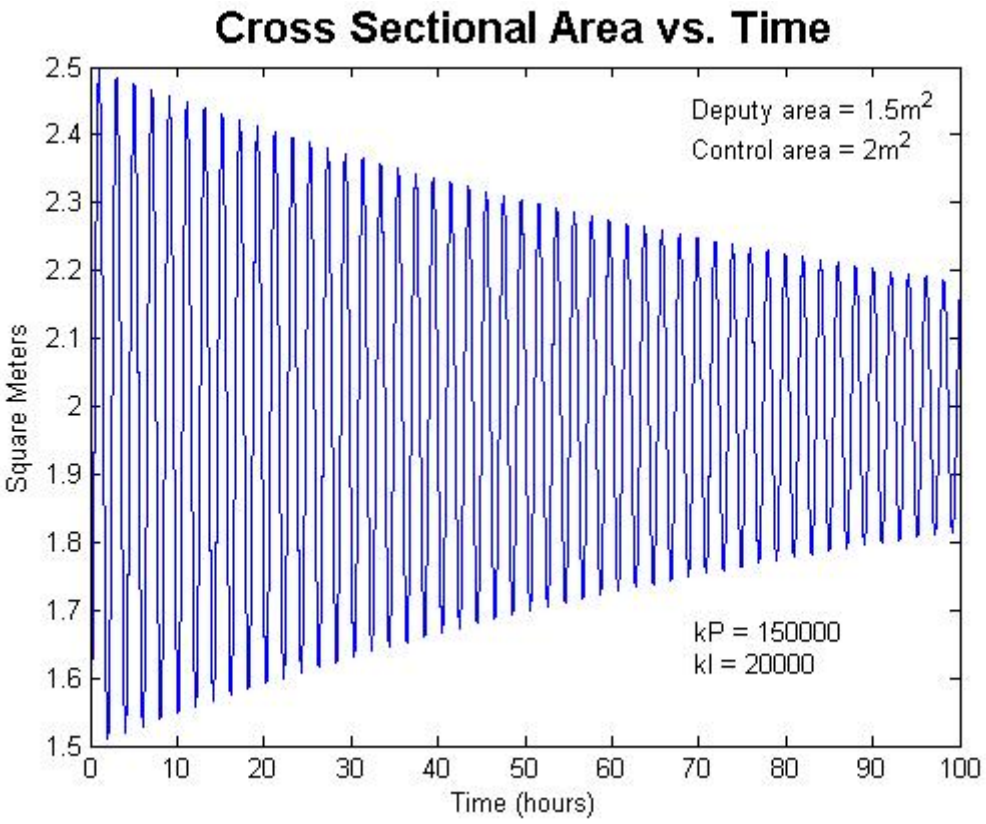

Figure 29. Cross sectional area vs. time maximum control (100 hours)

Figure 29 shows how the controller alters the deputy satellite's cross sectional area such that the orbits of the control and deputy satellites have the same energy. Because this particular controller is capable of producing large gains, the deputy satellite changes cross sectional area at a rapid pace and the separation distances can be kept to a minimum. In addition, as this controller continues to operate it will require less drastic cross sectional area changes and continue to oscillate closer to the cross sectional area of the control satellite. The controller used for this study only used proportional and integral control; however, the addition of a derivative control and further tuning of the controller gains would both help dampen the oscillation and allow the cross sectional area to settle down much more quickly (Ogata, 1970: 157). The derivative control action has

an anticipatory character and is only effective during transition periods (Ogata, 1970: 158).

The next step for examining the controlled in-plane formation involves examining how the formation will react to a controller that is not capable of generating large enough gains to immediately correct for the differential drag. The following graphs were propagated over longer periods of time so that the affect of the controller could be better characterized. The cross sectional areas displayed on the graphs are the initial cross sectional areas, however because the controller adjust the cross sectional areas it will change constantly throughout the simulation. The change in cross sectional area is presented in a later graph.

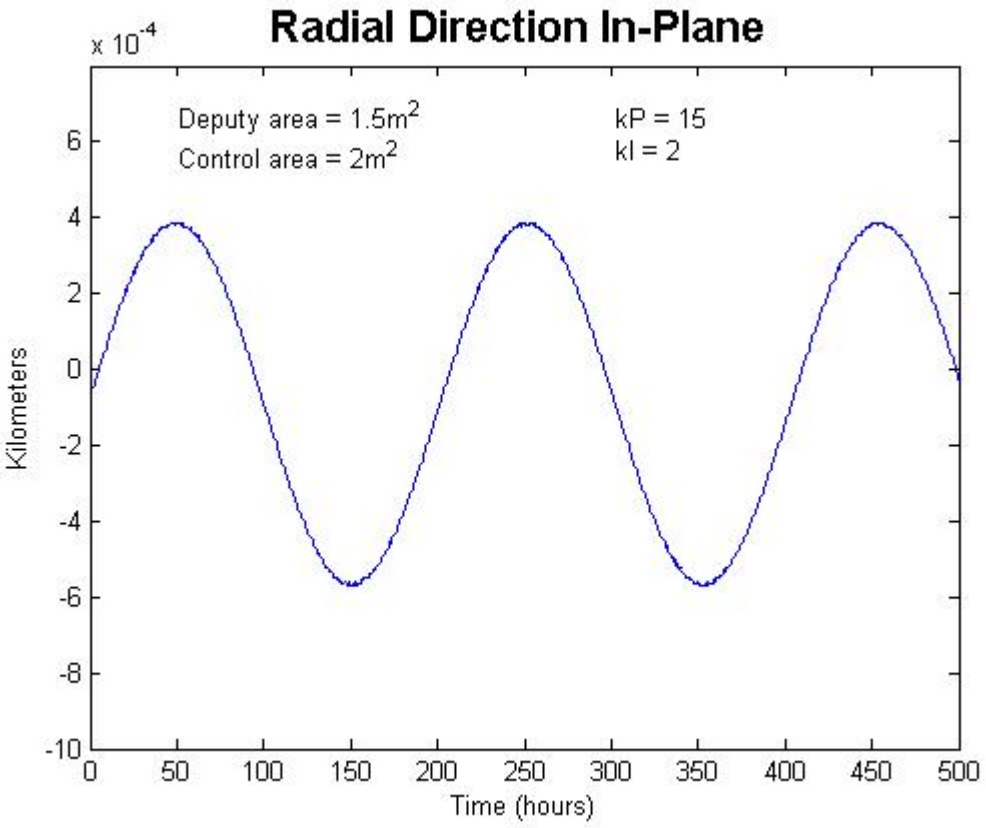

Figure 30. In-plane radial separation with minimum control (500 hours)

As the control satellite's orbit lowers the controller must adjust the cross sectional area of the deputy satellite such that both orbits have the same energy. To do this the controller increases the cross sectional area of the deputy satellite. The less powerful controller employed in this case cannot adjust the cross sectional area immediately (as the previous controller did). As the controller adjusts the cross sectional area it puts the deputy satellite into a slightly elliptical orbit so that the two satellites will maintain the same orbital energy. This causes the radial separation of the two satellites to vary periodically over a period of ~200 hours.

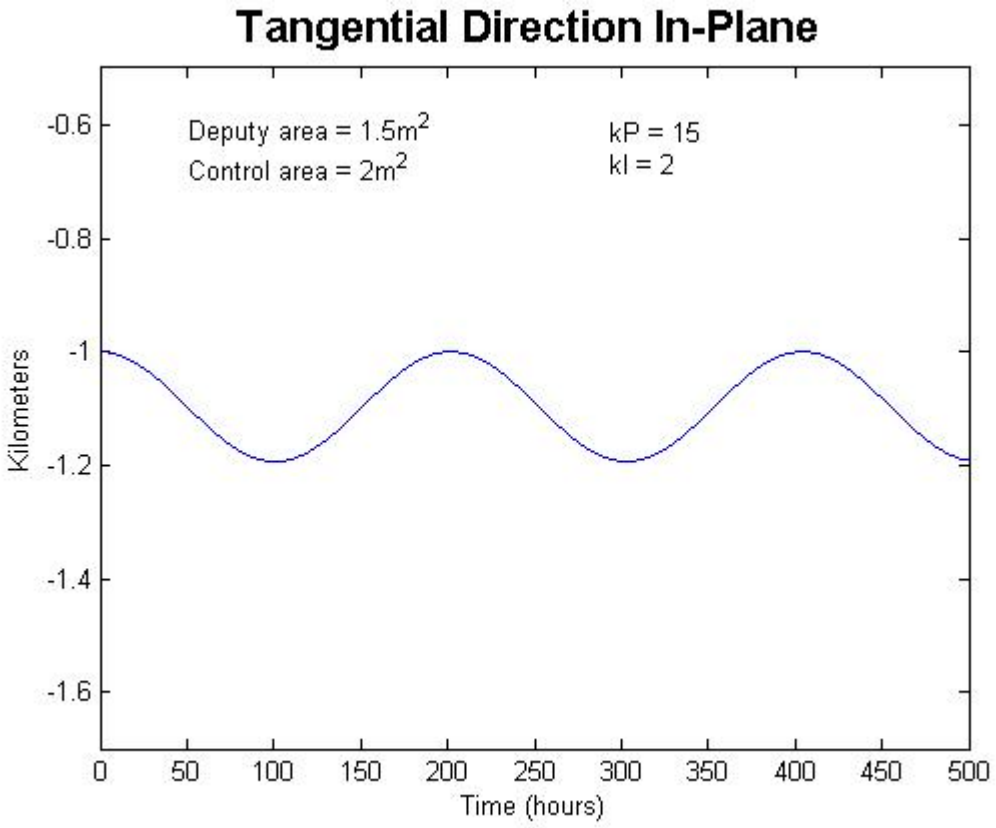

Figure 31. In-plane tangential separation with minimum control (500 hours)

The tangential separation between the two satellites follows a plot very similar to the radial separation plot. It is slowly increasing as the controller increases the cross sectional area and then slowly moves back toward the nominal separation.

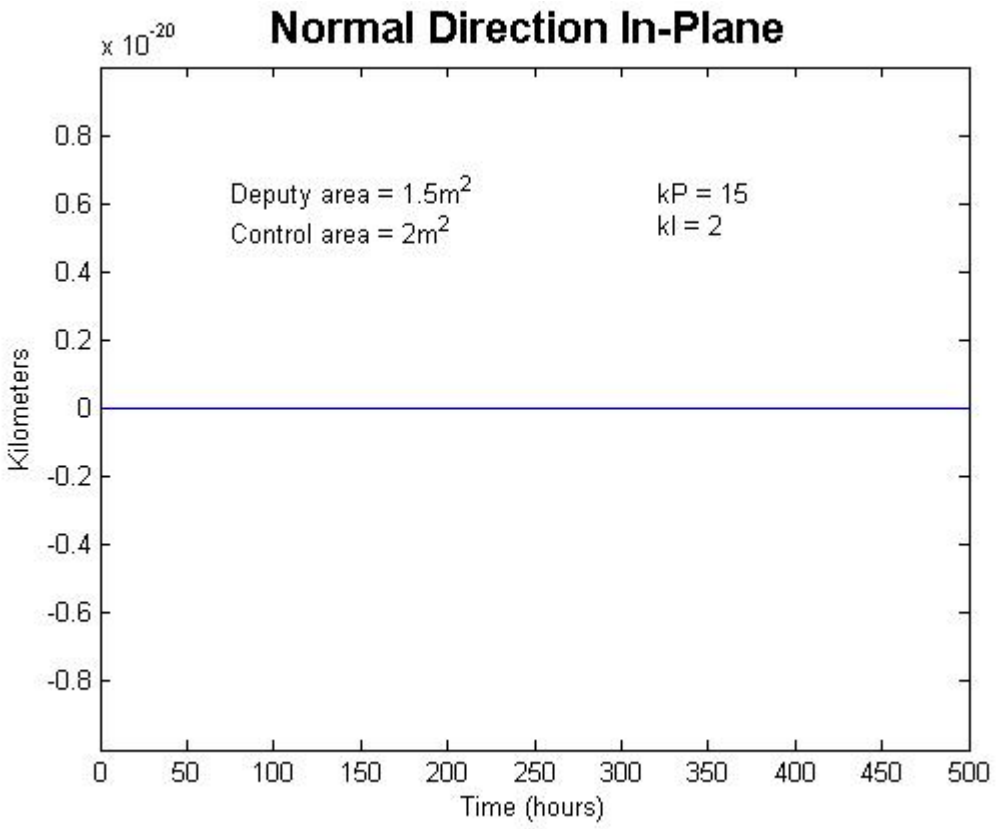

Figure 32. In-plane normal separation with minimum control (500 hours)

The normal separation continues to be a non-issue and for all intents and purposes it can be treated as zero.

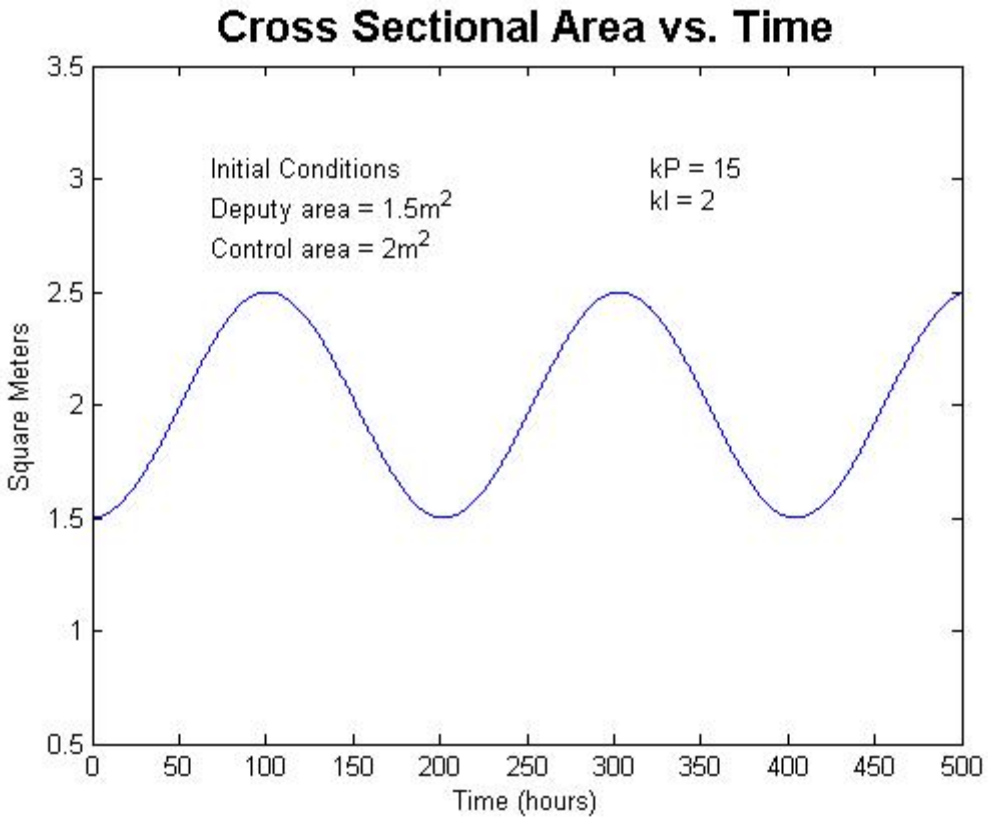

Figure 33. Cross sectional area vs. time with minimum control (500 hours)

At the initiation of the scenario, the control satellite has a larger cross sectional area than the deputy satellite and thus the controller begins to increase the cross sectional area of the deputy satellite in an attempt to equalize the orbital energies. By the time the controller has equalized the cross sectional areas of the two satellites the control satellite is already in a lower orbit. Hence, the controller continues increasing the cross sectional area of the deputy satellite as it works toward equalizing the orbital energies. When the deputy satellite's cross sectional area reaches approximately 2.5 meters squared the orbital energy of the two orbits are equal; however, the controller cannot reduce the cross sectional area of the deputy fast enough to keep the energies equal. Because the deputy satellite has a larger cross sectional area than the control satellite it will fall into a slightly lower orbit and the controller will begin to reduce the cross sectional area of the deputy

until it reaches 1.5 meters squared again. During this time the tangential separation is being reduced and the two satellites are moving back to the nominal separation of 1 km. However when the satellites reach the nominal separation of 1 km the cross sectional areas are also back at their initial values and the entire process starts over. Thus the periodic motion shown in the radial and tangential separation plots is also mirrored in the cross sectional area versus time plot that is displayed above.

This periodic motion could possibly be mitigated with the addition of a derivative control action (sometimes called rate control), or by better tuning the K_p and K_I gains. The derivative control action has an anticipatory character and is effective during transient periods; however the derivative control can never be used alone and must be implemented in conjunction with a proportional or a proportional plus integral control action (Ogata, 1970: 157).

Controlled In-Track Formation

The in-track formation demonstrated a diverging tendency similar to the in-plane formation. When the controller was added to the scenario it corrected the divergence but the results were slightly different. The in-track scenarios were all propagated using the original controller with large gains.

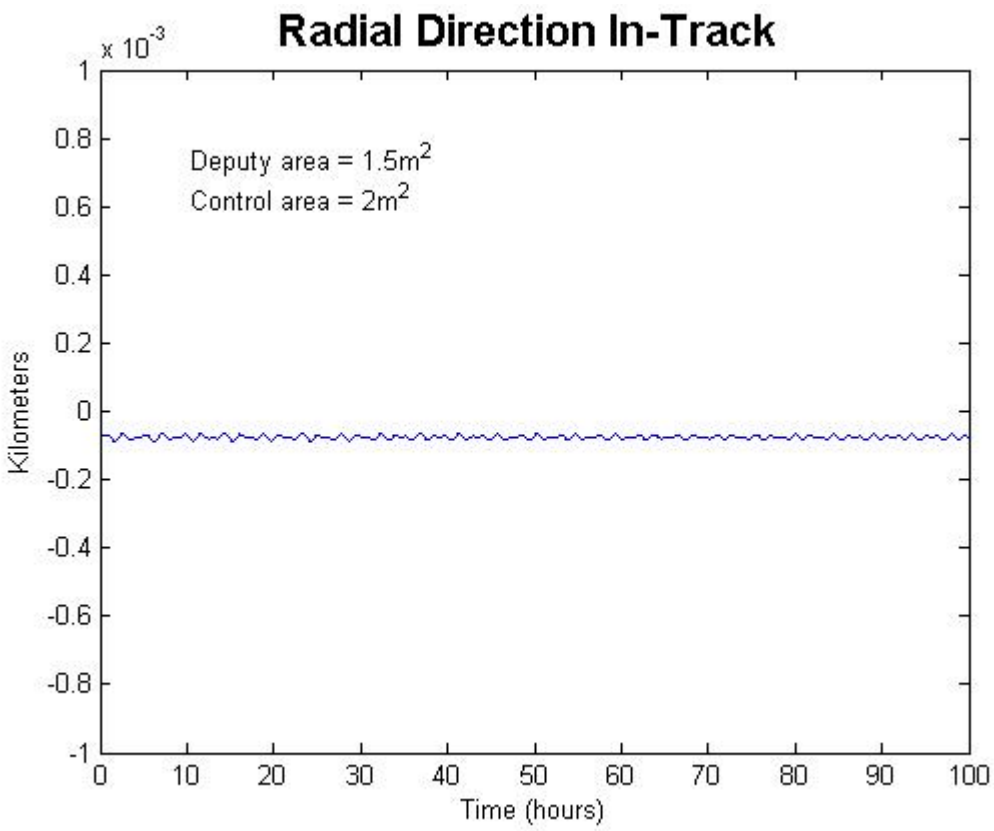

Figure 34. In-track radial separation with controller (100 hours)

In the uncontrolled scenario the radial separation changed by about 6.5 meters over a 10 hour time period shown. When the controller was employed, it reduced the maximum separation to less than one centimeter as shown by the above graph. If the controller is allowed to continue working, the maximum separation will continue to decrease over time.

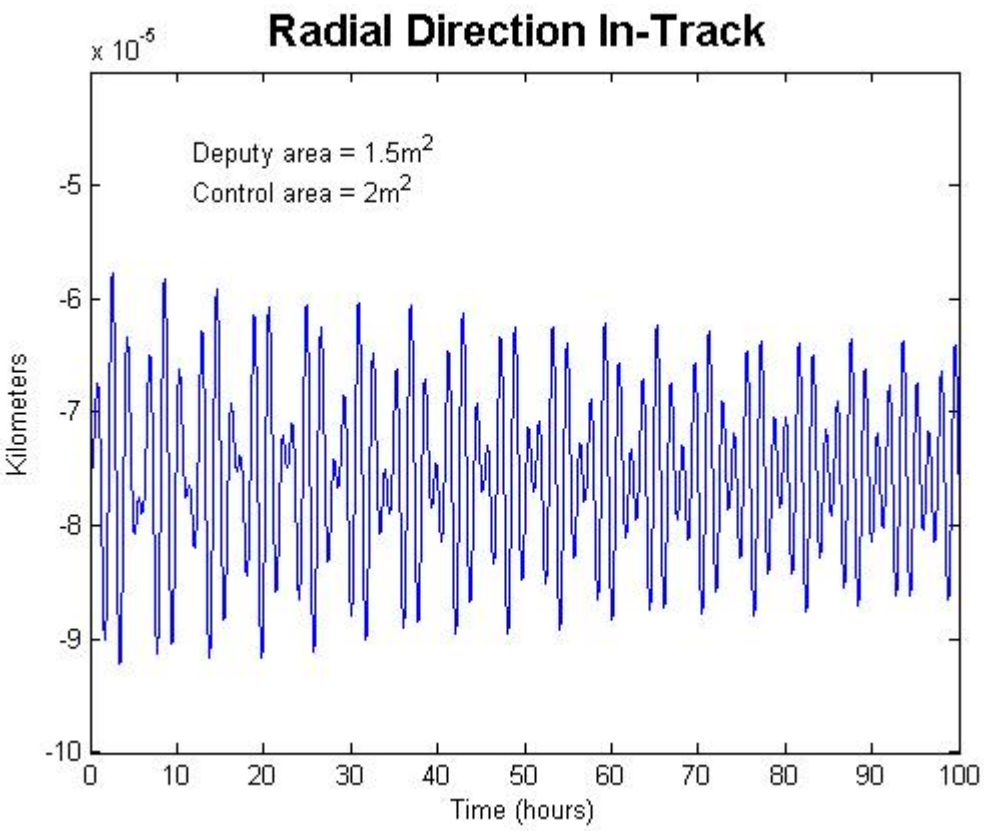

Figure 35. In-track radial separation with controller (100 hours zoom in)

When the in-track scenario was propagated over 100 hours, it becomes obvious that the radial separation will continue to decrease as the controller is allowed to operate and slowly reduce the oscillation to a near zero value.

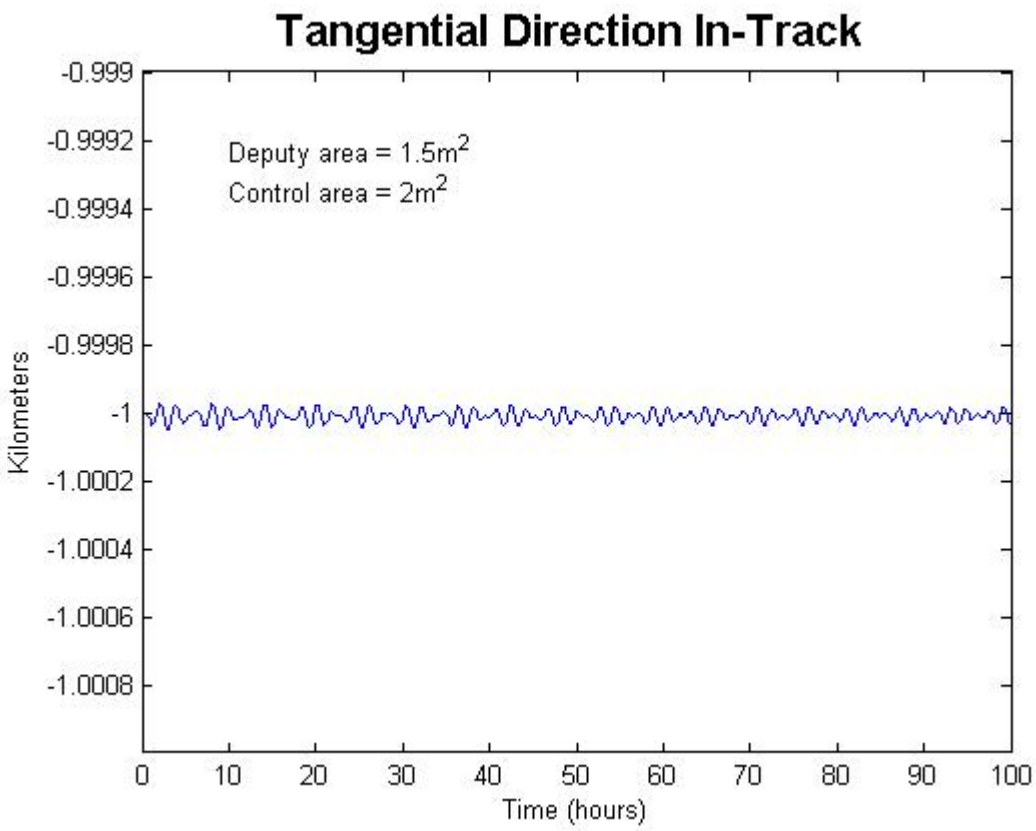

Figure 36. In-track tangential separation with controller (100 hours)

In the uncontrolled scenario the tangential separation began to grow at an ever increasing pace after a few hours; however, when the controller was implemented, the separation could be contained to a negligible value.

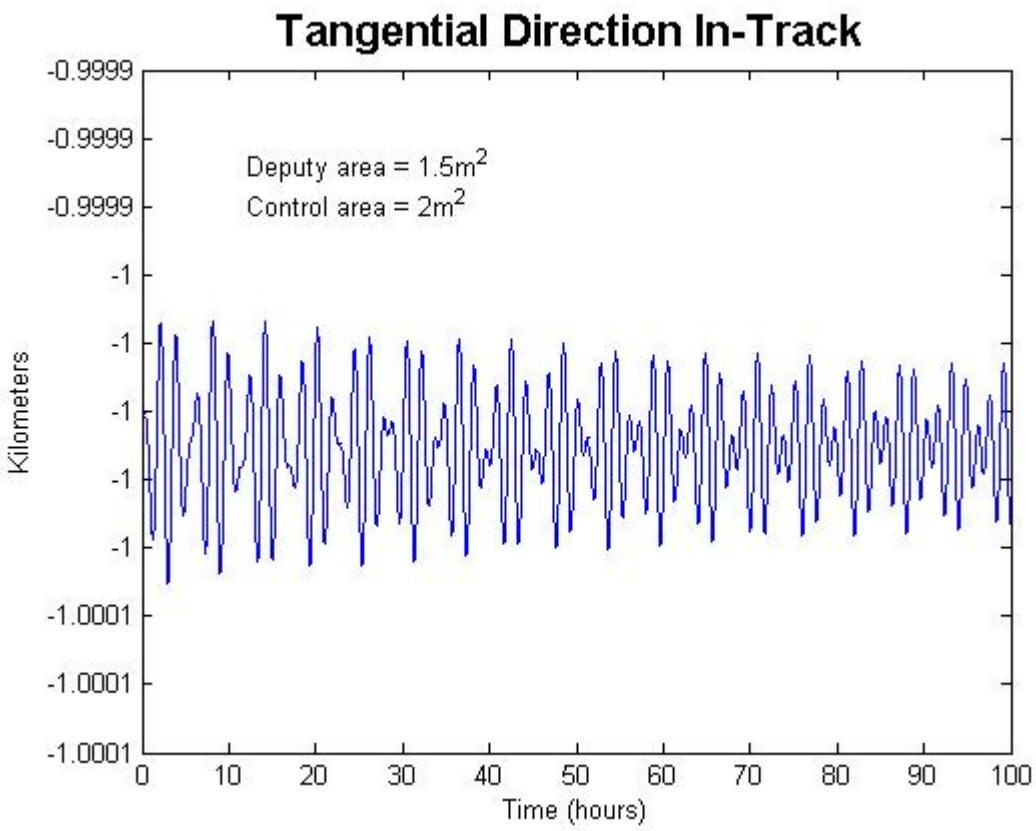

Figure 37. In-track tangential separation with controller (100 hours zoom in)

Propagating the in-track scenario over 100 hours and zooming in to the area of interest yields Figure 37. This graph is identical to Figure 36 only with a smaller range of values along the Y-axis. Clearly, as the controller continues to operate, the tangential separation will settle down closer and closer to a one kilometer separation.

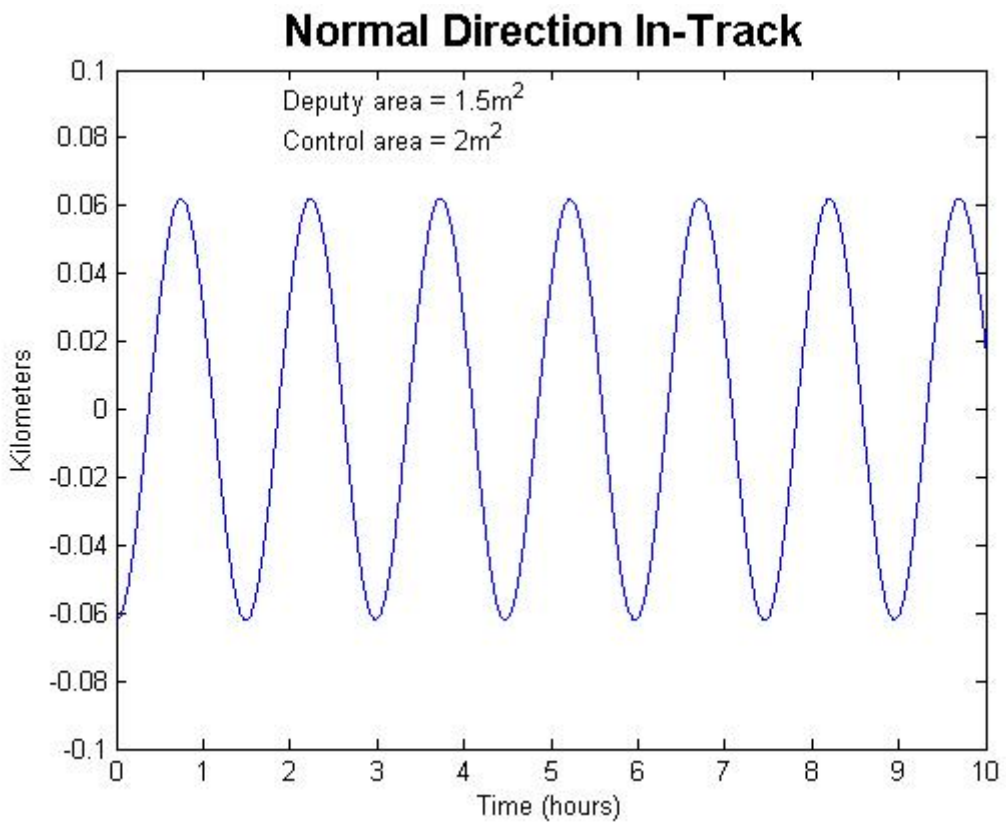

Figure 38. In-track normal separation with controller (10 hours)

For the in-track formation the only differences between the orbits of the deputy and control satellites are in the mean anomaly and the right ascension of the ascending node. The difference in right ascension of ascending node will cause the normal separation to oscillate around zero with the largest differences being when the satellites are near the equator.

A figure similar to Figure 28 could be displayed for the in-track scenario; however, the figure looks identical to that figure and thus has not been included.

Controlled Circular Formation

The circular formation was tested with exaggerated differences between the cross-sectional areas of the two satellites to show how the formation would degrade propagating the scenario over a reasonable amount of time. While it is not reasonable to imagine two satellites identical upon launch having such a wide disparity upon deployment, it does illustrate the trends of the formation quite well in an easy to read and understand plot. For the controlled scenarios the huge cross-sectional area differences will continue to be used to test the controller.

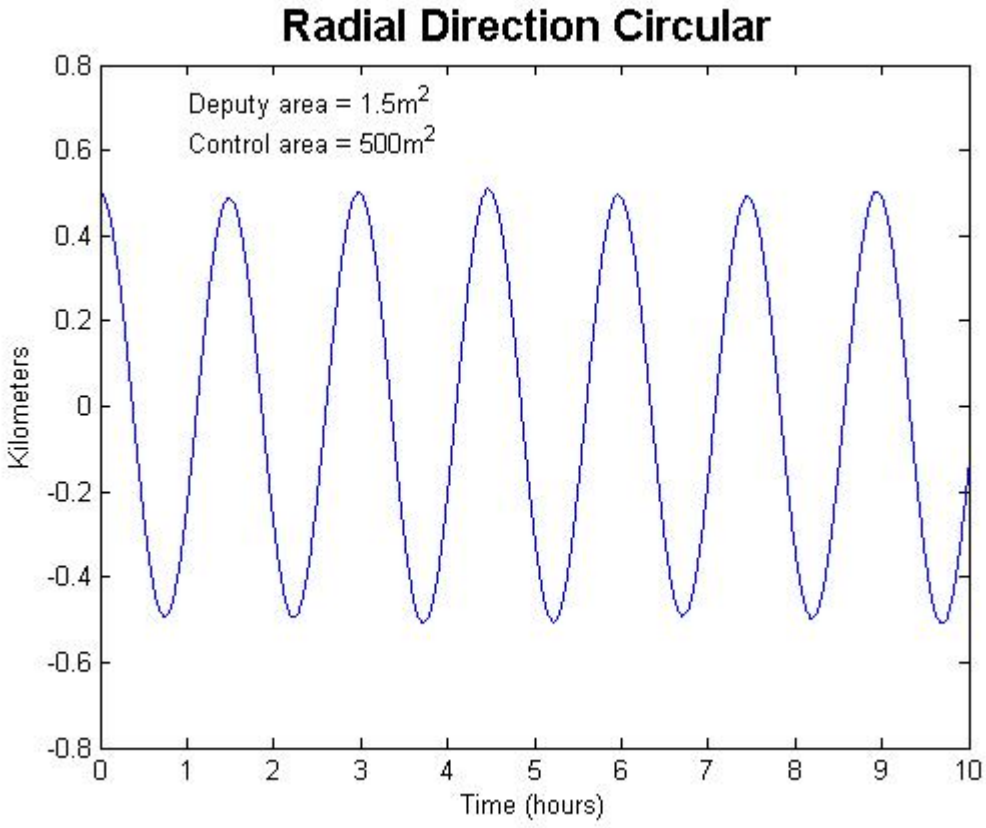

Figure 39. Circular radial separation with controller (10 hours)

For the uncontrolled scenario the separation began to expand in a noticeable manner after the plotted ten hour period. However with the controller employed the radial separation maintains the constant oscillation that is expected of two satellites with the same semi-major axis yet slightly different eccentricities.

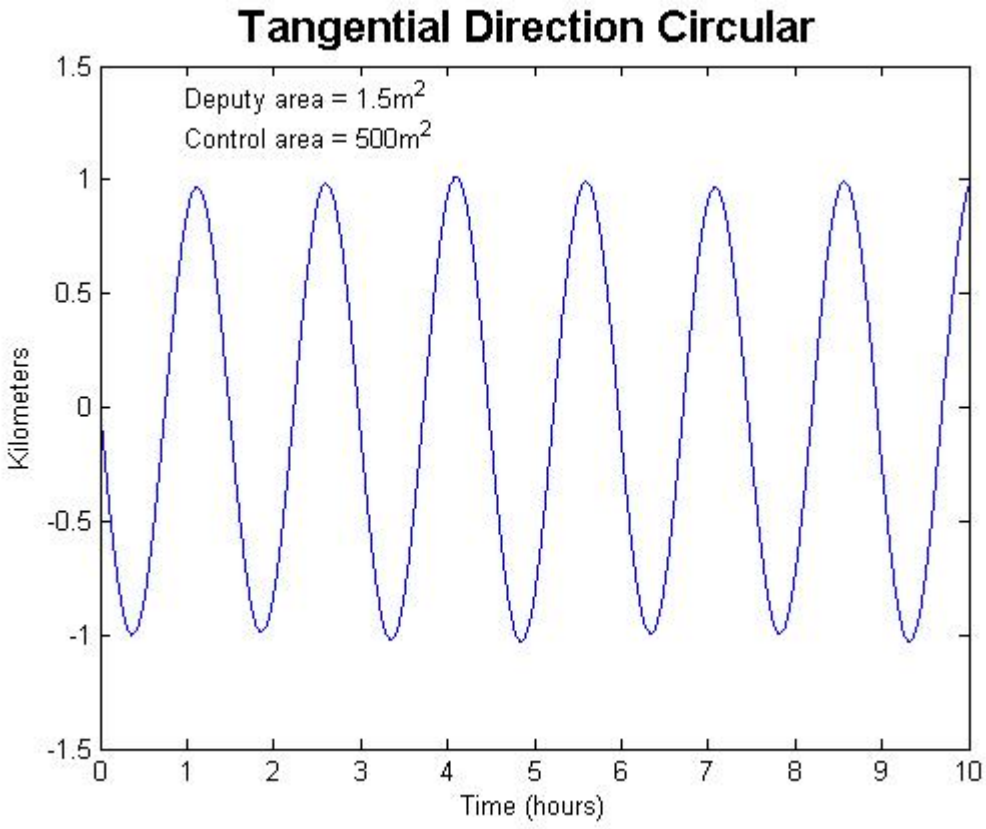

Figure 40. Circular tangential separation with controller (10 hours)

The tangential direction of separation quickly diverged from zero when tested in the un-controlled scenario, but as expected once the controller was added to the scenario it settled down and oscillated around zero without diverging. The points of maximum separation occur near the north and south poles (which is consistent with the design of the circular formation used for these scenarios).

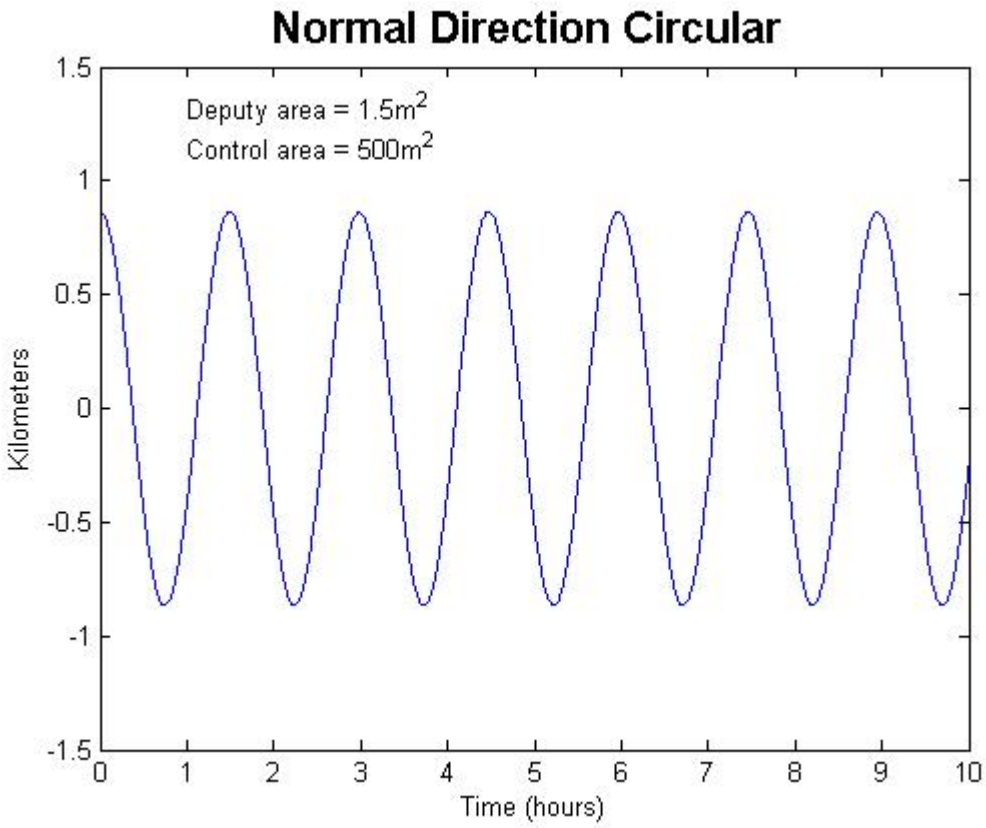

Figure 41. Circular normal separation with controller (10 hours)

Once again no major changes occurred in the normal direction of the un-controlled scenario so no changes are expected in the controlled scenarios. Figure 41 shows that the separation in the normal direction is no different than the un-controlled scenario and it continues to oscillate around zero depending upon which part of the orbit the satellites occupy at the current time.

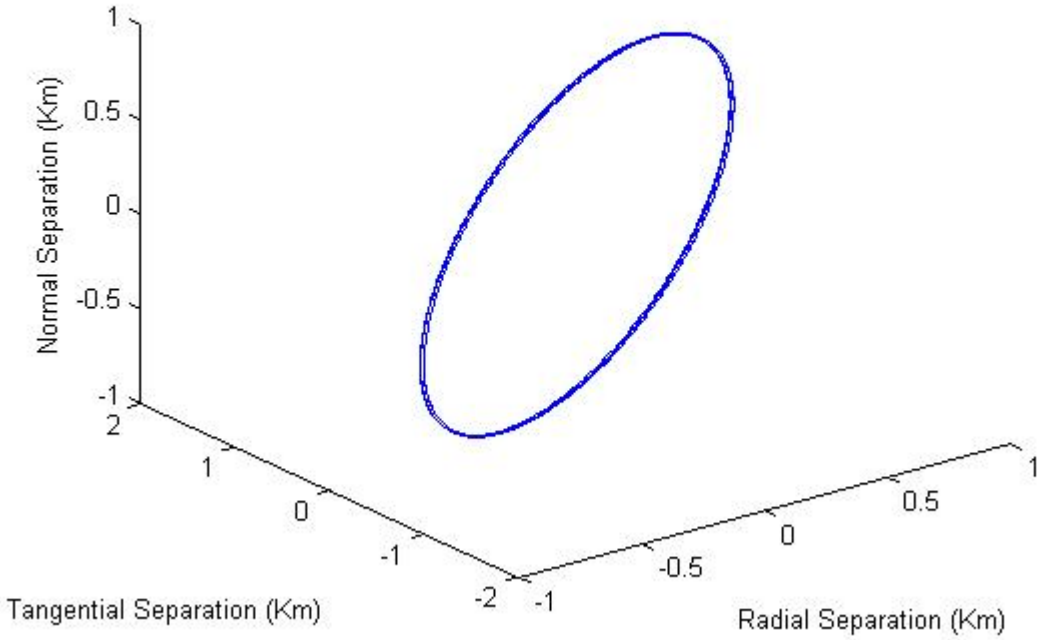

Figure 42. Circular 3-D separation with controller (10 hours)

Figure 42 is a three dimensional plot of the controlled circular formation with the exaggerated cross-sectional area differences. In the un-controlled scenario the tangential direction of separation quickly expanded and the circular formation degraded. The addition of the controller has solved that problem and the circular formation remains stable while the controller is applied.

V. Conclusions and Recommendations

Conclusions

The objective of this research was to study the effects of drag on anomalous satellites within a cluster and determine how quickly the cluster formation will deteriorate. Obviously this question depends a lot on the drag differential present between the satellites. This study examined two satellites with a 25% difference in cross sectional area and found (as expected) that the formations quickly deteriorated and the primary direction of separation was in the tangential direction. It quickly became obvious that none of the studied formations would be able to maintain their formation without some type of controlling mechanism.

Of the three formations (in-plane, in-track, and circular) examined in this research, the satellites in the circular formation maintained proximity for the longest period of time; however, this research did not include the effects of the J2 perturbation which would greatly affect the stability of the circular formation.

Many future formations will require precise satellite positioning and any small differences in cross sectional areas will cause the satellites to diverge from the designed formation. Therefore, if some type of controlling mechanism can be implemented to alleviate the differential drag between the satellites, the formation may be able to retain its integrity and functionality for extended periods of time.

This study implemented a controller that adjusted the cross sectional areas of the satellites such that the energies of the orbits would remain equal. If this type of controller can be implemented with large enough gains then the differential drag can be corrected immediately and the formation will remain true to its design. However if a controller

with smaller gains is used for the controlling actions the formations will degrade (depending of the cross sectional area difference) before the controller can fully correct the problem. Then the satellites will remain in close proximity but the integrity of the formation design will not be maintained and the total separation between the satellites will vary from the initial separation distance to an arbitrary maximum distance based on the drag differential and the controller gain. For this research, the arbitrary distance was 20% larger than the initial separation and the separation between the two satellites varied along a sine curve between the initial separation and maximum separation.

At some point satellite clusters will become imperative to the advancement of military ISR systems and at that point a controlling system that can compensate for drag differences and other perturbations will also become necessary to ensure the success of those systems.

Recommendations for Future Research

This research characterized the manner in which the separation between clustered satellites in different formations would diverge if one of the satellites experienced an anomaly which effected its cross sectional area. In addition, a proportional/integral controller was employed to compensate for the different cross-sectional areas. This type of controller is fairly straight-forward and the possibility of expanding the scope and complexity of the controller would be interesting. Adding a differential control component to the controller and fine tuning the proportional and integral gains of the controller would be a logical step forward. Further verification of the controller in a non-linear environment may also be necessary. Studying the dynamics and consumable

budgets of a formation that is forced to depend on this style of controller to maintain the functional formation would also be a logical step forward.

Increasing the cross sectional area to mitigate the differential drag is a viable option for controlling the satellites in formation, but it may also reduce the lifetime of the formation (more drag = shorter lifetime). Additional research could be done that studies the impact on formation lifetime. Along those same lines, a study that examined how attitude control could be used to correct for differential drag would be very interesting.

Another possible research area is the adaptation of a more accurate atmospheric model into the code. The current atmosphere model is satisfactory for the context; however, results obtained from a higher fidelity model would be important in the long run. Along similar lines, a study that implemented the full scope of orbital perturbations instead of just two body motion and atmospheric drag would provide higher fidelity results and may uncover some different issues related to the stability and behavior of these formation designs.

In addition to the three types of formations discussed in this research, there are other possible formation designs that could be explored. Other formation types will likely require extensive formation keeping. Unless those hurdles can be overcome in an efficient manner, there may not be a need to develop a differential drag controller to be implemented on the formation satellites.

Appendix A - Characterization Code

The following code was written and executed using MATLAB version 7.0.

```
function []=orbit_propagator()

%  Simulation of a satellite in orbit with two-body motion only

% Initial and Final Time (seconds)

t0 = 0;
tf = 36000;  % in seconds, 100 hrs = 360000

t_vec=t0:10:tf;

% Initial Satellite Orbital Parameters

% Orbit Altitude (Kilometers)

Sat_Alt = 250;

Earth_Radius = 6378.1;

Sat_SemiMajor = Earth_Radius + Sat_Alt;  % Compute Semimajor Axis

% Constants

% Earth Gravitational Parameter (km^3/sec^2)

mu = 3.98601e5;

% Gravitational constant
% Expressed in N m^2/kg^2

G = 6.67e-11;

% Mass of the Earth expressed in kg

MassEarth = 5.9742E24;

% Rotational rate of Earth (rad/s)

Earth_rate = 7.2722e-5; % corresponds to 15 degrees/hour

% Orbit Eccentricity
```

```
Sat_Ecc = 0;  % Eccentricity assumed zero

% Orbit Inclination (radians)

Sat_Inc = pi/2;

% Right Acsension of Ascending Node (radians)
%    Angle between vernal equinox direction and  point at which the satellite passes
%    the equator going north

Sat_RAAN = 0;

% Argument of Perigee (radians)
% Argument of Perigee undefined for circular orbit, assume zero as placeholder

Sat_ArgPeri = 0;

% Argument of Latitude at epoch (radians)
%    Angle between the ascending node direction and the satellite position vector
%    at the start time of the sim

Sat_ArgLat = 0;

% Argument of Latitude at epoch (radians)
%    For an in-plane satellite that is approximately 1 km behind the
%    control satellite.  Calculation 2pi*radius of sat orbit =
%    circumference of orbit
%    circumference/360 = 115.68 km/degree
%    1/115.68 = .008644 degrees for a one km separation.
%    .008644*pi/180 = .000150873

PSat_ArgLat = 2*pi - 0.000150873;

%    Angle between prime meridian and vernal equinox direction at start time of sim.
%    This is an arbitrary assignment unless we want sim time to have some real meaning
%    with respect to a true astronomical time system

Earth_Pos = 0;

% The in-track formation has satellites that occupy the same ground track.
% The deputy satellite starts off 1 Km behind the control and in a
% slightly different track.
% This is accomplished by offsetting their RAAN by

Period_initial = sqrt((4*(pi^2)*(Sat_SemiMajor*1000)^3) / (G*MassEarth));
```

```
intrack_RAAN = (2*pi-PSat_ArgLat)/(2*pi) * Period_initial * Earth_rate;

% Degree to Rad Conversion and reverse

degtorad = pi/180;
radtodeg = 180/pi;

% Convert Initial Orbit Parameters to
% Cartesian Position and Velocity
% Uses "posvel" function given at end of this code

[r0,v0] = posvel(Sat_SemiMajor, Sat_Ecc, Sat_Inc, Sat_RAAN, Sat_ArgPeri,
Sat_ArgLat, mu);

[r0plane, v0plane] = posvel(Sat_SemiMajor, Sat_Ecc, Sat_Inc, Sat_RAAN, Sat_ArgPeri,
PSat_ArgLat, mu);

[r0track, v0track] = posvel(Sat_SemiMajor, Sat_Ecc, Sat_Inc, intrack_RAAN,
Sat_ArgPeri, PSat_ArgLat, mu);


state0=[r0;v0];

stateplane0=[r0plane;v0plane];

statetrack0=[r0track;v0track];

% Propagate satellite position using two-body orbit assumptions
% Uses ode45 numerical integrator and
% "twobody" function given at end of this code

% Set max stepsize for integration.  I chose a number that
% gives quick results without losing too much accuracy
% over a 10 hour period of propagation

options = odeset('MaxStep',50);

[t,state]=ode45(@twobody,[t_vec],state0,options);

staterad = state(:,1:3);
statevel = state(:,4:6);

statevellength = length(statevel);

%Initialize period vector, because it changes slightly as drag effects
```

```
%satellite
Pvector=zeros(statevellength,1);

%Initialize RTN velocity vector
RTNstatevel=zeros(statevellength,3);

%Initialize true anomaly vector (ta)
ta=zeros(statevellength,1);

for i=1:statevellength
   velmag(i)=norm(statevel(i,:));
   radmag(i)=norm(staterad(i,:));

   Pvector(i,:)=sqrt((4*(pi^2)*(radmag(i)*1000)^3) / (G*MassEarth));

   % Determine the true anomaly by dividing time by period
   % Then divide remainder by period and multiply by 2pi
   ta(i)=(rem(t_vec(i),Pvector(i))/Pvector(i))*2*pi;

   ECItoRTN = [(cos(Sat_ArgPeri + ta(i))*cos(Sat_RAAN))-(sin(Sat_ArgPeri +
ta(i))*cos(Sat_Inc)*sin(Sat_RAAN)),...
   cos(Sat_ArgPeri + ta(i)) * sin(Sat_RAAN) + sin(Sat_ArgPeri + ta(i)) * cos(Sat_Inc)*
cos(Sat_RAAN),...
   sin(Sat_ArgPeri + ta(i)) * sin(Sat_Inc);...
   -sin(Sat_ArgPeri + ta(i)) * cos(Sat_RAAN) - cos(Sat_ArgPeri + ta(i)) * cos(Sat_Inc)*
sin(Sat_RAAN),...
   -sin(Sat_ArgPeri + ta(i)) * sin(Sat_RAAN) + cos(Sat_ArgPeri + ta(i)) * cos(Sat_Inc) *
cos(Sat_RAAN),...
   cos(Sat_ArgPeri + ta(i)) * sin(Sat_Inc);...
   sin(Sat_Inc) * sin(Sat_RAAN),...
   -sin(Sat_Inc) * cos(Sat_RAAN),...
   cos(Sat_Inc)];

   RTNstatevel(i,:)= ECItoRTN*statevel(i,:)';
   RTNvelmag(i)=norm(RTNstatevel(i,:));
   RTNdiff(i)=velmag(i)-RTNvelmag(i);


end


timehrs=t/3600;

figure(1)
plot(timehrs, radmag)
title('Orbit Radius of Sat#1 vs. Time(hrs)','fontsize',16,'fontweight','bold')
```

```
figure(2)
plot(timehrs, velmag)
title('Magnitude of Velocity of Sat#1vs. Time(hrs)','fontsize',16,'fontweight','bold')



% Start Code for second satellite with different drag characteristics
%%%%%%%%%%%%%%%%%%%%%%%%%%%%%%%%%%%%%%%%%
%%%%%%%%%%%%%%%%%%%%%%%%%
% The in plane formation

[t2,state2]=ode45(@twobody2,[t_vec],stateplane0,options);

staterad2 = state2(:,1:3);
statevel2 = state2(:,4:6);

statevellength2 = length(statevel2);


%Initialize period vector
Pvector2=zeros(statevellength,1);

%Initialize RTN velocity vector
RTNstatevel2=zeros(statevellength,3);

%Initialize true anomaly vector (ta)
ta2=zeros(statevellength,1);

%Initialize RTN position vector
relposRTN=zeros(statevellength,3);

%Initialize relative position vector
relative_position=zeros(statevellength,3);

for i=1:statevellength2
   velmag2(i)=norm(statevel2(i,:));
   radmag2(i)=norm(staterad2(i,:));

   Pvector2(i,:)=sqrt((4*(pi^2)*(radmag2(i)*1000)^3) / (G*MassEarth));

   % Determine the true anomaly by dividing time by period
   % Then divide remainder by period and multiply by 2pi

   ta2(i)=(rem(t_vec(i),Pvector2(i))/Pvector2(i))*2*pi;
```

```
   ECItoRTN2 = [(cos(Sat_ArgPeri + ta2(i))*cos(Sat_RAAN))-(sin(Sat_ArgPeri +
ta2(i))*cos(Sat_Inc)*sin(Sat_RAAN)),...
   cos(Sat_ArgPeri + ta2(i)) * sin(Sat_RAAN) + sin(Sat_ArgPeri + ta2(i)) *
cos(Sat_Inc)* cos(Sat_RAAN),...
   sin(Sat_ArgPeri + ta2(i)) * sin(Sat_Inc);...
   -sin(Sat_ArgPeri + ta2(i)) * cos(Sat_RAAN) - cos(Sat_ArgPeri + ta2(i)) *
cos(Sat_Inc)* sin(Sat_RAAN),...
   -sin(Sat_ArgPeri + ta2(i)) * sin(Sat_RAAN) + cos(Sat_ArgPeri + ta2(i)) *
cos(Sat_Inc) * cos(Sat_RAAN),...
   cos(Sat_ArgPeri + ta2(i)) * sin(Sat_Inc);...
   sin(Sat_Inc) * sin(Sat_RAAN),...
   -sin(Sat_Inc) * cos(Sat_RAAN),...
   cos(Sat_Inc)];

   RTNstatevel2(i,:)= ECItoRTN2*statevel2(i,:)';
   RTNvelmag2(i)=norm(RTNstatevel2(i,:));
   RTNveldiff2(i)=velmag2(i)-RTNvelmag2(i);  % To keep the origin around sat 1 do it
this way

   relative_position(i,:)=staterad2(i,:)-staterad(i,:);
   relposRTN(i,:)=ECItoRTN2*relative_position(i,:)';
end


timehrs2=t2/3600;


figure(3)
plot(timehrs2, relposRTN(:,1))
title('Radial Direction In-Plane ', 'fontsize',16,'fontweight','bold')
xlabel('Time (hours)')
ylabel('Kilometers')
%gtext({'Deputy area = 1.5m^2', 'Control area = 2m^2'})

figure(4)
plot(timehrs2, relposRTN(:,2))
title('Tangential Direction In-Plane','fontsize',16,'fontweight','bold')
xlabel('Time (hours)')
ylabel('Kilometers')
%gtext({'Deputy area = 1.5m^2', 'Control area = 2m^2'})

figure(5)
relative_position=state2(:,1:3)-state(:,1:3);
plot3(relative_position(:,1),relative_position(:,2),relative_position(:,3))
xlabel('x', 'fontsize',16,'fontweight','bold')
ylabel('Y', 'fontsize',16,'fontweight','bold')
```

```
zlabel('Z', 'fontsize',16,'fontweight','bold')
axis('equal')
title('Relative position','fontsize',16,'fontweight','bold')


figure(6)
plot(timehrs2, relposRTN(:,3))
title('Normal Direction In-Plane ', 'fontsize',16,'fontweight','bold')
xlabel('Time (hours)')
ylabel('Kilometers')
%gtext({'Deputy area = 1.5m^2', 'Control area = 2m^2'})

for i=1:statevellength2
absdist(i) = norm(relposRTN(i,:));
end

% Plots the separation between the two in-plane satellites
figure(19)
plot(timehrs, absdist)
title('Separation Between Satellites(In-Plane)', 'fontsize',16,'fontweight','bold')
xlabel('Time (hours)')
ylabel('Kilometers')
%gtext({'Deputy area = 1.5m^2', 'Control area = 2m^2'})

% Start Code for satellite in an in-track orbit
% with different drag characteristics
%%%%%%%%%%%%%%%%%%%%%%%%%%%%%%%%%%%%%%%%%%%%%%%%%%%%%%%%%%%%%%%%%%%%%%%%%%%%%

[t3,state3]=ode45(@twobody3,[t_vec],statetrack0,options);

staterad3 = state3(:,1:3);
statevel3 = state3(:,4:6);

statevellength = length(statevel3);

%Initialize momentum vector
Hvector3=zeros(statevellength,3);

%Initialize period vector
Pvector3=zeros(statevellength,1);

%Initialize RTN velocity vector
RTNstatevel3=zeros(statevellength,3);

%Initialize true anomaly vector (ta)
```

```
ta3=zeros(statevellength,1);

%Initialize RTN position vector
relposRTN3=zeros(statevellength,3);

%Initialize relative position vector
relative_position3=zeros(statevellength,3);

for i=1:statevellength
   velmag3(i)=norm(statevel3(i,:));
   radmag3(i)=norm(staterad3(i,:));
   Hvector3(i,:)=cross(staterad3(i,:), statevel3(i,:));
   eccen3(i,:)=(1/mu)*(cross(statevel3(i,:), Hvector3(i,:))-mu*staterad3(i,:)/radmag3(i));

   Pvector3(i,:)=sqrt((4*(pi^2)*(radmag3(i)*1000)^3) / (G*MassEarth));

   % Determine the true anomaly by dividing time by period
   % Then divide remainder by period and multiply by 2pi

   ta3(i)=(rem(t_vec(i),Pvector3(i))/Pvector3(i))*2*pi;

   ECItoRTN3 = [(cos(Sat_ArgPeri + ta3(i))*cos(intrack_RAAN))-(sin(Sat_ArgPeri +
ta3(i))*cos(Sat_Inc)*sin(intrack_RAAN)),...
   cos(Sat_ArgPeri + ta3(i)) * sin(intrack_RAAN) + sin(Sat_ArgPeri + ta3(i)) *
cos(Sat_Inc)* cos(intrack_RAAN),...
   sin(Sat_ArgPeri + ta3(i)) * sin(Sat_Inc);...
   -sin(Sat_ArgPeri + ta3(i)) * cos(intrack_RAAN) - cos(Sat_ArgPeri + ta3(i)) *
cos(Sat_Inc)* sin(intrack_RAAN),...
   -sin(Sat_ArgPeri + ta3(i)) * sin(intrack_RAAN) + cos(Sat_ArgPeri + ta3(i)) *
cos(Sat_Inc) * cos(intrack_RAAN),...
   cos(Sat_ArgPeri + ta3(i)) * sin(Sat_Inc);...
   sin(Sat_Inc) * sin(intrack_RAAN),...
   -sin(Sat_Inc) * cos(intrack_RAAN),...
   cos(Sat_Inc)];

   RTNstatevel3(i,:)= ECItoRTN3*statevel3(i,:)';
   RTNvelmag3(i)=norm(RTNstatevel3(i,:));
   RTNveldiff3(i)=velmag3(i)-RTNvelmag3(i);  % To keep the origin around sat 1 do it
this way

   relative_position3(i,:)=staterad3(i,:)-staterad(i,:);
   relposRTN3(i,:)=ECItoRTN3*relative_position3(i,:)';
end

timehrs3=t3/3600;
```

```
figure(7)
plot3(relposRTN3(:,1),relposRTN3(:,2),relposRTN3(:,3))
title('In-Track 3-D', 'fontsize',16,'fontweight','bold')
xlabel('Radial Direction (Kilometers)')
ylabel('Tangential Direction (Kilometers)')
zlabel('Normal Direction (Kilometers)')

figure(8)
plot(timehrs3, relposRTN3(:,1))
title('Radial Direction In-Track', 'fontsize',16,'fontweight','bold')
xlabel('Time (hours)')
ylabel('Kilometers')
%gtext({'Deputy area = 1.5m^2', 'Control area = 2m^2'})

figure(9)
plot(timehrs3, relposRTN3(:,2))
title('Tangential Direction In-Track', 'fontsize',16,'fontweight','bold')
xlabel('Time (hours)')
ylabel('Kilometers')
%gtext({'Deputy area = 1.5m^2', 'Control area = 2m^2'})

figure(10)
plot(timehrs3, relposRTN3(:,3))
axis([0 10 -0.1 0.1])
title('Normal Direction In-Track', 'fontsize',16,'fontweight','bold')
xlabel('Time (hours)')
ylabel('Kilometers')
%gtext({'Deputy area = 1.5m^2', 'Control area = 2m^2'})

%%%%%%%%%%%%%%%%%%%%%%%%%%%%%%%%%%%%%%%%%%%%%%%%%%
%%%%%%%%%%%
%  Start code for satellite in a circular formation  %
%%%%%%%%%%%%%%%%%%%%%%%%%%%%%%%%%%%%%%%%%%%%%%%%%%
%%%%%%%%%%%

% Start determining characteristics of a satellite in a circular formation
% with the reference satellite.  All values are originally in an RTN
% coordinate system with the reference satellite at the origin

% distance (km) between reference satellite (master) and slave satellite

r0circ = 1;

% Mean motion is needed for the equations and we know that the two orbits
% must have the same semi-major axis or their orbits would diverge very
% quickly
```

```
ncirc = sqrt(mu/Sat_SemiMajor^3);

% use equations 24-28 in Sabol paper to determine the other initial
% conditions

ynot = 0;
xnot = 0.5;
znot = xnot * sqrt(3);
ydotcirc = -0.0005850427710543116;
xdotcirc = ynot*ncirc/2;
zdotcirc = sqrt(3)*xdotcirc;              % Use positive because slave is at apogee

% Change the difference in position and velocity of the two satellites from
% RTN coords to ECI coords

diffcircpos0RTN = [xnot, ynot, znot]
diffcircvel0RTN = [xdotcirc, ydotcirc, zdotcirc]

% RTNtoECI = ECItoRTN';
RTNtoECI=[1 0 0;0 0 -1;0 1 0];

diffcircpos0ECI = RTNtoECI * diffcircpos0RTN';
diffcircvel0ECI = RTNtoECI * diffcircvel0RTN';
statecircpos0ECI = diffcircpos0ECI + r0;

statecircvel0ECI = diffcircvel0ECI + v0;

[t4,state4]=ode45(@twobody4,[t_vec],statecirc0,options);

staterad4 = state4(:,1:3);
statevel4 = state4(:,4:6);

statevellength = length(statevel4);

%Initialize period vector
Pvector4=zeros(statevellength,1);

%Initialize RTN velocity vector
RTNstatevel4=zeros(statevellength,3);

%Initialize true anomaly vector (ta)
ta4=zeros(statevellength,1);

%Initialize RTN position vector
relposRTN4=zeros(statevellength,3);
```

```
%Initialize relative position vector
relative_position4=zeros(statevellength,3);

for i=1:statevellength
   velmag4(i)=norm(statevel4(i,:));
   radmag4(i)=norm(staterad4(i,:));

   Pvector4(i,:)=sqrt((4*(pi^2)*(radmag4(i)*1000)^3) / (G*MassEarth));

   % Determine the true anomaly by dividing time by period
   % Then divide remainder by period and multiply by 2pi

   ta4(i)=(rem(t_vec(i),Pvector4(i))/Pvector4(i))*2*pi;

   e_r_hat = staterad4(i,:)/norm(staterad4(i,:));
   e_n = cross(staterad4(i,:),statevel4(i,:));
   e_n_hat = e_n/norm(e_n);
   e_t_hat = cross(e_n_hat,e_r_hat);

   ECItoRTN4 = [e_r_hat; e_t_hat; e_n_hat];

   RTNstatevel4(i,:) = ECItoRTN4*statevel4(i,:)';

   relative_position4(i,:)=staterad4(i,:)-staterad(i,:);
   relposRTN4(i,:)=ECItoRTN4*relative_position4(i,:)';

   energy4(i) = 0.5*norm(statevel4(i,:))^2 - mu/norm(staterad4(i,:));
end


timehrs4=t4/3600;

figure(11)
plot3(relposRTN4(:,1),relposRTN4(:,2),relposRTN4(:,3))
title('Circular 3-D', 'fontsize',16,'fontweight','bold')
xlabel('Radial Direction (Kilometers)')
ylabel('Tangential Direction (Kilometers)')
zlabel('Normal Direction (Kilometers)')

figure(12)
plot(timehrs4, relposRTN4(:,1))
axis([0 100 -0.8 0.8])
title('Radial Direction Circular', 'fontsize',16,'fontweight','bold')
xlabel('Time (hours)')
ylabel('Kilometers')
```

```
gtext({'Deputy area = 1.5m^2', 'Control area = 2m^2'})

figure(13)
plot(timehrs4, relposRTN4(:,2))
axis([0 100 -1.8 1.8])
title('Tangential Direction Circular', 'fontsize',16,'fontweight','bold')
xlabel('Time (hours)')
ylabel('Kilometers')
gtext({'Deputy area = 1.5m^2', 'Control area = 2m^2'})

figure(14)
plot(timehrs4, relposRTN4(:,3))
axis([0 100 -1.4 1.4])
title('Normal Direction Circular', 'fontsize',16,'fontweight','bold')
xlabel('Time (hours)')
ylabel('Kilometers')
gtext({'Deputy area = 1.5m^2', 'Control area = 2m^2'})


end % main program

function statedot=twobody(t,state)
% Equations of motion
% for two-body orbital motion
% does not account for any perturbations
%
% States:
% Cartesian Position (states 1-3)
% Cartesian Velocity (states 4-6)

Earth_Radius = 6378.1;

%  Earth Gravitational Parameter (km^3/sec^2)
mu = 3.98601e5;

% Magnitude of the radius vector
r = sqrt(state(1)^2 + state(2)^2 + state(3)^2);

% Magnitude of the velocity vector
v = sqrt(state(4)^2 + state(5)^2 + state(6)^2);


% All stuff I'm adding for drag
% for a height of 250 km, (Table on 537 Vallado)
hellp = r - Earth_Radius;          % in km
h0 = 200;                          % in km
```

```
H = 37.105;                    % in km
rho0 = 2.789e-11;              % in kg/m^3

% compute the atmospheric density (rho) in kg/m^3
% rho = rho0 * exp(-(hellp-h0)/H);
rho = rho0 * exp(-(r-6378.1-h0)/H);

A = 2;            % area in m^2 of a 2m x 2m satellite
Cd = 2.2 ;        % Normal value for coefficient of drag
mass = 100;       % in kg

B = (Cd*A)/mass;


% Equations of motion
% Since the satellite is in a polar orbit drag will only be affecting it in
% two dimensions

% multiplying the total Accel of drag times the unit vector in the
% desired direction gives the desired Ad component

statedot(1:3) = state(4:6);
statedot(4) = -(mu/r^3)*state(1) - (1/2*B*rho*v^2*state(4)/v);
statedot(5) = -(mu/r^3)*state(2) - (1/2*B*rho*v^2*state(5)/v);
statedot(6) = -(mu/r^3)*state(3) - (1/2*B*rho*v^2*state(6)/v);

statedot=statedot';


end % twobody function

function statedot2=twobody2(t2,state2)
% Equations of motion
% for two-body orbital motion
% does not account for any perturbations
%
% States:
% Cartesian Position (states 1-3)
% Cartesian Velocity (states 4-6)

Earth_Radius = 6378.1;

%  Earth Gravitational Parameter (km^3/sec^2)
mu = 3.98601e5;

% Magnitude of the radius vector
```

```
r2 = sqrt(state2(1)^2 + state2(2)^2 + state2(3)^2);

% Magnitude of the velocity vector
v2 = sqrt(state2(4)^2 + state2(5)^2 + state2(6)^2);


% All stuff I'm adding for drag
% for a height of 250 km, (Table on 537 Vallado)
hellp = r2 - Earth_Radius;          % in km
h0 = 200;                          % in km
H = 37.105;                         % in km
rho0 = 2.789e-11;                   % in kg/m^3

% compute the atmospheric density (rho) in kg/m^3
% rho = rho0 * exp(-(hellp-h0)/H);
rho2 = rho0 * exp(-(r2-6378.1-h0)/H);

A2 = 1.5;           % area in m^2 of a 2m x 2m satellite
Cd2 = 2.2;          % Normal value for coefficient of drag
mass2 = 100;        % in kg

B2 = (Cd2*A2)/mass2;


% Equations of motion
% Since the satellite is in a polar orbit drag will only be affecting it in
% two dimensions

% multiplying the total Accel of drag times the unit vector in the
% desired direction gives the desired Ad component

statedot2(1:3) = state2(4:6);
statedot2(4) = -(mu/r2^3)*state2(1) - (1/2*B2*rho2*v2^2*state2(4)/v2);
statedot2(5) = -(mu/r2^3)*state2(2) - (1/2*B2*rho2*v2^2*state2(5)/v2);
statedot2(6) = -(mu/r2^3)*state2(3) - (1/2*B2*rho2*v2^2*state2(6)/v2);

statedot2=statedot2';


end % twobody2 function

function statedot3=twobody3(t3,state3)
% Equations of motion
% for two-body orbital motion
% does not account for any perturbations
%
```

```
% States:
% Cartesian Position (states 1-3)
% Cartesian Velocity (states 4-6)


Earth_Radius = 6378.1;

%  Earth Gravitational Parameter (km^3/sec^2)
mu = 3.98601e5;

% Magnitude of the radius vector
r3 = sqrt(state3(1)^2 + state3(2)^2 + state3(3)^2);

% Magnitude of the velocity vector
v3 = sqrt(state3(4)^2 + state3(5)^2 + state3(6)^2);


% All stuff I'm adding for drag
% for a height of 250 km, (Table on 537 Vallado)
hellp = r3 - Earth_Radius;          % in km
h0 = 200;                       % in km
H = 37.105;                      % in km
rho0 = 2.789e-11;                  % in kg/m^3

% compute the atmospheric density (rho) in kg/m^3
% rho = rho0 * exp(-(hellp-h0)/H);
rho3 = rho0 * exp(-(r3-6378.1-h0)/H);

A3 = 1.5;           % area in m^2 of a 2m x 2m satellite
Cd3 = 2.2 ;         % Normal value for coefficient of drag
mass3 = 100;        % in kg

B3 = (Cd3*A3)/mass3;


% Equations of motion
% Since the satellite is in a polar orbit drag will only be affecting it in
% two dimensions

% multiplying the total Accel of drag times the unit vector in the
% desired direction gives the desired Ad component

statedot3(1:3) = state3(4:6);
statedot3(4) = -(mu/r3^3)*state3(1) - (1/2*B3*rho3*v3^2*state3(4)/v3);
statedot3(5) = -(mu/r3^3)*state3(2) - (1/2*B3*rho3*v3^2*state3(5)/v3);
statedot3(6) = -(mu/r3^3)*state3(3) - (1/2*B3*rho3*v3^2*state3(6)/v3);
```

```
statedot3=statedot3';


end % twobody3 function


function statedot4=twobody4(t4,state4)
% Equations of motion
% for two-body orbital motion
% does not account for any perturbations
%
% States:
%
% Cartesian Position (states 1-3)
% Cartesian Velocity (states 4-6)
%

Earth_Radius = 6378.1;

%  Earth Gravitational Parameter (km^3/sec^2)
mu = 3.98601e5;

% Magnitude of the radius vector
r4 = sqrt(state4(1)^2 + state4(2)^2 + state4(3)^2);

% Magnitude of the velocity vector
v4 = sqrt(state4(4)^2 + state4(5)^2 + state4(6)^2);


% All stuff I'm adding for drag
% for a height of 250 km, (Table on 537 Vallado)
hellp = r4 - Earth_Radius;          % in km
h0 = 200;                       % in km
H = 37.105;                       % in km
rho0 = 2.789e-11;                   % in kg/m^3

% compute the atmospheric density (rho) in kg/m^3
% rho = rho0 * exp(-(hellp-h0)/H);
rho4 = rho0 * exp(-(r4-6378.1-h0)/H);

A4 = 1.5;           % area in m^2 of a 2m x 2m satellite
Cd4 = 2.2;          % Normal value for coefficient of drag
mass4 = 100;        % in kg

B4 = (Cd4*A4)/mass4;
```

```
% Equations of motion
% Since the satellite is in a polar orbit drag will only be affecting it in
% two dimensions

% multiplying the total Accel of drag times the unit vector in the
% desired direction gives the desired Ad component

statedot4(1:3) = state4(4:6);
statedot4(4) = -(mu/r4^3)*state4(1) - (1/2*B4*rho4*v4^2*state4(4)/v4);
statedot4(5) = -(mu/r4^3)*state4(2) - (1/2*B4*rho4*v4^2*state4(5)/v4);
statedot4(6) = -(mu/r4^3)*state4(3) - (1/2*B4*rho4*v4^2*state4(6)/v4);

statedot4=statedot4';


end % twobody4 function


function [r,v]=posvel(a,e,inc,Omg,w,nu,mu)
%compute position and velocity vectors from classical orbital elements
% [r,v]=posvel(a, e, inc, Omg, w, nu,mu)
% Input all angles in radians
% r and v output in IJK unit vectors
%
% if mu is not present, assume canonical units
%
% CIRCULAR ORBIT
% if e=0 and inc~=0, w is not used and nu is assumed to be argument of
% latitude (u0)
%
% EQUATORIAL ORBIT
% if inc=0, Omg is not used and w is assumed to be Longitude of Periapsis
% (PI)
%
% CIRCULAR, EQUATORIAL ORBIT
% if e=0 and inc=0, Omg and w are not used and nu is assumed to be True
% longitude (l0)
%
if nargin<6
   display('Not enough input parameters')
end
if nargin==6
   mu=1;
   display('Assuming Canonical Units with Mu=1.0')
```

```
end

if e==0 & inc~=0
   w=0.0;
   disp('Circular Orbit, Argument of Latitude substituted for True Anomaly')
end

if e~=0 & inc==0
   Omg=0.0;
   disp('Equatorial Orbit, Longitude of Periapsis substituted for Argument of Perigee')
end

if e==0 & inc==0
   w=0;
   Omg=0;
   disp('Circular, Equatorial Orbit, True Longitude substituted for True anomaly')
end

% Compute orbit parameter (p)

p=a*(1-e^2);

% Compute Position and Velocity Vectors in Perifocal Coordinate System

rp = zeros(3,1);
rp(1) = p*cos(nu)/(1+e*cos(nu));
rp(2) = p*sin(nu)/(1+e*cos(nu));

vp = zeros(3,1);
vp(1) = -sqrt(mu/p)*sin(nu);
vp(2) = sqrt(mu/p)*(e + cos(nu));

% Rotate from Perifocal Coordinate System to IJK system

% Rotation matrix for -w angle rotation about axis normal to orbit plane

Rw = [cos(-w) sin(-w) 0; -sin(-w) cos(-w) 0; 0 0 1];

% Rotation Matrix for -inc angle rotation about first axis (periapsis
% direction in PQW, which should be aligned with node direction after
% rotation above)

Ri = [1 0 0; 0 cos(-inc) sin(-inc); 0  -sin(-inc)  cos(-inc)];

% Rotation Matrix for -Omg angle rotation about third axis (normal to orbit
% plane, which should be aligned with K after both rotations above)
```

```
RO = [cos(-Omg) sin(-Omg) 0; -sin(-Omg) cos(Omg) 0; 0 0 1];

% Compute Position and Velocity in IJK by rotation vectors in PQW coord

r = RO*Ri*Rw*rp;

v = RO*Ri*Rw*vp;


end % posvel function
```

Appendix B - Controller Code

The following code was written and executed using MATLAB version 7.0.

```
function []=orbit_propagator()

%  Simulation of a satellite in orbit with two-body motion and drag


global variable

variable.time = [];
variable.area = [];

% Initial and Final Time (seconds)
t0 = 0;
tf = 1800000;  % 10 hours = 36000;  1000 hours = 3600000

t_vec=t0:10:tf;

% Constants

% Earth Gravitational Parameter (km^3/sec^2)

mu = 3.98601e5;

% Initial Satellite Orbital Parameters

% Orbit Altitude (Kilometers)

Sat_Alt = 250;

Earth_Radius = 6378.1;

% Rotational rate of Earth (rad/s)

Earth_rate = 7.2722e-5; % corresponds to 15 degrees/hour .. expressed in rad/s

Sat_SemiMajor = Earth_Radius + Sat_Alt;  % Compute Semimajor Axis

% Orbit Eccentricity

Sat_Ecc = 0;  % Eccentricity

% Orbit Inclination (radians)
```

```
Sat_Inc = pi/2;

% Right Acsension of Ascending Node (radians)
%    Angle between vernal equinox direction and  point at which the satellite passes
%    the equator going north

Sat_RAAN = 0;

% Argument of Perigee (radians)
% Argument of Perigee undefined for circular orbit, assume zero as placeholder

Sat_ArgPeri = 0;

% Argument of Latitude at epoch (radians)
%    Angle between the ascending node direction and the satellite position vector
%    at the start time of the sim

Sat_ArgLat = 0;

% Argument of Latitude at epoch (radians)
%    For an in-plane satellite that is approximately 1 km behind the
%    control satellite.  Calculation 2pi*radius of orbit = circum of orbit
%    circum of orbit/2pi, then find how many radians for 1 km separation.

PSat_ArgLat = 2*pi - 0.000150873;

% Earth Rotational Position (radians)
%    Angle between prime meridian and vernal equinox direction at start time of sim.
%    This is an arbitrary assignment unless we want sim time to have some real meaning
%    with respect to a true astronomical time system

Earth_Pos = 0;

% The in-track formation has satellites that occupy the same ground track.
% The deputy satellite starts off 1 Km behind the control and in a
% slightly different track.
% This is accomplished by offsetting their RAAN by:


Period_initial = sqrt((4*(pi^2)*(Sat_SemiMajor)^3) / mu);

intrack_RAAN = (2*pi-PSat_ArgLat)/(2*pi) * Period_initial * Earth_rate

% Degree to Rad Conversion and reverse

degtorad = pi/180;
```

```
radtodeg = 180/pi;

% Convert Initial Orbit Parameters to
% Cartesian Position and Velocity
% Uses "posvel" function given at end of this code

[r0,v0] = posvel(Sat_SemiMajor, Sat_Ecc, Sat_Inc, Sat_RAAN, Sat_ArgPeri,
Sat_ArgLat, mu);

[r0plane, v0plane] = posvel(Sat_SemiMajor, Sat_Ecc, Sat_Inc, Sat_RAAN, Sat_ArgPeri,
PSat_ArgLat, mu);

[r0track, v0track] = posvel(Sat_SemiMajor, Sat_Ecc, Sat_Inc, intrack_RAAN,
Sat_ArgPeri, PSat_ArgLat, mu);


%%%%%%%%%%%%%%%%%%%%%%%%%%%%%%%%%%%%%%%%%%%%%%%%%%%%%%%%%%%%%%%%%%%%%%%%
% %%%%%%% Start code for satellite in a circular formation
%%%%%%%%%%%%
%%%%%%%%%%%%%%%%%%%%%%%%%%%%%%%%%%%%%%%%%%%%%%%%%%%%%%%%%%%%%%%%%%%%%%%%

% Start determining characteristics of a satellite in a circular formation
% with the reference satellite.  All values are originally in an RTN
% coordinate system with the reference satellite at the origin

% Choose the separation in the normal direction to be 0.5km

% Mean motion is needed for the equations and we know that the two orbits
% must have the same semi-major axis or their orbits would diverge very
% quickly

ncirc = sqrt(mu/Sat_SemiMajor^3);

% use equations 24-28 in Sabol paper to determine the other initial
% conditions as follows

ynot = 0;
xnot = 0.5;
znot = xnot * sqrt(3);
ydotcirc = -0.0005850427710543116;          %  for a 1 km separation
xdotcirc = ynot*ncirc/2;
zdotcirc = sqrt(3)*xdotcirc;                % Use positive because slave is at apogee
```

```
diffcircpos0RTN = [xnot, ynot, znot];
diffcircvel0RTN = [xdotcirc, ydotcirc, zdotcirc];

% RTNtoECI = ECItoRTN';
RTNtoECI=[1 0 0;0 0 -1;0 1 0];

diffcircpos0ECI = RTNtoECI * diffcircpos0RTN';
diffcircvel0ECI = RTNtoECI * diffcircvel0RTN';

r0circular = diffcircpos0ECI + r0;
v0circular = diffcircvel0ECI + v0;



% r0circular=[xnot;ynot;znot];
% v0circular=[xdotcirc;ydotcirc;zdotcirc];


%!!!!!!!!!!!!!!!!!!!!!!!!!!!!!!!!!!!!!!!!!!!!!!!!!!!!!!!!!!!!!!!!!!!!!!!!!!!!!!!!!!!!!!!!!!!!!!!!!!!!
!!!!!!!!!!%
% Choose the type of formation you want to analyze here, and comment out
% the othere initial conditions for the different formations     %%%%%%%%%%
state0=[r0;v0;r0plane;v0plane;0];  % Set to look at two in-plane satellites
%state0=[r0;v0;r0track;v0track;0];  % Set to look at two in-track satellites
%state0=[r0;v0;r0circular;v0circular;0];   %Set to look at two circular formation sats

% Note there is a 13th state above.  This state is going to
% integrate the difference in orbital energy and is part of the controller
%!!!!!!!!!!!!!!!!!!!!!!!!!!!!!!!!!!!!!!!!!!!!!!!!!!!!!!!!!!!!!!!!!!!!!!

% Propagate satellite position using two-body orbit assumptions
% Uses ode45 numerical integrator and
% "twobody_wdrag" function given at end of this code

% Set max stepsize for integration.  I chose a number that
% gives quick results without losing too much accuracy
% over a 10 hour period of propagation

options = odeset('MaxStep',50);

[t,state]=ode45(@twobody_wdrag,[t_vec],state0,options);

statelength = length(state);

staterad1 = state(:,1:3)';
statevel1 = state(:,4:6)';
```

```
staterad2 = state(:,7:9)';
statevel2 = state(:,10:12)';

d_pos = zeros(statelength,3);
d_vel = zeros(statelength,3);

for i=1:statelength

   e_r_hat = staterad1(:,i)/norm(staterad1(:,i));
   e_n = cross(staterad1(:,i),statevel1(:,i));
   e_n_hat = e_n/norm(e_n);
   e_t_hat = cross(e_n_hat,e_r_hat);

   ECItoRTN = [e_r_hat, e_t_hat, e_n_hat]';

%    RTNstatevel(i,:)= ECItoRTN*statevel(i,:)';
%    RTNvelmag(i)=norm(RTNstatevel(i,:));
%    RTNdiff(i)=velmag(i)-RTNvelmag(i);


d_pos(i,:) = ECItoRTN*(staterad2(:,i) - staterad1(:,i));
d_vel(i,:) = ECItoRTN*(statevel2(:,i) - statevel1(:,i));

d_energy(i) = 0.5*norm(staterad2(:,i))^2 - mu/norm(staterad2(:,i)) - ...
          0.5*norm(staterad1(:,i))^2 + mu/norm(staterad1(:,i));

end

timehrs=t/3600;

figure(1)
plot(timehrs,d_energy)

figure(2)
plot(d_pos(:,1),d_pos(:,2))
%axis([-0.001 0.001 -1.001 -.999])        %In-Plane parameters
title('Tangential vs. Radial Separation In-Plane ', 'fontsize',16,'fontweight','bold')
xlabel('Radial Separation (Km)')
ylabel('Tangential Separation (Km)')

figure(3)
plot(timehrs,d_pos)

figure(4)
plot3(d_pos(:,1),d_pos(:,2),d_pos(:,3))
xlabel('Radial Separation (Km)')
```

```
ylabel('Tangential Separation (Km)')
zlabel('Normal Separation (Km)')

figure(5)
plot(timehrs, d_pos(:,1))
title('Radial Direction In-Plane ', 'fontsize',16,'fontweight','bold')
axis([0 500 -10e-4 8e-4])          %In-Plane parameters
xlabel('Time (hours)')
ylabel('Kilometers')
gtext({'Deputy area = 1.5m^2', 'Control area = 2m^2'})
gtext({'kP = 15','kI = 2'})

figure(6)
plot(timehrs, d_pos(:,2))
title('Tangential Direction In-Plane ', 'fontsize',16,'fontweight','bold')
axis([0 500 -1.7 -0.5])           %In-Plane parameters
xlabel('Time (hours)')
ylabel('Kilometers')
gtext({'Deputy area = 1.5m^2', 'Control area = 2m^2'})
gtext({'kP = 15','kI = 2'})

figure(7)
plot(timehrs, d_pos(:,3))
title('Normal Direction In-Plane ', 'fontsize',16,'fontweight','bold')
%axis([0 500 -1.5 1.5])
xlabel('Time (hours)')
ylabel('Kilometers')
gtext({'Deputy area = 1.5m^2', 'Control area = 2m^2'})
gtext({'kP = 15','kI = 2'})

figure(8)
plot(variable.time/3600, variable.area)
title('Cross Sectional Area vs. Time', 'fontsize',16,'fontweight','bold')
xlabel('Time (hours)')
ylabel('Square Meters')
gtext({'Initial Conditions', 'Deputy area = 1.5m^2', 'Control area = 2m^2'})
gtext({'kP = 15','kI = 2'})


end % main program



function statedot=twobody_wdrag(t,state)
% Equations of motion
% for two-body orbital motion
```

```
% and adds drag plus a drag controller
%
% States:
%
% Satellite 1 Position (states 1-3)
% Satellite 1 Velocity (states 4-6)
% Satellite 2 Position (states 7-9)
% Satellite 2 Velocity (states 10-12)
% State 13 used for controller


global variable

%  Earth Gravitational Parameter (km^3/sec^2)
mu = 3.98601e5;

Earth_Radius = 6378.1; % kilometers


% Magnitude of the radius vector (sat 1)
r1 = sqrt(state(1)^2 + state(2)^2 + state(3)^2);

% Magnitude of the velocity vector (sat1)
v1 = sqrt(state(4)^2 + state(5)^2 + state(6)^2);

% Magnitude of the radius vector (sat 2)
r2 = sqrt(state(7)^2 + state(8)^2 + state(9)^2);

% Magnitude of the velocity vector (sat 2)
v2 = sqrt(state(10)^2 + state(11)^2 + state(12)^2);

% Drag Modeling
% for a height of 250 km, (Table on 537 Vallado)
% atmospheric density is based on satellite 1 altitude
hellp = r1 - Earth_Radius;          % in km
h0 = 200;                       % in km
H = 37.105;                       % in km
rho0 = 2.789e-11;                   % in kg/m^3

% Drag Modeling
% for a height of 250 km, (Table on 537 Vallado)
% atmospheric density is based on satellite 2 altitude
hellp2 = r2 - Earth_Radius;         % in km
h0 = 200;                       % in km
H = 37.105;                       % in km
rho0 = 2.789e-11;                   % in kg/m^3
```

```
% compute the atmospheric density (rho) in kg/m^3
% rho = rho0 * exp(-(hellp-h0)/H);
rho = rho0 * exp(-(r1-6378.1-h0)/H);

% compute the atmospheric density (rho) in kg/m^3
% rho = rho0 * exp(-(hellp-h0)/H);
rho2 = rho0 * exp(-(r2-6378.1-h0)/H);

% Compute Ballistic Coefficient for satelite one
A0 = 1.5;            % nominal area in m^2 of a micro satellite
dA1 = 0.5;           % delta-area (from damaged satellite, for example)
Cd = 2.2;            % Guesstimate for coefficient of drag
mass = 100;          % in kg
A1=A0+dA1;
B1 = (Cd*A1)/mass;    % ballistic coefficient


%--------- Controller  ------------------------
%
% Simple controller based on the period (energy) difference between the two
% satellites.  Computes Specific Mechanical Energy for both spacecraft and
% then assigns an Area for satellite two that is proportional to the energy
% difference.  If energy of satellite two is greater than satellite one,
% increase the Area of satellite two, increasing drag, and lowering energy.

% Compute Energy Difference

E1 = 0.5*v1^2 - mu/r1;

E2 = 0.5*v2^2 - mu/r2;

delta_E = E2-E1;

% Set second sat area

kP = 15;  %1.5e5;   %initial value  % Proportional Controller Gain----------------------------
-
kI = 2; % 2e4; %initial value % Integral Controller Gain-------------------------

A2 = A0 + kP*delta_E + kI*state(13);

variable.time = [variable.time t];
variable.area = [variable.area A2];
```

```
B2 = (Cd*A2)/mass;  % ballistic coefficient


% Equations of motion
% Since the satellite is in a polar orbit drag will only be affecting it in
% two dimensions

% multiplying the total Accel of drag times the unit vector in the
% desired direction gives the desired Ad component

statedot(1:3) = state(4:6);
statedot(4) = -(mu/r1^3)*state(1) - (1/2*B1*rho*v1*state(4));
statedot(5) = -(mu/r1^3)*state(2) - (1/2*B1*rho*v1*state(5));
statedot(6) = -(mu/r1^3)*state(3) - (1/2*B1*rho*v1*state(6));

statedot(7:9) = state(10:12);
statedot(10) = -(mu/r2^3)*state(7) - (1/2*B2*rho*v2*state(10));
statedot(11) = -(mu/r2^3)*state(8) - (1/2*B2*rho*v2*state(11));
statedot(12) = -(mu/r2^3)*state(9) - (1/2*B2*rho*v2*state(12));
statedot(13) = delta_E;    % This state is needed for the integral control

statedot=statedot';

end % twobody_wdrag function


function [r,v]=posvel(a,e,inc,Omg,w,nu,mu)
%compute position and velocity vectors from classical orbital elements
% [r,v]=posvel(a, e, inc, Omg, w, nu,mu)
% Input all angles in RADIANS
% r and v output in IJK unit vectors
%
% if mu is not present, assume canonical units
%
% CIRCULAR ORBIT
% if e=0 and inc~=0, w is not used and nu is assumed to be argument of
% latitude (u0)
%
% EQUATORIAL ORBIT
% if inc=0, Omg is not used and w is assumed to be Longitude of Periapsis
% (PI)
%
% CIRCULAR, EQUATORIAL ORBIT
% if e=0 and inc=0, Omg and w are not used and nu is assumed to be True
% longitude (l0)
%
```

```
if nargin<6
   display('Not enough input parameters')
end
if nargin==6
   mu=1;
   display('Assuming Canonical Units with Mu=1.0')
end

degtorad = pi/180;

if e==0 & inc~=0
   w=0.0;
   disp('Circular Orbit, Argument of Latitude substituted for True Anomaly')
end

if e~=0 & inc==0
   Omg=0.0;
   disp('Equatorial Orbit, Longitude of Periapsis substituted for Argument of Perigee')
end

if e==0 & inc==0
   w=0;
   Omg=0;
   disp('Circular, Equatorial Orbit, True Longitude substituted for True anomaly')
end

% Compute orbit parameter (p)

p=a*(1-e^2);

% Compute Position and Velocity Vectors in Perifocal Coordinate System

rp = zeros(3,1);
rp(1) = p*cos(nu)/(1+e*cos(nu));
rp(2) = p*sin(nu)/(1+e*cos(nu));

vp = zeros(3,1);
vp(1) = -sqrt(mu/p)*sin(nu);
vp(2) = sqrt(mu/p)*(e + cos(nu));

% Rotate from Perifocal Coordinate System to IJK system

% Rotation matrix for -w angle rotation about axis normal to orbit plane

Rw = [cos(-w) sin(-w) 0; -sin(-w) cos(-w) 0; 0 0 1];
```

```
% Rotation Matrix for -inc angle rotation about first axis (periapsis
% direction in PQW, which should be aligned with node direction after
% rotation above)

Ri = [1 0 0; 0 cos(-inc) sin(-inc); 0  -sin(-inc)  cos(-inc)];

% Rotation Matrix for -Omg angle rotation about third axis (normal to orbit
% plane, which should be aligned with K after both rotations above)

RO = [cos(-Omg) sin(-Omg) 0; -sin(-Omg) cos(Omg) 0; 0 0 1];

% Compute Position and Velocity in IJK by rotation vectors in PQW coord

r = RO*Ri*Rw*rp;

v = RO*Ri*Rw*vp;


end % posvel function
```

Bibliography

Adams, C., A. Robertson, K. Zimmerman, and J.P. How, "Technologies for Spacecraft Formation Flying," *Proceedings of ION GPS-96 Conference*. Kansas City MO, (September 1996).

Bauer, Frank H., Kate Hartman, Jonathon P. How, John Bristow, David Weidow, and Franz Busse. "Enabling Spacecraft Formation Flying through Spaceborne GPS and Enhanced Automation Technologies," *ION GPS-99 Conference*, 369-383. Nashville TN, (September 1999).

Carpenter, J., Jesse Leitner, Richard Burns, and David Folta. "Benchmark Problems for Spacecraft Formation Flying," *Proceedings of the 2003 Guidance, Navigation, and Control Conference and Exhibit*, Austin TX (August 2003).

Carpenter, J.R., David Folta, and D.A Quinn, "Integration of Decentralized Linear-Quadratic-Gaussian Control into GSFC's Universal 3-D Autonomous Formation Flying Algorithm." *AIAA GNC*, (August 1999).

Cobb, Richard G. Air Force Institute of Technology Professor, Dayton OH. Personal Interview. 22 Nov 2005.

Corazzini, T., A. Robertson, J.C. Adams, A. Hassibi, and J.P. How. "GPS Sensing for Spacecraft Formation Flying," *Proceedings of the ION-GPS-97 Conference*, (September 1997).

Clohessy W.H. and R.S. Wiltshire. "Terminal Guidance System for Satellite Rendezvous," *Journal of the Aerospace Sciences* 27:9 (September 1960).

de Selding, Peter B. "CNES Readies Essaim Satellites for December Launch," Space News (October 2004). 14 October 2005 http://www.space.com/spacenews/archive04/cnesarch_100404.html.

Ferguson, Phillip, Franz Busse, Brian Enberg, Jonathan How, Michael Tillerson, Nick Pohlman, Arthur Richards, and Robert Twiggs. "Formation Flying Experiments on the Orion-Emerald Mission," *Proceedings of the AIAA 2001 Space Conference and Exposition*. 28-30. Albuquerque NM (August 2001).

Folta, David, John Bristow, Albin Hawkins, and Greg Dell. " NASA's Autonomous Formation Flying Technology Demonstration, Earth Observing-1 (EO-1)," *Proceedings of the International Symposium on Formation Flying*, Toulouse, France (October 2002).

Francis, Scott, Samuel Stein, Thomas Celano, Jeremy Warriner, Jesse Leitner, Michael Moreau, Richard Burns, Robert Nelson, and Al Gifford. "Analytical Tools for Clocks in

Space." *Proceedings of the 2003 IEEE Frequency Control Symposium*. Tampa FL (May 2003).

Gaposhkin, E.M. and A. J. Coster. "Evaluation of New Parameters for Use in Atmospheric Models," Paper AAS-87-555. *Proceedings of the 1987 AAS/AIAA Astrodynamics Conference*. San Diego CA: AAS Publication Office, 1988

Gill, Eberhand. "First Results From a Hardware-in-the-loop Demonstration of Closed-loop Autonomous Formation Flying," *Advances in the Astronautical Sciences*, 113: 361-375. (2003).

How, J.P., R. Twiggs, D. Weidow, K. Hartman, and F. Bauer. "Orion: A Low-Cost Demonstration of Formation Flying in Space Using GPS," *Proceedings of the AIAA Astrodynamics Specialists Conference*. (August 1998).

Kang, W., Andy Sparks, and Siva Banda. "Multi-Satellite Formation and Reconfiguration," *Proceedings of the 2000 American Control Conference*. 379-383. Chicago IL, (June 2000).

Kitts, Christopher, Robert Twiggs, and Jonathon How. "Emerald: A Low-Cost Spacecraft Mission for Validating Formation Flying Technologies," *Proceedings of the IEEE Aerospace Conference*. 2: 217-226 (March 1999)

Larson, Wiley J. and James Wertz. *Space Mission Analysis and Design*. Torrance CA: Microcosm Press, 1991.

Leitner, Jesse. "Formation Flying: The Future of Remote Sensing from Space," Proceedings of the International Symposium on Space Flight Dynamics. Munich Germany (December 2004).

Leonard, C.L., W.M. Hollister, and E.V. Bergmann. "Orbital Formationkeeping with Differential Drag," *Journal of Guidance, Control, and Dynamics*,12: 108-113 (January 1989).

MacDowall, R., S. Bale, L. Gopalswarmy, D. Jones, M. Kaiser, J. Kasper, M. Reiner, and K. Weiler. "Solar Imaging Radio Array (SIRA): A Multi-Spacecraft Mission," *Proceedings of SPIE*. 284-292 (2005).

Mohammed, John L., "Mission Planning for a Formation-Flying Cluster," *Proceedings of the 14th Annual FLAIRS Conference*, 58-62, Key West FL, 2001.

Morring, Frank Jr. "Formation Flying," *Aviation Week and Space Technology*, 163: 38 (September 2005).

Ogata, Katsuhiko. *Modern Control Engineering.* Englewood Cliffs CA: Prentice-Hall Inc. 151-156. 1970.

Richelson, Jeffrey T. “U.S. Satellite Imagery, 1960-1999,” *National Security Archive Electronic Briefing Book No. 13,* (April 1999).

Roux, A., “Clusters Regroup for Relaunch,” *Aerospace America*, 36: 48-51 (August 1998).

Sabol, Chris, Rich Burns, and Craig McLaughlin. “Satellite Formation Flying Design and Evolution,” *Journal of Spacecraft and Rockets*, 38: 270-278 (March-April 2001).

Scharf, Daniel P., Fred Y. Hadaegh, and Scott R. Ploen. “A Survey of Spacecraft Formation Flying Guidance and Control (Part I),” *Proceedings of the American Control Conference*, 2: 1733-1739 (June 2003).

Storz, Mark. “High Accuracy Drag Model (HASDM),” *Proceedings of the AIAA/AAS Astrodynamics Specialist conference and exhibit*, Monterey CA 2002.

Vallado, David A. *Fundamentals of Astrodynamics and Applications.* El Segundo CA: Microcosm Press, 2001.

Wiesel, William E. *Spaceflight Dynamics*. Boston MA: Irwin/McGraw-Hill, 1997.

Zetocha, Paul, “Satellite Cluster Command and Control,” *Proceedings of the 2000 IEEE Aerospace Conference*. 7: 49-54. 2000.

REPORT DOCUMENTATION PAGE

Form Approved
OMB No. 074-0188

1. REPORT DATE *(DD-MM-YYYY)*	**2. REPORT TYPE**	**3. DATES COVERED** *(From – To)*
23-03-2006	Master's Thesis	August 2005 – March 2006

4. TITLE AND SUBTITLE
Characterizing and Controlling the Effects of Differential Drag on Satellite Formations

5a. CONTRACT NUMBER

5b. GRANT NUMBER

5c. PROGRAM ELEMENT NUMBER

6. AUTHOR(S)

Wedekind, James T., Captain, USAF

5d. PROJECT NUMBER

5e. TASK NUMBER

5f. WORK UNIT NUMBER

7. PERFORMING ORGANIZATION NAMES(S) AND ADDRESS(S)
Air Force Institute of Technology
Graduate School of Engineering and Management (AFIT/EN)
2950 Hobson Way, Building 640
WPAFB OH 45433-8865

8. PERFORMING ORGANIZATION REPORT NUMBER
AFIT/GSS/ENY/06-M14

9. SPONSORING/MONITORING AGENCY NAME(S) AND ADDRESS(ES)
AFRL/VS
Kirtland AFB, NM 87117

10. SPONSOR/MONITOR'S ACRONYM(S)
AFRL/VS

11. SPONSOR/MONITOR'S REPORT NUMBER(S)

12. DISTRIBUTION/AVAILABILITY STATEMENT

APPROVED FOR PUBLIC RELEASE; DISTRIBUTION UNLIMITED.

13. SUPPLEMENTARY NOTES

14. ABSTRACT

The ability to fly satellites in close formations represents a capability that could revolutionize the way satellite missions are designed in the future. This study examines three of the primary formation flying designs and characterizes the affect that an anomalous satellite with a slightly different cross-sectional area would have on the stability of the formation. Following the characterization of the effects a controller is implemented to mitigate the cross-sectional area differences between the satellites. With the addition of a straightforward controller, small cross-sectional area differences can be mitigated and corrected such that the satellites will remain in close proximity and in some cases the formation will remain stable.

15. SUBJECT TERMS
Satellite Constellations, Aerodynamic Drag, Maneuvering Satellites, and Orbiting Satellites

16. SECURITY CLASSIFICATION OF:			**17. LIMITATION OF ABSTRACT**	**18. NUMBER OF PAGES**	**19a. NAME OF RESPONSIBLE PERSON**
a. REPORT	**b. ABSTRACT**	**c. THIS PAGE**			Nathan A. Titus, Lt Col, USAF
U	**U**	**U**	**UU**	127	**19b. TELEPHONE NUMBER** *(Include area code)* (937) 255-6565, ext 4597 (Nathan.Titus@afit.edu)

Standard Form 298 (Rev. 8-98)
Prescribed by ANSI Std. Z39-18